PERFORMANCE ANALYSIS OF FSO COMMUNICATION SYSTEMS UNDER DIFFERENT IMPAIRMENTS

A Thesis Submitted to

Delhi Technological University

for the award of the Posthumous

degree of

Doctor of Philosophy

In

Electronics and Communication Engineering

By

late Mr. Piyush Jain

*(*Enrollment No. 2K18/PHDEC/516)

Under the supervision of

DR. N. JAYANTHI

Associate Professor in Dept. of ECE, DTU

DR. LAKSHMANAN. M

Dean IQAC and Professor in Dept. of Artificial Intelligence and Data Science, Sri Eshwar College of Engineering, Coimbatore, Tamil Nadu

Department of Electronics and Communication Engineering

Delhi Technological University, Delhi-110042, India

DELHI TECHNOLOGICAL UNIVERSITY

(Formerly Delhi College of Engineering)
Shahbad Daulatpur, Main Bawana Road, Delhi-42

CERTIFICATE

This is to certify that the thesis titled **"Performance Analysis of FSO Communication Systems under different impairments"** was originally undertaken by **Late. Mr. Piyush Jain** (Enrollment No.2K18/PHDEC/516) under the guidance of **Dr. N. Jayanthi** and **Dr. Lakshmanan .M**, in partial fulfillment of the requirements for the award of the Posthumous degree of **Doctor of Philosophy** (PhD) in Electronics and Communication Engineering, department at Delhi Technological University. It is with deep regret that we inform you that Mr. Piyush Jain passed away, before the completion of this thesis. In recognition of the significant work already accomplished by late Mr. Piyush Jain and in honor of his dedication towards his PhD work “Performance Analysis of FSO Communication Systems under different impairments", the supervisors have taken the responsibility to complete the thesis work on his behalf. This thesis is hereby submitted for the award of the degree of Doctor of Philosophy (PhD) posthumously, in memory of late Mr. Piyush Jain, whose passion and commitment to his research will always be remembered.

The results contained in this thesis have not been submitted to any other university or institute for the award of any degree or diploma.

Dr. N. Jayanthi
Associate Professor
Dept. ECE, Delhi
Technological University, Delhi,
India

DR. LAKSHMANAN. M
Dean IQAC and Professor in Dept. of
Artificial Intelligence and Data Science,
Sri Eshwar College of Engineering,
Coimbatore, Tamil Nadu,
India

DELHI TECHNOLOGICAL UNIVERSITY
(Formerly Delhi College of Engineering)
Shahbad Daulatpur, Main Bawana Road, Delhi-42

ACKNOWLEDGEMENT

First and foremost, thanks to the almighty for giving us strength and inspiration to complete the thesis on behalf of late Mr. Piyush Jain. This thesis stands as a testament to the dedication and hard work of the **Late Mr. Piyush Jain**, who embarked on this academic journey with passion and commitment. Tragically, Piyush passed away before the completion of this thesis. It is with deep respect and admiration that we acknowledge his invaluable contributions to this research. His intellectual curiosity, perseverance, and vision laid the foundation for this work, and we are honoured to have the opportunity to bring it to completion.

We immensely grateful to the **HOD ECE, DRC Chairperson, Dean Digital Education, Dean UG**, and **Dean PG** for their invaluable guidance throughout this journey. Words alone cannot express my gratitude. Also, we extend our appreciation to **Raj Shekhar Tiwari** (Enrolment No. 2K23/EC/160), who took on the responsibility of finalizing the formatting of this thesis with great care and dedication.

We would also like to acknowledge and appreciate **Piyush Jain's family** for their strength, understanding, and support during this difficult time. We extend our deepest gratitude to **Mr. Anil Kumar Jain, Mrs. Archana Jain, and Mr. Ayush Jain** for their kindness, support, and patience throughout this journey. Their trust in the university to complete this thesis has been deeply appreciated. This thesis is dedicated to the memory of late Mr. Piyush Jain, whose legacy will continue to inspire future generations of scholars.

Dr. N. Jayanthi (Supervisor)
Associate Professor
Department of ECE
Delhi Technological University
Delhi –110042, India

Dr. Lakshmanan. M (Co-Supervisor)
Dean IQAC and Professor in Department of
Artificial Intelligence and Data Science,
Sri Eshwar College of Engineering,
Coimbatore - 641202, Tamil Nadu, India

ABSTRACT

Free-space optical (FSO) communication is emerged as a promising technology for high-data-rate wireless communication due to its license-free spectrum, high security, and ease of deployment. However, FSO systems are highly susceptible to atmospheric turbulence, path loss, and pointing errors, which can significantly impact their reliability. To enhance system performance and mitigate these impairments, hybrid RF/FSO communication systems are proposed, leveraging the advantages of both RF and optical wireless channels. In a dual-hop RF/FSO system, the RF link ensures robust connectivity in adverse weather conditions, while the FSO link provides high-speed data transmission under favorable conditions. To accurately model channel fading effects, advanced statistical distributions are required, providing deeper insights into system performance under realistic conditions. This study investigates a dual-hop RF/FSO system by employing a Mixture Gamma (MG) distribution to model the RF channel and a Double Generalized Gamma (DGG) distribution for the FSO channel, analyzing key performance metrics such as outage probability, ergodic capacity, average capacity, and symbol error rate (SER) under varying turbulence conditions.

Considering a Dual Hop RF/FSO communication system, one hop is used as RF Signal and another as an FSO channel. Here, it uses Mixture Gamma Distribution to model the RF channel and a Double Generalized Gamma distribution to model the FSO channel. Also, as a special case, of Mixture Gamma, Rayleigh and Nakagami-m distribution is modelled at RF channel. In the first work, the mathematical and graphical analysis for different turbulence conditions are performed. The system's performance is analyzed in terms of Ergodic Capacity with different threshold SNR.

The analytical closed-form expression for the Outage and Ergodic Capacity is derived for the IM/DD detection approach to analyze the system's performance, The study finds that, given a particular threshold, the outage capacity decreases when the average electrical SNR rises and increases with the outage rate value rises. Also, it is noticed that as the average electrical SNR increases, Ergodic capacity increases for a specific threshold.

For the ergodic capacity, it is found that when the path loss increases, the ergodic capacity reduces for a given electrical SNR.

Next, the performance improvement of FSO system is analyzed in terms of AC and SER. Specifically, analytical expression of AC for Double Generalized Gamma fading

distribution under Equal Gain Combining (EGC) is presented. In addition, MGF based analytical expression of Symbol Error Rate (SER) of M-PSK and M-QAM for Double Generalized Gamma fading distribution under EGC scheme in terms of Fox-H is presented. Various special cases of proposed expressions are deduced for different fading distributions such as Double Weibull and Gamma-Gamma. It is evident from the results that increasing the diversity branches improve the performance in terms of AC and SER. However, the capacity improvement is more as it increases from L=1 to L=2 than L=2 to L=3 which is found in agreement with the literature. Further, at SNR of 30 dB, SER of QPSK are 3.7x10-19, 1.2x10-4 and 1.1x10-3 over weak, moderate and strong turbulence conditions respectively. Similarly, SER of BPSK, 4QAM and 8QAM is analyzed over weak, moderate and strong turbulence conditions. This implies that irrespective of fading scenario and/modulation scheme, the effect of moderate turbulence lies in between strong and weak turbulence conditions. This shows perfect agreement with the theoretical background. Finally, License free spectrum, high data rates and ease of installation make Radio on Free space optical (Ro-FSO) ubiquitous for upcoming generation of communication system. However, atmospheric turbulence induced fading and/or pointing error are the challenging issues of Ro-FSO system. The effects of these issues on performance of Ro-FSO is thoroughly analyzed by presenting closed form expressions under different turbulence conditions for different schemes. Specifically, BER of M-QAM and K-PSK modulation schemes over Double Generalized Gamma Fading distribution, under weak, moderate, and strong turbulence conditions, for OFDM based Ro-FSO system is analyzed by presenting closed form expressions for respective measures. Further, closed form expressions and in turn the presented analysis is based on with and without pointing errors. Furthermore, presented expressions are deduced over Gamma-Gamma and double Weibull fading as a special case of Double Generalized Gamma Fading distribution. BER of M-QAM and K-PSK modulation schemes for different values of K/M, different values of turbulence conditions and with or without pointing errors is observed numerically. Observation shows that irrespective of severity of turbulence be it strong or be it moderate an increase in order of modulation causes in an increase in BER. Also, pointing errors deteriorate the BER irrespective of severity and/or order of modulation schemes. Finally, it is observed that the effect of the order of modulation scheme on BER is more severe under moderate turbulence condition than under strong turbulence condition. Whereas, the effect of pointing error on BER is more under weak turbulence than under strong turbulence conditions.

Table of Contents

List of Figures

List of Tables

CHAPTER - 1
INTRODUCTION

In the past few years, there is an increasing bandwidth requirement and high data rate in communication area which makes to conduct various researches in the field of optical communication. Free Space Optical (FSO) communication fulfils the ever-increasing demand of data rate. It is the technology of transferring the data from one point to other by the help by optical signals. The components of the optical signals can be used to modulate information which has to be transferred [1]. FSO is a Line of Sight (LOS) communication technology which have many advantages over traditional RF communication like unlicensed spectrum, easy setup, higher data rate. High data rate, large bandwidth, less power requirement, low attenuation level and high transmission security among others makes the FSO system as most suitable for 5G [2]. Further, applications of FSO system also ranges from underwater to satellites communication. Also, FSO system is found suitable for future generation of mobile communication system. However, like any wireless system, in FSO too wireless link is always a weak link causing impairments. Specifically, apart from pointing errors (deviation from point-to-point LOS) fading, scattering, atmospheric turbulence and absorption are the serious concern of FSO system [3-4].

1.1 BASIC PROPERTIES OF FSO

Some of the basic attributes of FSO communication are listed below:

1.1.1 IMMENSE BANDWIDTH

In communication systems bandwidth of transmitted signal directly depended on the frequency of the carrier signal. Using optical signal as carrier whose frequency ranges from 10^{12} to 10^{16} Hz in FSO therefore result in high bandwidth compared to RF communication system [5]. The Optical communication promises increased amount of information due to its huge bandwidth.

1.1.2 NARROW SIZE OF BEAM

The transmitted signal is only focused within a very fine area with limited divergence of between 0.01– 0.1 milli rad. This indicates that the transmitted signal is very difficult to intercept making FSO highly secure way to communicate. Such a narrow area of signal, requires more sophisticated alignment of transmitter and receiver in communication system [2].

1.1.3 UNLICENSED SPECTRUM

Unlike RF communication use of FSO (optical frequency) is free of cost apart from its installation and maintenance. In order to use RF systems, it is required to buy costly spectrum. FSO is therefore considered as the cheap communication system as compared to other traditional systems [3].

1.1.4 LOW POWER REQUIREMENT

Optical wave has larger frequency than Radio waves so apparently it has much larger power. Thus, it is not necessary to invest large amount of power in transmission of optical signal. Therefore, Optical communication systems are power efficient.

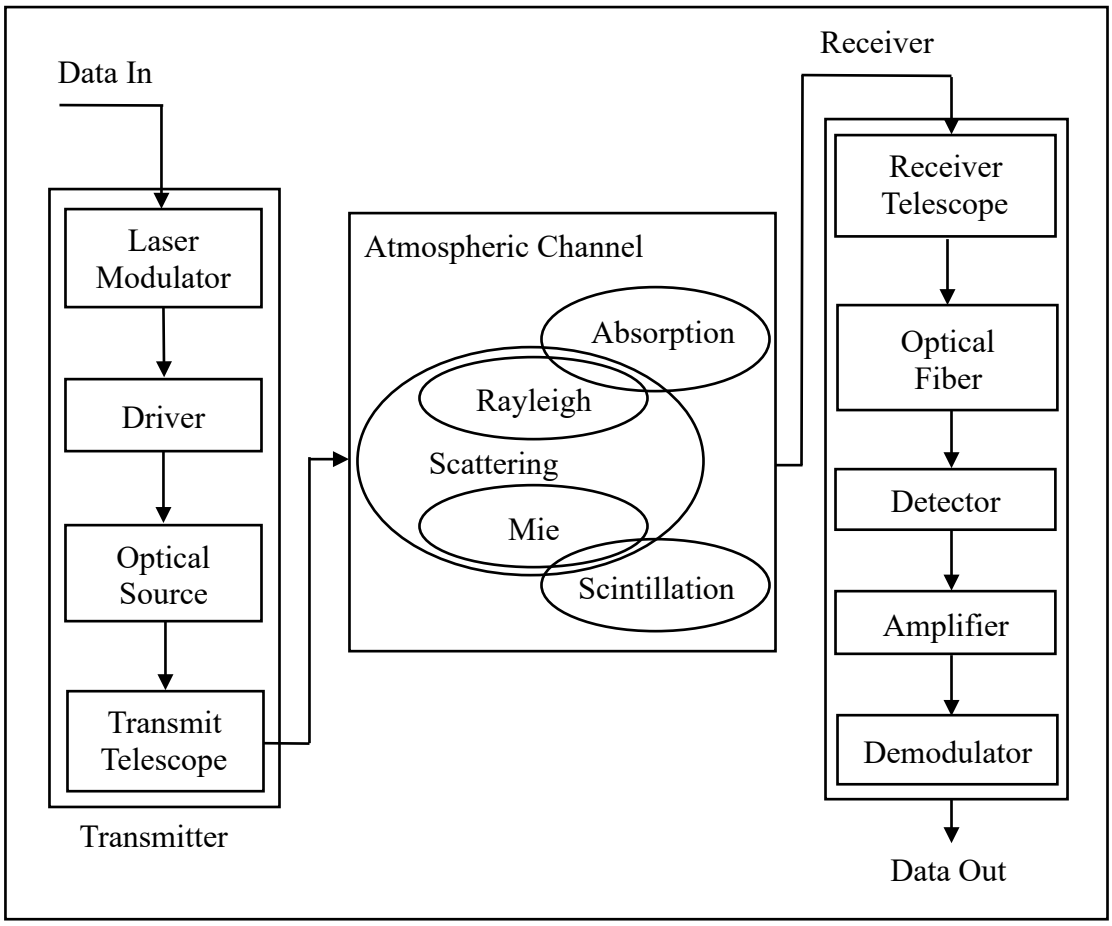

Fig.1.1 Block diagram of FSO communication system [4].

1.2. APPLICATIONS OF FSO

Some of the most common applications of FSO are listed below:

1.2.1. BACK UP FOR OPTICAL FIBER

FSO can be used to complement other technologies like optical fiber. It can be used as backup communication system when the fiber can suffer any damages.

1.2.2. DISASTER RECOVERY

In events of disaster FSO system can be proved to be highly useful due to the fact that FSO is easy to deploy and redeploy in any region. Since it is line of sight communication it does not need any large arrangements [4].

1.2.3. DIFFICULT TERRAINS

FSO can be used for communication in the region where it is very difficult to install and maintain wired link. For example, across the rivers or densely constructed area in city.

1.2.4. MILITARY USES

Since it is highly secured network it can be used in army for transfer of the sensitive information.

1.2.5. INTERSATELLITE COMMUNICATION

In order to achieve high quality of communication which is also power efficient between satellites, Free Space Optical Communication has been used. The application of FSO can be further extended in drones and other vehicles [5].

1.3. CHALLENGES IN FSO

Like other wireless communication systems, Free Space Optics (FSO) also faces certain limitations, including signal fading, scattering, and absorption of the transmitted light. These limitations are due to the fact that there is no fixed channel in FSO. Transmitting signal in the free space gives system more flexibility but it also induces certain impairments. Major problem in FSO is therefore uncertainty in the channel that is, free space. These disturbances will cause attenuation in the signal, which degrades the overall performance of the system. There are some of the problems listed below.

1.3.1. FSO LINK

When there is even small misalignment in position of transmitter and receiver, then it can cause huge loss of data and it degrades system performance. Misalignment in the systems can be due to many factors like human error, thermal expansion of buildings where system was held. The aperture size of the receiver lens must be adjusted according to the divergence angle to minimize losses.

1.3.2. ATMOSPHERIC TURBULENCE

The solar radiation on earth's surface causes air in lower region to heat and rise up this results in inhomogeneities in the temperature. This results in the random variation in refractive index of the air in certain areas, this condition is called atmospheric turbulence [6]. The atmospheric turbulence is categorized upon various magnitude of refractive index variation and inhomogeneities. Under these conditions when optical signal is transmitted there is the random phase and amplitude change which eventually results in performance degradation. Due to this receiver gets corrupted information and BitError Rate (BER) of the system increases. The turbulence can sometimes can causes the total optical link failure in communication system.

1.3.3. ATMOSPHERIC LOSSES

The reduction in the amplitude of the optical signal by atmospheric channel is called as Atmospheric losses. The major factors responsible for this loss are absorption and scattering of the optical signal. Our atmosphere is full of various types of gases (N2, H2) and liquid molecules (mist) which responsible for the absorption of the intensity of the optical signal. As a name suggest Scattering is process of deflection of component of light wave in optical communication. When photon of light wave in FSO hits certain specific size of the particles in the atmosphere there is random redistribution of the component of light wave. Fog, rain, snow and sand are the other factor that cause scattering and absorption which leads to the atmospheric losses [7].

1.4. ATMOSPHERIC TURBULENCE MODELS

In past years various statistical models have been introduced describe the probability density function (pdf) of irradiance fluctuation in order to model atmospheric turbulence. These are Negative Exponential, Log Normal, I-k distribution, negative exponential and

Gamma-Gamma distributions. In earlier studies Log-normal distribution has been used more often but it is limited for weak turbulence conditions only. It is shown that in strong turbulence condition there are many uncertainties in experimental results. Several other models have been developed further to model atmospheric turbulence under wide range of turbulence conditions.

Another decent distribution model, Gamma-Gamma fading distribution is further proposed which is suitable for all weak to strong turbulence condition. The gamma-gamma model is a two-parameter distribution; the product of small-scale fluctuations and large-scale fluctuations are considered as irradiance fluctuations. Two independent gamma distributions govern both the fluctuations.

A new statistical model, Double Generalized Gamma (double GG) has also been proposed in some recent literatures. This model is applicable for all range of atmospheric turbulence conditions from weak to strong. The double GG model considers the product of large-scale fluctuations and small-scale fluctuations as the irradiance fluctuation; both of these fluctuations are Generalized Gamma distributed.

Table 1.1 Channel models for different turbulence conditions [2]

WEAK TURBULENCE	MODERATE TURBULENCE	STRONG TURBULENCE
Log Normal Distribution	Log Normal Distribution	G-G Distribution
G-G Distribution	Negative Exponential	K-Distribution
K-Distribution	G-G Distribution	I-K-Distribution
I-K-Distribution	Double Weibull	Double Weibull
Exponentiated Weibull	Exponentiated Weibull	Exponentiated Weibull
Double Generalized Distribution	Double Generalized Distribution	Double Generalized Distribution

1.5. FSO MODULATION TECHNIQUES

In FSO, the modulation is used in order to achieve high transmission rate and low BER rate. The modulation techniques can further be utilized to reduce the impact of turbulence. Different modulation techniques, for example, PPM, BPSK and OOK have been examined. It is entirely appealing for the modulation technique to be power effective, yet this is anyway by all account not alone the main contributor in the decision of choice of modulation technique. The design complications of transmitter/receiver and the data transfer capacity are equally significant. Picking a modulation for a specific application in this manner involves trade-off among these variables.

PPM has poor transfer speed proficiency, BPSK is for the most part utilized as it gives the least BER. Sub carrier intensity modulation (SIM) is utilized as an option to OOK and it is concentrated throughout the years that BPSK SIM is better than the other regulation strategies, for example, QPSK, MPSK etc. [3]

1.5.1. TYPES OF MODULATIONS IN FSO

There are a wide range of kinds of modulation which are reasonable for wireless optical communication. Mainly digital modulations techniques are used are: OOK, pulse position modulation (PPM) and phase shift keying with SIM.

1.5.1.1. OOK

On-Off keying (OOK) is simplest and main modulation technique to be implemented in practical FSO systems. OOK can utilize either non-return to-zero (NRZ) or return to-zero (RZ) pulse format. In NRZOOK, an optical pulse of peak power $\alpha_e P_t$ is used to represent digital 0 while the transmission of an optical pulse of peak power P_t represent digital 1, where α_e is optical source extinction ratio. The implementation of OOK is easy but it is seen as imperfect over atmospheric disturbance channel. In turbulence conditions for OOK

to perform optimally it is required to have adaptive threshold level according to irradiance fluctuation and noise [8].

1.5.1.2. PULSE POSITION MODULATION (PPM)

In this type of modulation mapping of each block of $log_2 M$ data bit has been made at one of M probable symbols. Each symbol these M symbols is made of a fixed power P_t pulse, engaging single slot, together with M-1 empty slots. Pulse position is used to encode information. Due to the encoding of information on pulse position at the receiver of PPM system it needs both slot and symbol synchronization to obtain the information in communication systems. As compared to OOK it is more power efficient and does not require any adaptive threshold.

1.5.1.3. PHASE SHIFT KEYING (PSK)

BPSK: Binary phase shift keying is simple type of PSK where the 0's and 1's are represented by two different phase positions in the carrier signal that is $\theta = 0^{\circ}$ for binary 1 and $\theta = 180^{\circ}$ for binary 0.

MPSK: In m-ary phase-shift keying (MPSK), there are more than two phases' states, typically four (0, +90, -90, and 180 degrees) or eight (0, +45, -45, +90, -90, +135, -135, and 180 degrees) MPSK modulation has higher data rate than the case in BPSK. In this modulation technique the information bits in mapped on one of M phase shifted forms of the carrier to transmit the data. As a result, in transmitted signal all waveforms have different phases along with the same amplitude and frequency. In a typical SIM-based Free Space Optics (FSO) system, the intensity of the optical source is modulated by the electrical signal, transmitted through the free-space channel, and then directly detected at the receiver by a photodetector, which transforms back electrical signal from the received optical signal. The Double GG fading distribution is used to model our FSO

communication channel under moderate turbulence conditions. The optical signals are passed through an atmospheric turbulence channel and are detected at the receiver by a photoelectric detector.

1.6. FSO TRANSMITTER

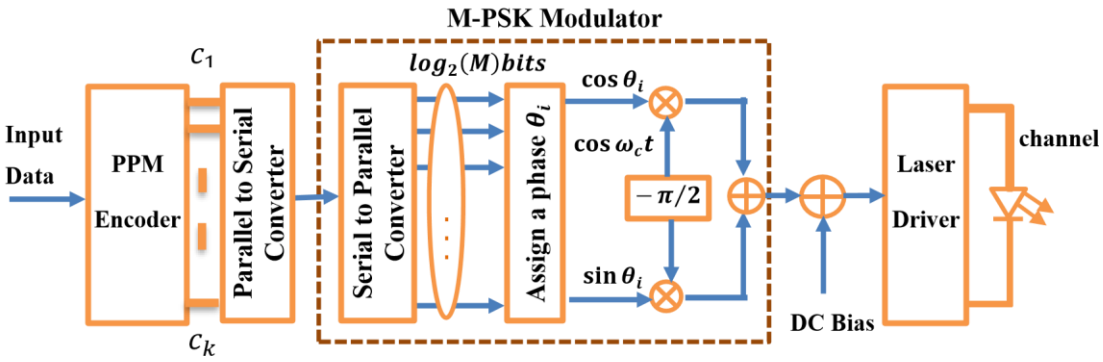

Fig.1.2. Block diagram of FSO transmitter [9], [10].

In the transmitter section PPM encoder converts the block of data bits $M = log_2 L$ into PPM code words where M is the number of bits per PPM symbol and L is the average PPM symbol length. The PPM code words are modulated by MPSK modulator on the optical signal intensity. is shown in Fig1.2.

Finally, the newly processed data array is modulated onto a subcarrier using an M-ary Phase Shift Keying (MPSK) scheme. Since the resulting MPSK-modulated subcarrier is a sinusoidal signal including both positive and negative values, a DC bias is added for the purpose of ensuring the total driving signal for the laser diode remains above the threshold current. This guarantees that the laser operates continuously and avoids signal distortion due to under-threshold operation.

1.7. FSO CHANNEL

In FSO communication channel modelled using Double GG fading distribution in which I is the received irradiance. This model is applicable for all regimes from weak to strong

turbulence conditions. The Double Generalized Gamma (Double GG) distribution extends the generalized gamma model by representing received irradiance fluctuations as the result of small-scale fluctuations modulated by large-scale fluctuations. Due to free space as a channel there are many factors in FSO systems such as Atmospheric Turbulence, Absorption and scattering of optical signal, beam wandering, beam spreading, background noise.

1.8. FSO RECEIVER

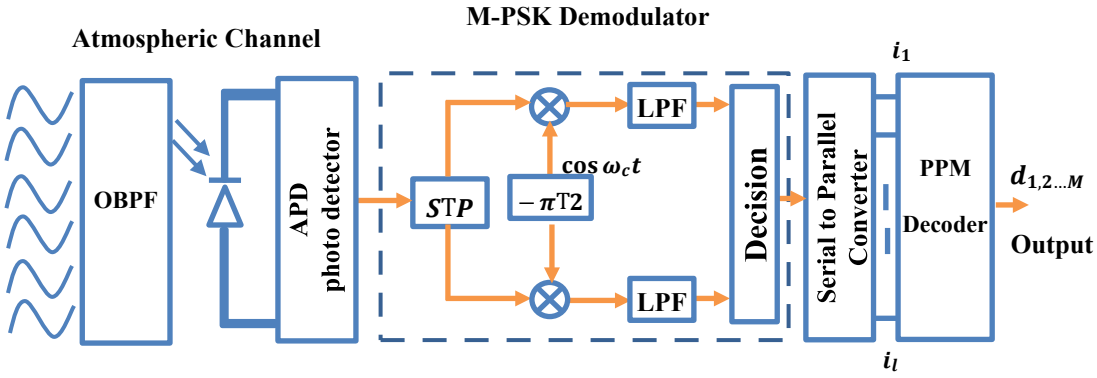

Fig.1.3. Block diagram of FSO receiver [9], [10].

In FSO system when optical signal reaches at receiver firstly optical band pass filter (OBPF) is used to pass out excessive noise elements. Next component avalanche photo detector (APD) is then use to detect optical signal and convert it into electrical signal. As the optical signal passes through the atmospheric channel, its amplitude and phase are distorted because of absorption and scattering effects. After passing through Low Pass Filter (LPF) and sampler, electric signal is obtained which is of low frequency bearing information. On further decoded by PPM Decoder obtaining output data.

1.9. DIVERSITY TECHNIQUES

Spatial diversity techniques are widely used technique to combat the effect of impairments/turbulence induced fading. Commonly utilised diversity combining schemes are equal gain combing (EGC), maximum ratio combining (MRC), optimal combining (OC), and selection combining (SC). It is noticeable that MRC provide optimum efficiency at the cost of computational complexity whereas EGC is least complex [8].

1.10. RESEARCH MOTIVATION

In recent years, the explosive growth of data-driven applications and emerging 5G/6G technologies has intensified the demand for high-speed, reliable, and secure communication systems. While Free Space Optical (FSO) communication stands out as a potential enabler due to its license-free spectrum, high data rates, and immunity to electromagnetic interference, its performance is severely hindered by environmental conditions such as atmospheric turbulence, pointing errors, and path loss. Conversely, Radio Frequency (RF) communication systems provide robust connectivity under adverse conditions but suffer from limited bandwidth and spectrum licensing issues.

This duality presents a compelling case for hybrid RF/FSO systems, particularly the dual-hop RF/FSO model, which combines the reliability of RF links with the high-throughput advantage of FSO channels. However, accurate performance prediction of such systems under realistic fading environments is challenging. Classical models like Rayleigh or Nakagami-m provide limited insight when dealing with the intricate interplay of RF and optical fading characteristics, especially under strong turbulence and pointing misalignments.

To bridge this gap, the thesis leverages advanced statistical models—namely the Mixture Gamma (MG) distribution for RF and the Double Generalized Gamma (DGG) distribution for FSO—to deliver a more holistic analysis. This allows for the derivation of

closed-form expressions for key performance metrics such as Outage Capacity, Ergodic Capacity, Average Capacity (AC), Symbol Error Rate (SER), and Bit Error Rate (BER) under a variety of conditions.

Moreover, the integration of Equal Gain Combining (EGC) diversity techniques and OFDM-based Ro-FSO architectures with and without pointing errors expands the scope of analysis, addressing practical deployment challenges in real-world systems. The novelty of the proposed analytical expressions and their validation through extensive MATLAB simulations makes this study both timely and significant for future wireless network evolution.

1.11. THESIS ORGANIZATION

This thesis is organized into seven chapters, each of which builds upon the preceding one to systematically explore and enhance the performance of dual-hop RF/FSO communication systems:

- **Chapter 1: Introduction:** This chapter introduces the fundamentals of FSO communication, highlighting its advantages over traditional RF systems and outlining the key challenges such as turbulence, pointing errors, and atmospheric losses. The motivation for hybrid RF/FSO systems and the need for advanced statistical modelling are also discussed.
- **Chapter 2: Literature Review:** A comprehensive survey of existing models and techniques for FSO and hybrid RF/FSO systems is presented. The limitations of classical fading models and the need for more accurate distributions like Double Generalized Gamma and Mixture Gamma are highlighted. The chapter also surveys various diversity schemes and modulation techniques used to mitigate performance degradation.

- **Chapter 3: Ergodic Capacity Analysis:** This chapter focuses on the derivation and analysis of Ergodic Capacity for a dual-hop RF/FSO system using Mixture Gamma and Double Generalized Gamma fading models. Both analytical and simulation-based evaluations are conducted under various path loss and SNR conditions, comparing the effects of Rayleigh and Nakagami-m distributions.
- **Chapter 4: Average Capacity and SER under EGC:** This chapter demonstrates closed-form expressions for Average Capacity (AC) and Symbol Error Rate (SER) for M-PSK and M-QAM schemes over DGG fading with EGC diversity. The analysis also incorporates the effect of weak, moderate, and strong turbulence conditions, and discusses how capacity improves with the number of diversity branches.
- **Chapter 5: Outage and Ergodic Capacity under Dual-Hop Framework:** Here, the Outage Capacity and Ergodic Capacity for the dual-hop RF/FSO system are further expanded, with distinct focus on the impact of different fading models (Rayleigh and Nakagami-m). Analytical expressions are derived and validated via simulations to demonstrate their accuracy under multiple turbulence regimes.
- **Chapter 6: BER Analysis of OFDM-Based Ro-FSO System:** This chapter introduces a Radio-over-FSO (Ro-FSO) system using OFDM, where novel closed-form BER expressions are derived for both M-QAM and K-PSK schemes under DGG fading with and without pointing errors. This section addresses real-world impairments like intermodulation distortion and laser non-linearity, making the analysis more application-oriented.
- **Chapter 7: Conclusion and Future Scope:** The final chapter summarizes the key contributions of the thesis, validates the proposed models, and highlights their significance for next-generation communication networks. It also outlines future

research directions including MIMO-based RF/FSO architectures, AI-driven channel prediction, and experimental validations through testbed deployments.

CHAPTER 2

LITERATURE REVIEW

Free Space Optical (FSO) Communication empowers wireless communication through space with the help of laser transmitters in infrared bands. These frameworks give high information rates practically identical to fiber optics. Free space optical frameworks involve an optical transceiver at the two terminations to give bidirectional capacity. FSO communication is certifiably not another advancement it is just more advanced now. FSO frameworks stood out at first as the last mile arrangement and can also be utilized in a vast exhibit of uses comprising of cell backhaul, between building associations in big business/grounds conditions, video reconnaissance/checking, fiber back-up, excess connection in catastrophe recuperation and aid projects among others.

The FSO has been achieved great attention in wireless communication. There were various literature focusing on different modulation technique and different. FSO involves the optical transmission of voice, video, and data using air as the medium of transmission as opposed to fibre optic cable. Transmission using FSO technology is relatively simple. It comprises two systems, each equipped with an optical transceiver that includes a laser transmitter and a receiver, enabling full-duplex communication.

2.1 LITERATURE ON FSO COMMUNICATION SYSTEM

In [11], the author estimates the probability distributions of power fades, he considers two basic types of disturbance in electromagnetic wave propagation through atmospheric turbulence: wave-front intensity fluctuations and wave-front distortion. The mitigation of aggregate loss probability associated with these two mechanisms is evaluated through spatial diversity, implemented using a multi-aperture receiver

configuration. Receiver performance degradation is analyzed using fractal techniques to model turbulence-induced wavefront phase distortion, while a log-normal distribution is assumed to model the fluctuations in the collected optical power.

A unified analytical framework is presented for accurately determining the average Symbol Error Rate (SER) of linearly modulated signals over generalized fading channels. The analysis is applicable to systems utilizing coherent demodulation along with maximal-ratio combining (MRC) across multiple channels. It assumes independently fading paths, which may have non-identical distributions. In all scenarios, the proposed method yields an average SER expression involving a single finite-range integral, which is straightforward to evaluate numerically. Additionally, SER expressions for single-channel reception are derived as special cases of the general analysis. These expressions reduce to well-known solutions, give alternative (often simpler) expressions for previous results, or provide new formulas that are either closed form expressions or simple to compute numerically [12].

Now a day the wireless technology has become popular in the wireless system. Free Space Optics (FSO) is a communication technology that broadcast information using light in the visible to near-infrared (NIR) spectrum through the atmosphere. FSO is gaining attention as a modern engineering solution to last-mile bottlenecks in local area access networks, offering high bandwidth, low-cost deployment over unlicensed spectrum, lower power consumption, and enhanced security compared to traditional RF technologies. Equally, the free space optical communication is extremely impressed by the various atmospheric conditions which cause the degradation of the carrying out of FSO link. This report introduces the study of the issue of the various atmospheric conditions on the FSO link. This report includes the result of the fog by analysis the

various fog models such as Kim Model, Kruse Model. And also, analysis the wet and dry snow over the FSO links [13].

In optical communication systems that utilize direct detection at the receiver, intensity modulation schemes like On-Off Keying (OOK) and Pulse Position Modulation (PPM) are commonly employed to transmit information. Consider the possibility of applying space-time coding in such a scenario, using, for example, an Alamouti-type coding scheme [14]. Implicit in the Alamouti code is the fact that the modulation that defines the signal set is such that it is meaningful to transmit and detect both the signal and its negative. While modulations such as PSK and QAM naturally fall into this class, OOK and PPM do not since the signal polarity (phase) would not be detected at the receiver. The authors investigate a modification of the Alamouti code to be used with such modulations that has the same desirable properties as the conventional Alamouti code but does not rely on the necessity of transmitting the negative of a signal [15].

The study investigates the utilization of multiple laser transmitters paired along with multiple photodetectors for atmospheric line-of-sight optical communication. It emphasizes multiple-pulse-position modulation (MPPM) as a power-efficient transmission technique, incorporating signal repetition across the laser array. The analysis assumes ideal photon-counting detectors, both in the presence and absence of background radiation. This configuration forms a multiple-input multiple-output (MIMO) channel, which offers the potential to mitigate fading effects caused by atmospheric turbulence—modeled using both log-normal and Rayleigh distributions. The work focuses on evaluating symbol error probability for uncoded transmission and channel capacity for coded transmission. Full spatial diversity is obtained naturally in this application [16].

Error control coding is a reliable approach for mitigating turbulence-induced fading in FSO communication links. This paper derives error performance bounds for

coded FSO systems operating over atmospheric turbulence channels modeled by the recently introduced Gamma-Gamma distribution. Initially, a pairwise error probability (PEP) expression is developed, which is then combined with the transfer function technique to establish upper bounds on the bit error rate (BER). Simulation results are further demonstrated to confirm the analytical results [17].

2.2 LITERATURE ON FSO COMMUNICATION SYSTEM USING DIFFERENT DISTRIBUTIONS

In [18], the author proposes a statistical channel model, named as Double Weibull, to describe the irradiance fluctuations in moderate and strong turbulence for FSO systems. Stochastic model is grounded in scintillation theory and is formulated as the product of two Weibull-distributed random variables. Closed-form expressions for the probability density function (PDF) and cumulative distribution function (CDF) are derived using Meijer's G-function. The model is compared with the classical Gamma-Gamma model, and its accuracy is evaluated through simulations under both plane and spherical wave conditions. Furthermore, the performance of an FSO system operating over the Double Weibull turbulence channel is analyzed. Closed-form expressions for the bit error rate (BER) and outage probability are derived, assuming intensity modulation along with direct detection (IM/DD) and On-Off Keying (OOK).

In [19], the author develops a new statistical model for the irradiance fluctuations of an unbounded optical wave front (plane and spherical waves) propagating through a turbulent medium under all irradiance fluctuation conditions in homogeneous, isotropic turbulence. The primary advantage of this model lies in its ability to yield closed-form, analytically solvable expressions for key channel statistics of an unbounded optical wavefront across all turbulence regimes. Moreover, it joins several existing statistical

models for irradiance fluctuations and shows strong agreement with experimental observations.

In [20], the author proposes a simple accurate closed-form approximation to the pdf of the sum of independent, identically distributed gamma-gamma random variables. It has been demonstrated that the probability density function (PDF) of the Gamma-Gamma (G-G) sum can be effectively estimated using the α-μ distribution. Leveraging this approach, accurate and simplified expressions for key performance metrics of MIMO free-space optical systems operating under G-G fading are derived. The validity and precision of the suggested schemes are confirmed through extensive numerical evaluations and computer simulations.

In [21], a Hybrid Modulation scheme based on PPM and BPSK-SIM schemes for free-space optical communications is proposed. The analytical bit error rate (BER) performance is evaluated under both weak and strong (saturated) turbulence conditions, and the outputs are validated through simulation. Findings indicate that the PPM-BPSK-SIM scheme consistently outperforms conventional BPSK-SIM across all turbulence regimes. Additionally, the signal-to-noise ratio (SNR) gain relative to standard PPM increases with the severity of atmospheric turbulence.

The author investigates spatial diversity techniques for subcarrier PSK-modulated optical wireless communication links over Gamma–Gamma fading channels. Together repetition coding and Alamouti-type orthogonal space-time block coding (OSTBC) schemes are analyzed. By employing a moment generating function (MGF) method alongside a series expansion of the modified Bessel function, highly accurate series expressions for the error rate are derived. Asymptotic analysis reveals that the system's diversity order is determined solely by the effective number of small-scale scattering cells in the atmosphere. Performance evaluations indicate that, for subcarrier PSK systems over

Gamma–Gamma channels, repetition coding consistently outperforms OSTBC. The asymptotic performance loss of the Alamouti-coded system with respect to the repetition-coded system is also quantified analytically [22].

In [23], the contributors theoretically study the performance of direct-detection free space optical communication systems using binary phase-shift keying sub carrier intensity modulation and APD. The bit-error rate and channel capacity of the system are analytically derived for both log-normal and Gamma-Gamma channel models, which represent weak-to-moderate and moderate-to-strong atmospheric turbulence conditions, respectively. The authors conduct a quantitative analysis of the optimal avalanche photodiode (APD) average gain, required transmitted optical power, and achievable bit-rate under varying turbulence levels, considering the impact of APD shot noise and thermal noise. Results indicate that an appropriate choice of APD average gain can significantly enhance system performance across both turbulence regimes. While the optimal APD gain remains relatively stable across different turbulence levels, it shows notable sensitivity to changes in the receiver noise temperature.

Now a day the wireless technology has become popular in the wireless system. The technology known as FSO transmits information by making use of the visible to near infrared (NIR) light that travels through the atmosphere. FSO communications are increasingly recognized as a modern engineering solution for addressing last-mile bottleneck challenges in local area access networks, thanks to their high bandwidth, low implementation cost in unlicensed spectrum, relatively low power consumption, and enhanced security compared to RF technologies. Equally, the free space optical communication is extremely impressed by the various atmospheric conditions which cause the degradation of the carrying out of FSO link. This report introduces the study of the issue of the various atmospheric conditions on the FSO link. This report includes the

result of the fog by analysis the various fog models such as Kim Model, Kruse Model. And also, analysis the wet and dry snow over the FSO links [24].

Atmospheric turbulence is a significant performance degrader for free space optical communication (FSO) systems. A promising strategy for reducing turbulence-induced fading is the use of spatial diversity techniques. The Double Generalized Gamma distribution, a brand-new general statistical model that encompasses all turbulence conditions, is used in this study to inspect the error rate performance of FSO links with spatial diversity over atmospheric turbulence channels. The authors assume intensity modulation/direct detection with on-off keying and present the BER performance of SIMO, MISO and MIMO FSO systems over this new channel model [25].

Free Space Optical (FSO) communication systems are wireless solutions that offer high-speed, secure, and cost-effective data transmission among two points. The FSO channel is modelled using the Málaga distribution, a generalized statistical model that encompasses a wide range of turbulence conditions and includes several earlier models as special cases. This work analyzes the performance of a Subcarrier Intensity Modulation (SIM)-based FSO system while considering the adverse impacts of atmospheric turbulence and pointing errors. Closed-form analytical expressions for the bit error rate (BER) and channel capacity are derived under these conditions. The results demonstrate the performance deterioration the system suffers because of the channel and also how the m-distribution model can be used to obtain the performance over other FSO channels [26].

When used in a FSO communication link, the authors investigate the effects of MIMO spatial diversity schemes in a variety of weather conditions, including very clear air, drizzle, haze, fog, and so on. The outage probability P out and the bit error rate (BER) are used to assess the performance. They demonstrate that, at low signal-to-noise ratios,

MIMO schemes result in a decrease in the BER and P out, which is more pronounced in conditions of very clear air and clear air than in conditions of haze and fog. At a BER, diversity gain is evaluated and found to rise in tandem with the number of transmit/receive apertures. However, for a given MIMO scheme and turbulence strength, it remains nearly constant across all weather conditions. A FSO link and MIMO scheme's performance are contrasted using aperture averaging. Owing to constraint on the receiver aperture diameter, the aperture averaging technique fails to give the same kind of performance as provided by the higher order MIMO schemes [27].

In [1], the author proposes a new probability distribution function which accurately describes turbulence-induced fading under a wide range of turbulence conditions. Based on a doubly stochastic theory of scintillation and developed through the product of two generalized gamma distributions, the proposed model is known as double-generalized gamma (double GG). The published simulation data for plane and spherical waves are well matched by the proposed double GG distribution, which applies to many of the existing turbulence channel models and is a good fit. The outage probability and average bit error of free-space optical communication systems over turbulence channels are expressed in closed form and asymptotically using this new statistical channel model. They demonstrate that the results previously reported for gamma–gamma, double-Weibull, and K channels as special cases are covered by our derived expressions.

PPM-MSK-SIM, a novel Hybrid Modulation scheme based on PPM and MSK subcarrier intensity modulation, is proposed to enhance the BER performance of BPSK-SIM-based FSO communication systems. PPM-MSK-SIM's BER performance for an FSO system in log-normal turbulence channels with avalanche photodiode detection is then thoroughly examined. PPM-MSK-SIM outperforms BPSK-SIM and PPM in terms

of improved BER performance, as demonstrated by the numerical simulation results. This makes PPMMSK-SIM a favourable candidate for the modulation technique in FSO communication systems [28].

Recently, the research community has been paying more and more attention to optical wireless communication technologies. In the context of atmospheric turbulence, the authors investigate how a free space optical communication system performs over the generic propagation model known as M-distributed channel. They analysed a SIM-FSO communication system using DPSK and closed form expressions are derived using Meijer G function for bit error rate, channel capacity and outage probability for M-distribution [29].

Due to its capability to achieve extremely high data rates over unlicensed optical spectrum, FSO communication has received a growing amount of attention in recent years. Atmospheric turbulence significantly reduces the system's performance, which is a major performance constraint for FSO systems. Multiple transmit and/or receive apertures can be used to solve this problem, and diversity gain can improve performance. In [30], the authors investigate the BER performance of FSO systems with transmit diversity or receive diversity with EGC over atmospheric turbulence channels described by the Double Generalized Gamma (Double GG) distribution. The recently proposed Double GG distribution offers a unified, closed-form model that generalizes numerous existing turbulences models and effectively captures all atmospheric turbulence conditions. Given that the bit-error rate (BER) expression involves the distribution of a sum of Double GG random variables (RVs), a closed-form upper bound for this sum is first derived. Building on this, a novel union upper bound for the average BER is developed, along with its corresponding asymptotic expression, both evaluated in terms of Meijer's G-functions.

The atmospheric turbulence has a negative impact on the FSO link's BER performance. The FSO communication system's error rate can be significantly improved by employing additional transmit and receive apertures at the transmitter and receiver, respectively. However, the advantages of the multiple transmit and/or receive apertures-based FSO communication system may be lost due to the PEs caused by building sway. Therefore, the impact of PEs on the GG fading atmospheric fluctuations is taken into consideration for a comprehensive and realistic study of the FSO MIMO system. The probability density function of the GG fading FSO links with PEs is given a new power series-based representation. In contrast to the closed-form representation, which includes the RV's Meijer-G function, the new series representation only includes terms with the RV's exponent. The average BER for the two combining strategies over the GG fading FSO links with PEs is then calculated. Both systems' combining gains and analytical diversity order are also obtained. In various scenarios, the impact of PEs on the performance of the schemes is examined, and it is discovered that PEs significantly reduce the diversity of the FSO MIMO system. Simulation and analysis have shown that the MRC scheme is more resistant to large PEs, despite the fact that the EGC scheme is simpler to implement [31].

In arid and semi-arid regions, dust particles suspended in the atmosphere can affect FSO communication systems. The optical link suffers severe effects when these particles are in the air, reducing its availability and resulting in service outages. A lot of research has been done in the literature on how dust affects microwave signals. However, information and research are still extremely limited, if not completely absent, for FSO communication systems that make use of shorter wavelengths. As a result, they investigate the performance of FSO links during dust storms in this letter. The author constructed a chamber to replicate this particular setting and conduct measurements. An

empirical model for the signal attenuation as a function of the visibility range is derived and proposed from the experiments. Under moderate and light dust conditions, the results demonstrate that FSO links can reach distances of hundreds of meters to a few kilometers with acceptable performance. Furthermore, a comparison analysis shows that the dust induces seven times higher attenuation than fog [32].

Atmospheric turbulence-induced fading poses a significant challenge to the performance of free-space optical (FSO) communication systems. Incorporating multiple lasers and photodetectors in MIMO FSO configurations offers a promising solution to counteract such fading effects. To enable an accurate and comprehensive analysis of these systems, this paper adopts the recently developed Double Generalized Gamma (Double GG) fading model, which effectively captures irradiance fluctuations under a wide range of turbulence conditions.

The study focuses on MIMO FSO systems employing subcarrier intensity modulation and investigates two common transmit diversity schemes: repetition coding (RC) and orthogonal space-time block coding (OSTBC). A novel power series representation for the probability density function (PDF) of the Double GG distribution is introduced. Using this, average bit-error rate (BER) expressions for both diversity schemes are derived in the form of double power series. The truncated versions of these series allow for efficient and accurate numerical computation of BER.

Additionally, asymptotic BER analyses at high electrical signal-to-noise ratios (SNR) are performed, leading to closed-form expressions for diversity order and coding gain. Simulation results, which align closely with the analytical findings, demonstrate that repetition coding consistently outperforms OSTBC in MIMO FSO systems using subcarrier intensity modulation under Double GG fading conditions. The asymptotic

coding gain of the RC scheme over the OSTBC scheme is analytically quantified for varying degrees of the fading strength [8].

In [33], they study the performance improvement of FSO communication system with spatial diversity techniques employing Hybrid PPM-BPSK-SIM. In diversity-based FSO systems, employing multiple photodetectors proves to be an effective approach for mitigating scintillation effects. In this study, the authors simulate the bit-error rate (BER) performance under varying parameters such as average SNR and link distance across different weather conditions. These simulations, conducted in the MATLAB environment, are validated against theoretical mathematical analyses. The results demonstrate that higher-order SIMO (Single Input Multiple Output) configurations offer enhanced BER performance. Moreover, the hybrid PPM-BPSK-SIM modulation scheme significantly outperforms conventional schemes like PPM and BPSK-SIM, highlighting its potential for improved reliability in FSO communication.

Free Space Optics (FSO) is a wireless communication technology that utilizes light to transmit data through free space. It offers several advantages, including the use of an unlicensed spectrum and the potential for high bandwidth. This paper provides an overview of the key benefits and limitations of FSO systems, highlights the major challenges associated with their deployment, and explores various channel models used to characterize FSO communication under different atmospheric conditions. To mitigate the turbulence in FSO the mitigation techniques like relaying, diversity schemes and adopting different modulation techniques used in different channels are discussed [2].

In recent years a large number of studies have been carried out on free-space optical communication, sometimes also called wireless optical communication with great interest on investigating the effects of the turbulent atmosphere on the communication link that mostly produces irradiance fluctuations in the received signal, greatly reducing

link performance [2][33]. Scintillation, or random fluctuations of the signal-carrying laser beam's irradiance, is the most obvious effect of atmospheric turbulence. However, other perturbations that affect the traveling wavefront include beam wander, which is a continuous random movement of the beam centroid over the receiving aperture plane; angle-of-arrival fluctuations, which are connected to image jitter at the receiver focal plane; and beam spreading, which is spreading beyond the beam radius's pure diffraction limit. In [34], author has carried out numerical simulations of waves traversing a three-dimensional random medium with Gaussian statistics and a power-law spectrum with inner-scale cutoff. The pdf of irradiance is provided by the distributions of irradiance on the final observation screen. In the strong-fluctuation regime, the simulation PDFs for initially plane and initially spherical waves fall somewhere in the middle of a log-normal-convolved-with-exponential distribution and a K distribution. A plot of the PDF of scaled log-normal irradiance has been provided by the author.

In [35], the author presents a fading model that captures the nonlinear characteristics of the propagation medium. This model leads to the derivation of the α-μ distribution, which is essentially a reformulation of the Stacy distribution. Notably, the α-μ distribution encompasses several well-known fading models as special cases, including the Gamma distribution (and its discrete forms such as Erlang and central Chi-squared), Nakagami-m, exponential, Weibull, one-sided Gaussian, and Rayleigh distributions. Based on this generalized fading model, the paper derives closed-form expressions for various higher-order statistical measures. More specifically, level-crossing rate, average fade duration, and joint statistics (joint probability density function, general joint moments, and general correlation coefficient) of correlated α-μ variants are obtained, and they are directly related to the physical fading parameters

In [36], the BER parameter is usually mentioned by FSO manufacturers, but it is not defined what conditions a certain value of BER stands for. This article deals with problems of measuring the BER of free space optical link and with questions how to determine the probability of unavailability of a certain link. The implementation of bit error rate tester with the E1 interface system is presented. BER is one of the most important parameters for analysis of channel in wireless communications.

In [37], the performance of a FSO communication system under strong turbulence regime that follows the K distribution is evaluated. The outage probability and ergodic capacity of a single-input, single-output FSO link are evaluated, along with some useful closed-form channel statistics. It has been shown, as was expected, that the outage probability increases whereas the bandwidth efficiency reduces when the turbulence gets stronger.

Turbulence-induced fading is a major impairment impacting the performance of free-space optical (FSO) communication systems. In this work, the contributors analyze the performance of FSO systems also referred to as wireless optical communication systems—under log-normal and Gamma-Gamma fading models, which effectively represent atmospheric turbulence due to their strong alignment with experimental data. The study derives closed-form expressions for key performance metrics, including the average (ergodic) capacity and outage probability, for both channel models. Additionally, the authors investigate the influence of various factors—such as atmospheric conditions, link distance, and receiver aperture diameter—on overall system performance. The derived analytical expressions are verified by various numerical examples and can be used as an alternative to time-consuming Monte-Carlo simulations [38].

In [39], considering the $\alpha-\mu$ channel fading model and evaluating the MGF for the probability density function characterizing this new channel model. The bit error rate

for various coherent modulation strategies over this generalized fading channel is evaluated using the derived MGF expression. For this channel model, there is also a derived expression for the outage probability. The well-known fading channel distributions in the literature, such as the Rayleigh, Nakagami-m, and Weibull model, can be reduced to the general closed forms of all derived expressions. In [40], author performs the experimental research of the atmosphere impact on FSO link attenuation is studied. Experiment is performed on a mountain observatory Milesovka of severe weather conditions. The empirical relationships on 830 nm only between FSO attenuation on one hand and atmospheric visibility V or wind turbulent energy E_T on the other hand are presented and discussed.

In [41], there's study on the performance of free space optical links with fading statistics modelled by the negative exponential distribution which describes channels under strong atmospheric turbulence conditions. In the course of the evaluation of the outage probability as well as the outage and average capacity, the analysis is carried out on the availability and the bounds of the practical channel capacity for links with fast and slow fading statistics, line-of-sight architecture, and intensity modulation with direct detection. In addition, an estimate is made of the average error probability for on-off keying scenarios. Extract closed-form mathematical expressions for practically valuing the performance of the link for these very significant magnitudes. The Exponentiated Weibull (EW) distribution is an innovative approach to modelling the fading channel in free-space optical links that was recently proposed. In the absence of aperture averaging, it has been proposed that the EW distribution can represent the probability density function (PDF) of the irradiance in weak to strong conditions.

In [42], author has carried out an analysis of probability of fade and bit error-rate (BER) performance using simulation results and experimental data. New expressions are

derived from the BER analysis, which presumes intensity modulation and direct detection with on-off keying. The statistics of the EW fading channel model are used to model the data, and the results are compared to the Gamma-Gamma and Lognormal distributions, which are currently the models that are most commonly accepted. The suggested EW model is demonstrated to be valid under all of the validated conditions and even to perform better than the GG and LN distributions, which are only valid in certain situations.

In [43], derivation for mathematical expressions for the evaluation of the average (ergodic) capacity of free-space optical (FSO) communication systems, atmospheric turbulence conditions are modelled using the I-K distribution.

In [44], author has given a detailed study for FSO link based on vendor's specifications is presented. Analytical analysis and link investigation concluded that, NRZ line code with 1550 nm operating wavelength utilizing APD receiver in different weather conditions achieves a remarkable performance in order to keep an acceptable received signal power and BER levels. Pointing error effect on the performance of the FSO link is a critical aspect especially in deteriorating weather conditions. Pointing error angles in the range of micro radians could lead to a link failure.

In [45], author discussed the performance analysis of FSO communication link in weak atmospheric turbulence has been analyzed for different atmospheric transmission windows using OOK modulation. Bit error rate was used as the performance metric in the analysis.

In [46], author have designed a 2.5 Gbit/s FSO system and presented analysis of 2.5 Gbit/s FSO system with different weather condition by distance of 9 km. From the result, it is evident that the transmission range and Q factor will decrease as they transition

from clear weather to heavy fog. It presented an FSO system whose maximum transmission range is 9 km at attenuation 1 dB/km which is clear weather conditions.

In [47], author evaluates the bit error rate performance of the FSO system; to design a high-performance communication link for the atmospheric FSO channel, it is of great importance to characterize the channel with proper model. The performance of high-speed, high-efficiency FSO communication systems is often constrained by factors such as scintillation and atmospheric turbulence. Incorporating Orthogonal Frequency Division Multiplexing (OFDM) into FSO systems enhances their resilience to frequency-selective fading, narrowband interference, and improves overall spectral efficiency. This study evaluates the performance of various modulation schemes—Binary Phase Shift Keying (BPSK), Quadrature Phase Shift Keying (QPSK), and 8-PSK—over Lognormal and Negative Exponential turbulence channel models. A comparative analysis of Bit Error Rate (BER) versus Signal-to-Noise Ratio (SNR) is presented, offering valuable insights into system performance across different modulation techniques and channel conditions.

In [48], the mathematical integral calculus considering all integrals from simpler ones to complex ones are explained and formulas have been provided in a systematic manner with proper explanation.

In [49], the focus is on outdoor terrestrial OWC links which operate in near IR band. In the literature, these are frequently referred to as FSO communication. Free Space Optical (FSO) systems are employed for high-rate communication over distances of several kilometers between fixed points. Compared to radio frequency (RF) links, FSO offers significantly higher optical bandwidth, enabling much greater data rates. These systems are ideal for applications such as metropolitan area network (MAN) extension, LAN-to-LAN connectivity, fiber backup, wireless cellular network backhaul, disaster recovery, high-definition television and medical image/video transmission, wireless video

surveillance, and quantum key distribution, including others. A current survey of FSO communication systems is presented in this paper. The transmitter/receiver structures and FSO channel models are discussed in the first section. The second section discusses the algorithmic level system design research activities and information theoretical limits of FSO channels.

In [50], the transmission in FSO is dependent on the medium because the presence of foreign elements like rain, fog, and haze, physical obstruction, scattering, and atmospheric turbulence are some of these factors. The paper discusses multiple investigations into weather phenomena and the approaches adopted to mitigate their influence.

In [51], author embodies the H-transform theory into a unifying framework for modelling and analysis in wireless communication. The authors develop a unifying H-transform analysis for the amount of fading, error probability, channel capacity, and error exponent in wireless communication using the new systematic language of transcendental H functions. Author then proposes a new methodology for modelling and analysis in wireless communication is developed, which resorts to the H-transform theory. Author then put forth two classes of fading models—namely, H-fading and degree-2 irregular H fading—to account for (i)composite effects of multipath fading and shadowing; and (ii) specular or inhomogeneous radio propagation, respectively. These H-modelling subsumes most of known fading models and enables more importantly the unified analysis for the error probability, channel capacity, and error exponent in terms of H-transforms. In a nutshell, H-transform framework provides a very general way applicable to the accurate channel modelling and unified analysis for emerging wireless applications.

In [52], Outdoor FSO communication systems are sensitive to atmospheric impairments, such as turbulence and fog, in addition to being subject to pointing errors.

Fog presents a significant challenge for FSO communication systems, causing attenuation that can range from a few decibels to several hundred decibels per kilometer. Additionally, pointing errors further degrade link performance by misaligning the optical beam and introducing signal fading. In this study, the author analyzes the performance of FSO systems under foggy conditions and pointing errors, focusing on outage probability as the primary performance metric. The paper also investigates the effectiveness of various mitigation strategies—such as multi-hop relaying, transmit laser selection, and hybrid RF/FSO integration—in enhancing system reliability.

Closed-form expressions for outage probability are derived, and a series of practical numerical examples are provided to illustrate and validate the findings. Outcomes indicate that FSO system performance is significantly bounded, especially in wireless microcell environments with a minimum cell radius of 500 meters. Performance deterioration is further exacerbated by the presence of pointing errors. While increasing transmit power offers some improvement under light to moderate fog, it has minimal effect in dense fog conditions. The study concludes that implementing appropriate mitigation techniques is essential for extending communication range and reducing outage probability in fog-affected scenarios.

In [53], FSO is a wireless communication technology which uses light to transmit the data in free space. Higher bandwidth and unlicensed spectrum are two of FSO's advantages. The author discusses the advantages and disadvantages of the FSO system, its difficulties, and various channel models in this paper. Relaying, diversity schemes, and adopting various modulation techniques used in various channels are discussed and their performance is compared as means of mitigating the turbulence in FSO.

In paper [54], a detailed study of performance analysis of outage probability, average BER and ergodic capacity has been shown. The imprecise channel model is

treated as the superposition of exact channel gain and a Gaussian random variable, and atmospheric turbulence and pointing errors are taken into account when modelling the exact FSO links as a Gamma–Gamma fading channel. Expressions for the outage probability, average bit error probability (BEP), and ergodic capacity are derived in terms of Meijer's G-functions, based on the probability density function (PDF), cumulative distribution function (CDF), and the nth moment of the imprecise channel gain. Analytical and numerical findings are presented. Communication performance deteriorates in the imprecise channel model, according to the simulation results, but approaches exact performance curves as the channel model becomes more accurate.

In [55], there is detailed discussion about outdoor channel modelling i.e about atmospheric channel which is a very complex and dynamic environment that can affect the characteristics of the propagating optical beam (laser in most cases), thus resulting in optical losses and turbulence-induced amplitude and phase fluctuation The properties of the atmospheric channel is random in nature; therefore its effects can be characterized by statistical means there are a number of models in the literature to characterize the statistical nature of the atmospheric channel; these will be discussed in this section. One can estimate the received optical irradiance at the receiver based on the type of model and its accuracy.

In [56], it is observed that besides providing various advantages FSO suffers from a lot of impairments out of which atmospheric turbulence is the major one. There are many techniques used to enhance the system performance. Depending on the turbulence conditions researchers developed various channel models such as log-normal model is used for weak to moderate turbulence conditions, gamma–gamma is used for moderate to strong fluctuations, K distribution is used only for strong atmospheric turbulences.

Gamma–Gamma model is best suitable as it works under all kinds of atmospheric conditions.

In [57], the authors have presented a novel analytical expression for the bit error rate under OOK modulation for Free Space Optical Communication using α−μ distribution. Numerical comparison between the PDF, CDF and BER using α−μ and Gamma-Gamma distribution has been performed. The relative error between PDF and CDF of Gamma Gamma and α−μ demonstrates the viability of α−μ as alternative to Gamma-Gamma distribution.

In [58], polar codes are employed in a MIMO FSO communication system to mitigate turbulence induced fading. The spatially correlated fading situation is considered in a polar-coded MIMO FSO system. The ergodic capacity of the MIMO FSO channel is calculated from the perspective of information theory to confirm the superiority of the polar codes in a MIMO FSO system.

However, the uncertainty in the atmospheric channel creates various challenges for the FSO systems. One of the main issues arises from the presence of the atmospheric turbulence, which creates fluctuation in the transmitted optical signals. There are various literatures, having different channel distributions to model the atmospheric channel and having different modulation techniques to improve the system performance.

The bit-error-rate (BER) performance of free-space optical (FSO) communication systems is improved by employing binary phase-shift keying subcarrier intensity modulation (BPSK-SIM), an innovative hybrid modulation scheme called PPM-MSK-SIM is proposed, which is based on pulse position modulation (PPM) and minimum shift keying (MSK) subcarrier intensity modulation [9]. PPM-MSK-SIM's BER performance for an FSO system in log-normal turbulence channels with avalanche photodiode detection is then thoroughly examined. The results of the numerical simulation in [9]

show that PPM-MSK-SIM has the advantages of improving the BER performance compared with BPSK-SIM and PPM.

2.3 LITERATURE ON FSO COMMUNICATION SYSTEM INCORPORATING DIVERSITY TECHNIQUES

The performance improvement of free space optical (FSO) communication system with spatial diversity techniques employing hybrid pulse position modulation binary phase shift keying-subcarrier intensity modulation (PPM-BPSK-SIM) is studied in [59]. A good way to get around scintillation in diversity-based FSO systems is to use multiple photodetectors. Simulated weather conditions also affect the bit error rate (BER) in relation to various parameters like average SNR and link distance. The simulation results are verified in Matlab environment with the mathematical analysis [59]. The hybrid PPM-BPSK-SIM modulation scheme in FSO communication systems employs spatial diversity techniques like EGC and MRC. The study demonstrates that the BER performance of the hybrid PPM-BPSK-SIM modulation is significantly improved by approximately 6.5 dB in comparison to that of the BPSK-SIM method. It is observed from the simulation result that unlike single input single output (SISO) system, an increase in the number receivers for single input multiple output (SIMO) system results in better system performance as N= 1 to N= 4 in clear air condition the BER improvement is about 4.7 dB and in light fog case it is about 13.3 dB in [59]. However, the bit error rate decreases in various weather conditions when the attenuation level increases, from clear air to light fog, but the BER performance is improved when hybrid PPM BPSK- SIM with higher order diversity is used. The simulation reveals that the rate of BER change from clear air to light fog is significantly lower in higher diversity order N= 4 (1 x 4 SIMO) than in N= 1 (1 x 1 SISO).

Thus, hybrid PPMBPSKSIM modulation scheme with spatial diversity is a better approach for mitigation of scintillation up to some extent [59].

The BER under DPSK modulation and ergodic capacity of FSO rely system including dual hop RF FSO and FSO-FSO links is evaluated [60]. To demonstrate diversity enhancement's impact on system performance and capacity, the authors investigate the dual hop variable gain FSO relay and dual branch FSO selection combining that operate on such channels with the impact of pointing errors. First, they use the H-function and the G-function to describe the statistical properties of the maximum and minimum of double generalized gamma random variables when pointing errors are taken into account. In particular, they find the cumulative distribution function (CDF), the probability density function (PDF), the moment generating function (MGF), and the moments in closed-form [60].

The BER performance of FSO links with spatial diversity over atmospheric turbulence channels described by the Double GG distribution is analyzed and obtained an efficient and unified closed-form expression for the BER of SIMO FSO systems with OC receiver which generalizes existing results as special cases [61]. On the basis of numerical calculations of the integral expressions, the BER performance of MISO and MIMO systems is presented. The numerical results have shown that spatial diversity schemes can significantly enhance system performance and outperform SISO systems in terms of performance. The error rate performance of single-input multiple-output (SIMO), multiple-input single-output (MISO), and multiple-input multiple-output (MIMO) FSO systems employing intensity modulation/direct detection (IM/DD) with on-off keying (OOK) is analyzed over independently and identically distributed (i.i.d.) turbulence channels modeled by the Double Generalized Gamma (Double GG) distribution [61].

Optical communications using subcarrier phase shift keying (PSK) intensity modulation through atmospheric turbulence channels is studied in [62]. The bit error rate (BER) is derived employing either OOK or subcarrier PSK intensity modulation. It is shown that signal scintillation caused by atmospheric turbulence severely degrades the performance of optical communication systems. Increasing the detector collection aperture will not further reduce the scintillation level once it reaches a certain size.

It is shown that subcarrier phase-shift keying (PSK) intensity modulation is superior to OOK in the presence of atmospheric turbulence. Analysis of BER for optical communication systems using OOK and disadvantage is identified. Analysis of the BER for optical communication systems employing subcarrier PSK intensity modulation [58]. Simulation results are presented for optical communications systems employing convolutional codes with either OOK or subcarrier PSK intensity modulation. For optical communication through channels of atmospheric turbulence, the use of convolutional codes is discussed.

The effect of multi-input multi-output (MIMO) spatial diversity schemes when used in a free space optical (FSO) communication link in the presence of turbulence and varied weather conditions such as very clear air, drizzle, haze, fog is studied in [63]. Outage probability Pout and bit error rate (BER) are used to assess performance. It demonstrates that MIMO schemes result in a decrease in the BER and Pout, which is more pronounced at low signal-to-noise ratios in conditions of very clear air and clear air as opposed to haze and fog. The performance of FSO link with MIMO schemes is compared with a FSO link using aperture averaging [63]. The aperture averaging method does not provide the same level of performance as higher-order MIMO schemes because of restrictions placed on the receiver aperture diameter.

Free Space Optical (FSO) communication is evaluated in indoor and outdoor experimental environments for other communication applications, which opens the study of environmental effects in FSO communications, these effects represent the nature environments around us such as rain and fog, which are termed by mathematical distribution models such as lognormal and Gamma-gamma distribution. One of the major solutions that proposed to reduce these effects and enhance the received signal is the use of Multiple Input Multiple Output MIMO diversity techniques in FSO. A Multi-input multi-output free space optical channel model is impaired with atmospheric turbulence, gamma-gamma distribution and the diversity gain only on the atmospheric parameters; also, it is independent from the number of transceivers and atmospheric fading parameters [60]. The bit error rate for different diversity combining techniques is analysed and it is found that the system performance is increased. Another different procedure is utilized to examine the diversity combining techniques to minimize the fading and also as a solution for conflicting turbulence-induced fading over FSO links [64].

Atmospheric turbulence causes random fluctuations in transmitting laser beam which gives rise to scintillation. Compared to the large data rates, scintillation process is slow in optical transmission. In order to mitigate this harmful effect of atmospheric turbulence and beam wander, multiple input and multiple output (MIMO) is used. A multiple input multiple output (MIMO) channel is created by using multiple lasers and multiple output apertures to reduce scintillation. In MIMO system different diversity combining techniques are used. A model for FSO-MIMO channels impaired in the presence of atmospheric fading, the diversity gain depends only on the atmospheric parameters and is independent of both the number of transceivers and atmospheric fading parameters [65]. The system's performance is improved by analyzing the outage probability and bit error rate for various diversity combining methods. The results confirm

that the performance of the threshold combining is better when compared with the EGC, SC and MRC techniques [66]. By increasing the number of transmitter antennas and receiver antennas, diversity gain is increased and the performance of the system is increased. The system's performance is improved by analyzing the outage probability and bit error rate for various diversity combining methods.

An adaptive subcarrier phase shift keying (PSK) intensity modulation for free space optical (FSO) communication systems operating over Malaga atmospheric turbulence channel, which is a generalized statistical model proposed for FSO communications is studied in [67]. By utilizing adaptively the modulation order of subcarrier PSK, the proposed transmission method makes efficient use of the FSO channel capacity in accordance with the instantaneous state of turbulence-induced irradiance fluctuation and a target bit error rate (BER). Moreover, a closed-form expressions for the average BER of non-adaptive strategy, the achievable spectral efficiency and the average

BER of proposed adaptive subcarrier PSK FSO system are derived in terms of the Meijer's *G*-function [68]. The proposed scheme offers an achievable spectral efficiency gain without increasing transmitted average optical power or compromising BER requirements, according to numerical results.

Bridging the so-called "last mile" in communication networks has revived keen interest in free-Space Optics (FSO), also known as fibre-free or fibreless optics, which is a technology that transports data via laser technology. It is a line-of-sight technology that currently enables optical transmission up to 2.5 Gbps of data, voice and video through the air at long distances (4km), allowing optical connectivity without deploying fiber optic cable or securing spectrum licenses. It is moving closer to being a realistic alternative to laying fiber in access networks. An introduction to FSO and the current state of its

technology is presented in [69]. The growth of communications networks has accelerated last-mile access needs for high-speed links. FSO is a viable choice for connecting the LAN, WAN, and MAN; carrying voice, video and data at the speed of light. However, due to lower atmospheric transmission losses and increased system reliability, FSO links in the mid-infrared spectrum appear to be preferable, particularly in poor weather with low visibility. While fiber-optic communication has gained acceptance in the telecommunications industry, FSO communication is still a relatively new entrant [69]. Its apprehension has not been universal; its development activity is concentrated in the US. High throughput, solid security, and low cost are its primary advantages. With current availability of up to 1.25 Gbps, throughputs of hundreds of Gbps are possible in the future. Free space optics is a technology that is poised for exponential growth in the coming years [63].

The case of long-range FSO links with APD-based receivers is considered and optimal signal demodulation for the case of NRZ OOK signalling is investigated, in the presence of signal-dependent shot noise [64]. For optimal OOK signal demodulation, the receiver requires the knowledge of the instantaneous channel attenuation coefficient. Due to the computational complexity of the estimators, the authors proposed an ML channel estimator based on the iterative EM algorithm. In [70], the performance of the proposed EM-based estimator through numerical simulations is investigated, which alleviated the advantage of this estimator compared to the three other methods. The relatively low computational complexity and the low estimation delay of the proposed method and the fact that it does not rely on the transmission of pilot sequences, makes it particularly suitable for implementation in FSO communication links.

Free space optics is replacing radio frequency communication because of its high speed, large bandwidth, maximum performance, minimum error and efficient

communication. All these is achieved by using free space optical communication system. Because FSO system is license free and cost effective, therefore, it has become need of the hour. Turbulence manifests in increased Bit Error Rate (BER) leading to degradation in the link performance. In [71], a comprehensive survey of FSO communication system with main focus on the study of different turbulent conditions of atmosphere is done. Moreover, work done by different researchers in the field of FSO system using different modulation techniques in various turbulence models is discussed. Also, methods for performance enhancement of FSO link are described in the work.

When propagated over a clear atmosphere, free-space optical communications (FSO) experience irradiance fluctuations brought on by minute but sporadic changes in atmospheric temperature. As a result, performance is harmed and the signal-to-noise ratio (SNR) is reduced. The error performance of the FSO using a subcarrier intensity modulation (SIM) based on a binary phase shift keying (BPSK) scheme in a clear but turbulent atmosphere is presented [72]. The probability density function (pdf) of the received irradiance after traversing the atmosphere is modelled using the gamma-gamma distribution in order to evaluate the system error performance in turbulence regimes ranging from weak to strong. On the other hand, the negative exponential distribution is used to model turbulence in the saturation region and beyond. The effect of turbulence induced irradiance fluctuation is mitigated using spatial diversity at the receiver [72].

The error rate performance of binary phase shift keying based subcarrier intensity modulated free space optical (SIM–FSO) communication system over gamma–gamma channel with pointing errors is investigated [73]. For the average bit error rate of a single-input multiple-output FSO (SIMO–FSO) system using a variety of combining schemes, novel closed-form analytical expressions are derived. In [73], it is observed that SC provides the best BER performance compared to other considered combining schemes.

The study also demonstrates that increasing the number of receiving apertures significantly improves BER performance. Additionally, simulations of BER for SIMO systems with up to seven receiver apertures are presented. Using SIMO with selection combining (SC), a BER of 10^{-5} is achieved at an SNR of 30 dB, indicating enhanced performance.

2.4 LITERATURE ON MIXED RF-FSO COMMUNICATION SYSTEM

The performance of mixed RF–FSO system with hybrid PPM–BPSK–SIM and fixed-gain relay in [68]. Both the FSO link and the RF link are subjected to Rayleigh distribution, and Gamma–Gamma distribution in multiple ways. The hybrid RF–FSO system's unconditional BER expression is derived. Influences of the FSO link, such as atmospheric turbulence and pointing error, are investigated using the above mathematical representation.

In [74], the result of this study shows that the BER performance of the hybrid system could be improved when it adopts hybrid PPM–BPSK–SIM, and the specific improvement effect has a lot to do with the length of symbol, L [74]. As L increases, the hybrid system's BER decreases, and when L is greater than eight, the hybrid system performs better than BPSK. The mixed RF–FSO system's performance is noticeably and steadily improved by the hybrid PPM–BPSK–SIM even under severe pointing error conditions and strong turbulence. The FSO channel's turbulence effect and pointing error have an impact on the outage probability as well as the average capacity of the channel.

This paper proposes the Hybrid PPM-BPSK modulation scheme [75]. The simulation results for the PPM-BPSK modulation scheme's bit error rate (BER) performance in the lognormal atmospheric channel are presented for a variety of turbulence variances. In this work [76], a new hybrid PPM-BPSK modulation scheme is proposed and used simulation to investigate its efficiency and compare results with PPM

and BPSK SIM techniques. Additionally, experimental performance findings are also provided for the 4PPM and BPSK (SIM) techniques. The output is investigated and compared for N = 1 of PPM-BPSK, 4PPM, and BPSK (SIM). The results showed that PPM BPSK provided comparable performance to 2-PPM, superior performance compared to BPSK-SIM while providing the same bandwidth but less than 4-PPM performance for turbulence level.

The selection combining (SC), the equal gain combining (EGC), and the maximum ratio combining (MRC) are suggested in FSO systems [77]. MRC provides the optimum performance preceded, respectively, by EGC and SC. Implementation of MRC however involves a highly complex program and hardware. Therefore, this paper considers only the EGC. In this paper [77], on 2-PPM BPSK-SIM, spatial diversity is investigated with EGC schemes. The empirical BER using the linear EGC is measured, compared to BPSK-SIM using a lognormal and negative exponential model. The results of the simulation showed an increase in SNR Increases with turbulent intensity. The income from SNR also increases with an increase in receiver numbers. However, the number of receivers beyond the SNR gain is not significant.

In paper [78], the average BER performance of hybrid SIM with LPPM and MSK over double GG distribution is analysed for received average irradiance. The performance is analysed for different values of L in LPPM-MSK-SIM i.e., for L=2, 4, and 8, and for average irradiance range between -12bBm to 4dBm. It is observed that the BER get reduced for the lower average length L of PPM symbol [78]. Hybrid LPPM-MSK-SIM modulation technique over double GG distribution performed better for weak, moderate and strong turbulence condition.

According to [79], the performance parameters are analyzed for the system model which follows the Nakagami-m & Double Generalized Gamma fading distribution since,

it comes up with the maximum suitability and closeness with our proposed model. They use PDF (Probability Density Function) and derive CDF (Cumulative Distribution Function) from its PDF and also derive the novel expression, also analyzed is the system performance and graph using MATLAB software and validated the obtained results through Monte Carlo simulation. The system performance is calculated through Outage Probability, Outage Capacity, BER in the presence of pointing errors with LOS (Line of sight) signaling mechanism.

In [80], the paper discusses the performance of FSO/RF which is a two-way mixed- relaying system is investigated, and Co-Channel Interference are considered. Nakagami-m and Gamma Gamma distribution over various turbulence condition like Weak, Strong and Moderate with pointing errors. Closed novel expressions for OP (Outage Probability) and BER are found and simulated for RF and FSO. Compare and examine the impact of different parameters on system performance. The outcome shows that increasing the power and the number of interferences reduces system performance, and increasing the interference powers makes the effect of the number of interferences more severe. This means that the RF link will dominate and its performance is limited by the same channel interference. Observation says better reflect practical scenes; Important factor that cannot be ignored in the system model are Co-Channel Interference.

In [81], the paper illustrates the performance of the dual-hop FSO/RF system. The FSO link operates under Gamma-Gamma distribution including the pointing errors. The RF link operates under α-F distribution fading. Various performance metrics are evaluated using Fox H-functions, like the BER, OP, Channel capacity, and ergodic capacity. The derived expressions are validated using Monte Carlo simulation. Diversity orders for end-to-end transmissions are related to the nonlinear parameter of the propagation modes, the number of multipath clusters, the detection method, and the turbulence conditions.

Expectedly severe atmospheric turbulence deteriorates the system performance along with non-linearity and shadowing parameters.

In [82], the performance of a transferring framework comprising of FSO which is multi-jump, where hidden connections are accepted by the Double Generalized Gamma technique including some pointing errors. Inferred articulations for the BER (Bit Error Rate) and Outage Probability and also consider for fixed-gain and CSI-helped, relaying and also analyzed the asymptotic exhibition to get variety orders. See that variety gains are an element of turbulence boundaries, recognition strategy and pointing errors of all things are considered. Accepting a steady normal SNR for the principal FSO connection, where the SNR of any remaining connections increments endlessly, a diversity request of zero is acquired (i.e., a error floor occurs) for both fixed gain retransmission and CSI - helped handing-off.

In [83], the authors analyzed the ergodic capacity and the ABER, dependence on atmospheric turbulence conditions, correlation coefficient, pointing errors strength, average SNR per RF hop, electrical SNR per FSO hop and different PRS, structures. High upsides of the coefficient of correlation (implying that the obsolete serial communications interface and actual serial communications interface for the SR channel at the time of transmission of signal are more correlated) keeps an eye on progress of the ABER (Bit error Rate). The slope of the correlation coefficient (CC) and ergodic capacity curve is around the same in all turbulence conditions like weak, Strong and Moderate. The more grounded is the impact of number of transfers, the higher is the value of correlation coefficient on the ergodic capacity.

In [84] literature paper, the authors discuss the OP and average Bit Error rate expressions with and without the pointing errors by deriving analytical expressions of CDF and PDF functions. RF and FSO link operate under Nakagami-m and gammagamma

fading. The paper also firmly addresses about adding of RF link which can effectively increase the performance of the given FSO model. The adaptive combining technique provides better performance in both the outage probability performance metrics. To get the best outage performance, the switching threshold should be greater than or significantly equal to the outage threshold because the OP is found out to be fixed value and minimum in the range of the switching value of threshold.

In [85], the Mixture Gamma (MG) distribution is considered which is better for composite channels and for small-scale fading. The Mixture Gamma gives a good accurate representation of the channels like composite fading which is not provided by the K and other models. Because of its high accuracy and mathematically tractable form, the Mixture Gamma distribution so allows fast evaluation of the performance metrics such as Outage capacity, channel capacity etc.

In [86], FSO frameworks apply to multiplex Radio Frequency signals from various clients and is utilized to send with the high data transfer capacity. In this type of systems, the SR link (Source to Relay link) and RD link (Relay to Destination link) assumed Nakagami-m fading and M-distribution fading respectively. Novel closed- form equations of CDF for the Channel, ergodic channel capacity and the outage probability is derived for the system with IM/DD or heterodyne receiver. M-distribution is used as a generalized channel model, from which one can appropriately derive the presentation of elective free space turbulence models as special cases. The final results showed that heterodyne detection performed better than IM/DD, so FSO channel model.

In [87], they consider fixed gain relaying technique in mixed FSO (Free Space Optical Communication). This paper considers that η-μ distribution on SR (RF link) and M- distribution on RD (FSO link). For numerical analysis first derive novel form of CDF (Cumulative density function) and also included the effect of pointing error after that use

those expressions of outage probability, ergodic capacity and bit error rate performance. In this work also see effect of variable gain relaying and multiuser diversity. In this get more insight of outage probability under asymptotic. After analyze the result it is clearly shown that performance of the system depends on the value of g. If there is no pointing error then the performance of the system is increased by the using multiuser diversity technique.

The paper [88] prescribes that RF and FSO signal power have to increase at the similar rate because a small increase in any of them with greater than other yields to a zero gain in performance. It also revealed that implementing higher number of relay circuits improves the performance. The paper has worked upon the analysis of the behavior of the dual-hop RF-FSO transmission systems. The FSO part is subjected with the Double Generalized Gamma (DGG) fading under the effect of nonzero boresight error. The Cumulative and Probability density functions, MGF are also obtained as statistics for the SNR values. The closed-form mathematical equations for the performance indexes like the OP, ABER and SE are also obtained. Detection methods like the IM/DD and heterodyne detection methods are used to examine the system model. This paper concluded that high number of relays can't operate in low SNR values.

A dual-hop multi-input serial output (MISO) mixed radio frequency and serial input multi output (SIMO) FSO RF FSO structure model is studied here. During the first jump the Multi input Single Output (MISO) RF approach is used which operates under the Rayleigh fading. The paper also considers ASTBC and TAS which are different schemes used from the source to relay part. Considered is the Amplitude and Forward fixed gain and variable gain method. The Free Space Optical part in the second hop suffers the gamma- gamma fading using the SIMO technique which improves the system model execution of the FSO connect at very convenient cost. The paper contains the analytical

articulations of different execution parameters like OP and average SER. EMGBF is used to determine the logical articulations of Ergodic capacity along with outage capacity. The paper finds that ASTBC plan has the preferable exhibition over the TAS scheme. It finds that the power of the ASTBC articulation is twice of the TAS articulation for specific bit encountered [89].

In this particular literature, a dual-hop model is assumed which further leads to the derivation of Moment Generating Function (MGF)which operates under Direct and forward link. For high values of SNR an accurate model of MGF is also derived. The scientific articulations of the Ergodic/Average Capacity and Bit Error Rate also acquired. The mathematical quantities thus obtained conveyed about the average SNR on the system evaluation of a dual-hop system model. Numerical Articulations for the OP is also derived. Paper also gives a likewise short examination of the conduct of the FSO link in a dual jump RF-FSO framework operating under κ-μ/Inverse Gaussian distribution respectively [90].

The paper [91] discusses the generalized numerical articulations for the BER of the DPSK FSO framework model involving or not involving of considering the two branch TLS variety plots which work over the double GG disturbance channel is studied. As the double Generalized Gamma distribution is assumed to be a generic model this means that the analyzed scientific articulations is thought of as a generic expression and thus are utilized proficiently for successfully analyzing overall system model execution of the DPSK FSO system model utilizing the TLS variety plot in diverse disturbance conditions parameters.

In [92], an original double jump remote electrical cable blended correspondence system utilizing Direct and Forward transfer instrument mechanism and further the pdf articulation for the same start to finish Signal to Noise Ratio of the framework model is

gotten. Accordingly, the articulation for the scientific normal BER for the framework viable. Further, the authors get careful shut structure articulation for the blackout likelihood and a surmised articulation of the normal channel capacity of the framework. It is gathered from the mathematical plots that the appearance likelihood of the hasty clamour and the indiscreet commotion record boundary of the added substance commotion on the PLC link adversely impact the conduct of the proposed agreeable correspondence framework. Helpful experiences into the framework execution are ascertained through the patterns acquired in different mathematical plots.

In [93], the numerical articulations for the Probability Density Function and Cumulative Distribution Function of the dual-hop mixed Direct and Forward relaying system. In the thought about framework, the RF linkage operates under the κ−μ fading approximation and the FSO link goes through though the EW disturbance distribution. The Outage Probability is determined as far as Meijer G work dependent on the CDF. Also, the ABER and EC are also acquired by the method of generalized Gauss-Laguerre integral. The precision of the determined insightful articulations is additionally confirmed with the reenactment results. This writing additionally recommends that any progressions in the boundary of the RF connection can impact the general framework execution. It is also inferred that grave disturbance conditions can debilitate the impact of any progressions in the RF interface boundaries. It is also seen that the FSO (Free Space Optical) interface rules the presentation than the RF part, of a double bounce blended RF/FSO framework model under moderate to solid choppiness condition. Lately, Performance parameters like the OP, ABER and EC are successfully analyzed for various disturbance conditions with the “aperture averaging technology”. Severe turbulence drastically reduces the system performance, but the aperture averaging technology

fundamentally rises the performance of the double jump RF/FSO framework model by restraining the blurring brought about by the disturbance.

In [94], the authors illustrate about the numerical articulations that are inferred for CDF, PDF, MGF of a dual-hop Radio Frequency/Free Space Optics channel model with the pointing errors. Those mathematical expressions are used to novel form derive the analytical novel closed form for the performance matrices like outage probability, Average Bit Error Rate of the system model for both heterodyne detection and IM/DD detection techniques. The RF link is assumed under the Rayleigh fading distribution while the FSO channel is assumed to be operating as Malaga fading distribution. The effects of fading, turbulence, jitter, and pointing error is also completely investigated on the performance parameters of the proposed RF/FSO system. It is inferred that the atmospheric turbulences (weak, moderate, strong) and the pointing errors severely degrade the performance of the proposed dual hop RF/FSO system model. Also derived are the parameters like the diversity order and coding gain which are helpful in better understanding the complex mathematical expressions for the CDF and PDF.

The [95] paper presents the performance parameters like the OP investigation of the various blended Amplitude and Forward relaying RF/FSO framework. In a stark contrast to all the previous system models, this system model works upon the Variable gain AF relays, the selection of the active relay is entirely based on the PRS system mechanism. Assumes the RF link to experience the Rayleigh fading environment used over the fast- fading statistics. This means the Outdated Channel state Information mechanism of the RF channel is employed for the PRS system mechanism and also for the transfer gain identification. For the FSO part, the intensity fluctuations in the dedicated optical signals are assumed to operate under the Malaga distribution environment considering the effects of pointing errors. Based on these preconditions the

analytical expression for the performance parameters like the outage probability is derived. [96] also provides the approx. high SNR equations are also analyzed. These analytical results are numerically presented and checked through the Monte Carlo simulations method. The system model is thoroughly examined under various channel and system parameters. Outdated CSI used for the relay gain parameter can influence the outage probability performance for the different turbulence parameters in presence of the pointing errors. [96], is expected under hurtful conditions like strong environmental turbulences and severe pointing errors.

In [97], discusses about the performance matrices such as the outage probability (OP), Average Bit Error Rate (ABER), and ergodic capacity for the dual-hop based RF/FSO system model, assumed under the κ-μ and the M-distribution in addition to the pointing errors and different atmospheric turbulences, based upon the AF relaying scheme. The mathematical expressions thus derived are general in nature as they are also valid for various other distributions including the Nakagami-m distribution for RF link and the Gamma-Gamma distribution for the FSO link. [97] presents exact results for some of the at high SNR values and it provides essential information about the behavior of the proposed system in the presence of different channel parameters. Simulation results are presented to validate the derived analytical expressions. In case of severe pointing errors and atmospheric turbulences the system performance is seen to be deteriorating. The additional inference that can also be taken into account in particular is that the average Bit Error Rate with BPSK as the modulation scheme is found to be better than that of the DPSK modulation scheme.

ABER execution of the Direct and Forward dual-hop FSO/RF urban communication system model is briefly calculated in [98]. The RF part is assumed to be working under the RF distribution (Nakagami-m) fading environment and the FSO seems

to operates under the distributed turbulence environment along with the nonzero boresight pointing errors. The approx. closed form equations of the ABER with the modulation scheme as BPSK is derived and validated via the Monte Carlo (MC) simulations to validate the accuracy of the proposed ABER system model. [99], discusses the of the ABER results of the FSO and RF links on the performance of the ABER. For the severe turbulence in the FSO link the ABER will suffer directly by the fading in the RF link. In addition to it, the NBPE and ZBPE in the FSO part will result in heavy performance loss. In order to mitigate these losses, the aperture averaging technique is used to see significant improvement on the ABER performance for the system model with non-zero boresight or zero boresight pointing errors. The proposed dual hop system model in [99] strictly applies to the urban areas.

Dual hop RF / FSO performance consisting of Double Generalized Gamma fading distribution-based system model is concentrated in [100]. Various closed-form mathematical expressions, including the Cumulative Distribution Function (CDF). The corresponding Outage Probability as the measure of the execution for the system framework is also analyzed. It is concluded that at any instant for any threshold as the Average Electrical SNR increases then the performance parameter which in this case is Outage Probability, decreases. And, this same performance parameter (OP) increases when the value of the Average Electrical SNR increases. With these results a particular trend is seen which indicates that as the Average Electrical SNR increases at an even higher rate, then the percentage change in the value of Outage Probability will in fact decrease. It is also inferenced that the increasing fading turbulence from moderate to strong parameters degrades system model performance. This model serves as the basis for the calculation of Other Performance Parameters which include the Average Symbol Error Rate (ASER/ABER), Average capacity and OC.

In [101], the authors studied the performance of a dual-hop RF/FSO consisting of Mixed Weibull and Gamma-Gamma based system model employing CSI-assisted Amplitude & Forward (AF) relaying protocol. End-to-end SNR CDF, PDF, and ASER closed-form terms are derived from both heterodyne and IM / DD detection techniques. The exact observations are also validated and verified using computer-based simulations like Monte Carlo simulation mechanism.

In [102], Dual hop RF / FSO performance consisting of Rayleigh and Double Generalized Gamma fading distribution-based system model is concentrated. Various closed-form mathematical expressions, including the Cumulative Distribution Function (CDF). The corresponding Outage Probability as the measure of the execution for the system framework is also analyzed. It is concluded that at any instant for any threshold as the Average Electrical SNR increases then the performance parameter which in this case is Outage Probability, decreases. And, this same performance parameter (OP) increases when the value of the Average Electrical SNR increases. With these results a particular trend is seen which indicates that as the Average Electrical SNR increases at an even higher rate, then the percentage change in the value of Outage Probability will in fact decrease. It is also inferenced that the increasing fading turbulence from moderate to strong parameters degrades system model performance. This model serves as the basis for the calculation of Other Performance Parameters which include the Average Symbol Error Rate (ASER/ABER), Average capacity and OC.

Starting with the double generalized Gamma (GG) model to describe turbulence induced fading in free-space optical (FSO) systems, in [103], the authors propose a new unified model that accounts for the impact of pointing errors and type of receiver detector. In terms of the Meijer's G-function, unified closed-form expressions for the cumulative distribution function, probability density function, moment generating function, and

moments of the end-to-end signal-to-noise ratio (SNR) of a single link FSO transmission system are provided. Asymmetric RF-FSO dual-hop relay transmission systems with fixed gain relay and a single FSO link operating over double GG fading models are both evaluated using these unified expressions to determine performance metrics like the bit error rate, outage probability, and ergodic capacity. All of the earlier expressions can be expressed in terms of elementary functions by employing an asymptotic expansion of the Meijer's G-function at high SNR.

Composite fading is a phenomenon that arises when shadowing and multipath fading occur simultaneously in wireless channels. The generalized-K model for composite fading was developed through the application of the Nakagami probability density function (PDF) to the simulation of multipath fading and the Gamma PDF to the simulation of shadowing. However, the computational and analytical difficulties associated with the resulting special functions make further derivations using the generalized K PDF quite challenging. The moment matching method is used to investigate how a Gamma PDF can approximate the generalized-K PDF. Subsequently, an adjustable form of the expressions obtained by matching the first two positive moments, to overcome the arising numerical and/or analytical limitations of higher order moment matching, is proposed [104]. For various integer and non-integer values of the multipath fading and shadowing parameters, the optimal values of the adjustment factor are provided. Moreover, the approach introduced in this paper [104] can be used to well-approximate the distribution of the sum of independent generalized-K random variables by a gamma distribution; the need for such results arises in various emerging distributed communication technologies and systems such as coordinated multipoint transmission and reception schemes including distributed antenna systems and cooperative relay networks.

In this letter [105], the secrecy performance of the classic Wyner's wiretap model over the generalized Gamma fading channels is studied. The lower bound for secure outage probability and closed-form expressions for the probability of strictly positive secrecy capacity are derived. The derived analysis is confirmed by Monte-Carlo simulations.

In this paper [106], the performance of an optical wireless communication system is investigated and reported the achievable BER and average channel capacity using different modulation schemes such as: on-off keying (OOK), quadrature phase shift keying (QPSK) and pulse position modulation (PPM). For the free space optics (FSO) system, a comparative study based on these three schemes has been conducted. The atmospheric channel is modeled with the combined effects of turbulence and pointing errors for weak to strong atmospheric turbulence. Gamma-Gamma (G-G) and lognormal (LN) distribution channel models are used to model the FSO link here. A closed-form mathematical expression for the average channel capacity and bit error rate (BER) for various modulation schemes, such as To evaluate the FSO system's efficiency, OOK, QSPK, and PPM are presented. The Gamma-Gamma and Lognormal distribution channel model's simulated BER and channel capacity for various modulation techniques are presented in this paper.

In [107], the authors investigate the performance of hybrid L-ary quadrature amplitude modulation-multi-pulse pulse-position modulation (LQAM-MPPM) techniques over exponentiated Weibull (EW) fading free-space optical (FSO) channel, considering both weather and pointing-error effects. Taking into account the effects of fog, beam divergence, and pointing error, upper bound and approximate-tight upper bound expressions for the bit-error rate (BER) of LQAM-MPPM techniques over EW FSO channels are derived. The LQAM-MPPM/FSO system's transmitter and receiver

setup block diagrams are described and illustrated. The numerical evaluation of the BER expressions reveals that the LQAM-MPPM technique performs better than conventional LQAM and MPPM schemes under various weather conditions and fading levels. In addition, the effect of the modulation index is investigated, and it was discovered that a modulation index greater than 0.4 is necessary for system performance optimization.

In recent years, free-space optical (FSO) communication has received a lot of attention as a low-cost, license-free, and wide-bandwidth access method for applications with high data rates. However, the atmospheric conditions that cause turbulence-induced fading severely affect the performance of FSO communication. To take advantage of the advantages of spatial diversity and mitigate turbulence fading, multiple laser transmitters and/or receivers can be positioned at both ends. For channels with strong turbulence, where a single-input, single-output (SISO) link performs very poorly, spatial diversity is especially important. In outdoor FSO systems, atmospheric-induced strong turbulence fading can be modelled as a multiplicative random process that follows the K distribution.

In this paper [108], the authors investigate the error rate performance of FSO systems for K distributed atmospheric turbulence channels and potential advantages of spatial diversity deployments at the transmitter and/or receiver. The results show that using multiple transmitters and receivers in FSO channels increases diversity significantly. In addition, effective approximated closed-form expressions for the average bit-error rate (BER) of FSO systems with multiple inputs and outputs (MISO) and single inputs and outputs (SIMO) are provided by the authors.

This paper [109] investigates the bit error rate (BER) performance of spatial diversity free-space optical (FSO) communication systems using on-off keying modulation. This study examines Free Space Optical (FSO) channels characterized by correlated log-normal fading, while also accounting for path loss caused by weather

conditions. The system employs intensity modulation with direct detection (IM/DD). To analyze the joint behaviour of correlated log-normal channels, approximated moment generating functions (MGFs) are utilized. By employing MGF approximations, bit error rate (BER) expressions are derived for repetition codes (RCs) and orthogonal space-time block codes (OSTBCs) operating over correlated log-normal channels. In conditions of correlated channels, the findings demonstrate that RCs perform better than OSTBCs. In addition, the effect of different weather conditions (e.g., haze, rain and fog) on the BER performance of the FSO links are studied. The validity of the proposed mathematical analysis is further supported by the Monte Carlo simulation results.

Due to their compact size, ease of deployment, and use of license-free spectrum, free-space optical (FSO) communication systems are attracting significant research and commercial interest. However, the receiver's signal quality can be significantly distorted due to the atmosphere's time-varying characteristics and variable composition of scatterers and absorbent matter, which is the optical signal's propagation path. Thus, in this work [110], the authors investigate the performance of an FSO link using receivers' spatial diversity scheme and optimal combining reception. On wireless optical links, the performance is evaluated using the average bit error rate metric for some of the most widely used modulation formats, taking atmospheric turbulence, which is modelled using either the gamma-gamma or the negative exponential distribution model, and the pointing errors effect into account. More specifically, for the purpose of estimating the average bit error rate, brand-new closed-form mathematical expressions are derived. These expressions can be easily implemented for wireless optical links. In the final section, the conclusions drawn from the results and the corresponding numerical results are discussed.

Based on the joint probability density function of Malaga atmospheric turbulence and pointing errors, the asymptotic expressions of the average BER for MIMO system

with three combing methods including maximum ratio combining (MRC), equal gain combining (EGC) and select combining (SC) are derived in [110]. When the receiver radius is fixed, the influence of different beam waist radius and jitter deviation on the average BER of the system is analyzed. Meanwhile, the performance of BER and diversity gain of MRC system is better than that of the other two combining methods When the receiving aperture is 4, the diversity gain of MRC can reach 25dB.

Irradiance fluctuations in free space optical (FSO) communication channels are influenced by atmospheric turbulence and pointing errors. To describe the beam's irradiance fluctuations as it moves through a turbulent medium, a new generalized statistical model called Málaga was developed recently. In this paper [111], an approximate finite-series probability density function (PDF) for composite turbulence with pointing errors is verified. Specific closed-form expressions for the average symbol error rate (ASER) and outage probability are derived taking into account multiple pulse-position-modulation (MPPM) with intensity modulation and direct detection. ASER and outage probability over the Málaga channel with pointing errors are also given asymptotic expressions. Last but not least, expressions for ASER and outage probability are derived for each of the three turbulence regimes—strong, moderate, and weak. As a result, simulation results are presented to confirm the proposed expressions' accuracy. At a distance of one kilometer, the findings indicate that the optimal beam divergence angle is 1 mrad for zero-boresight displacement and 2 mrad for nonzero-boresight. Atmospheric turbulence is found to have a greater impact than boresight displacement when the range is increased to 5 km. In addition, the transmit power, normalized boresight, and link distance of the system at the optimized divergence angle are examined.

Unmanned aerial vehicles (UAVs) have recently received a lot of attention due to their potential for recent applications like 6G, the internet of things, and disaster management.

Platforms at low, medium, and high altitudes are becoming increasingly attractive, particularly for inter-UAV communications. UAV communication relies heavily on free space optical (FSO) communication to provide a high data rate, wider bandwidth, and secure transmission. In this paper [112], first time author introduced heterodyne detection (HD) in FSO based inter UAV communication. The proposed system's outage and average bit error rate (BER) performance is compared to that of the existing intensity modulation direct detection (IM/DD). The authors investigated how the proposed system's BER and outage performance were affected by turbulence and pointing errors. The Rytov Variance, field-of-view, Transmitter UAV orientation, Receive UAV orientation, link range, and Beam width are all plotted in the results. The Monte-Carlo simulations confirm the analytical findings.

Line-of-sight free-space optical (FSO) communication uses data to modulate the infrared or visible laser light that travels from the transmitter to the receiver through the air. FSO is widely regarded as a technology for the next generation of high-speed wireless communication because it ensures data transmission that is quick, safe, and dependable. For most commercial metro network systems connecting fixed locations, FSO systems serve as the "last mile solution." FSO systems are being considered for use in military systems due to their inherent advantages of mobility, quick deployment, security, and high data rates. The license-free band, cost-effectiveness, and high bandwidth access of the FSO system have allowed it to rapidly gain popularity as a method for transferring data at high rates over short distances. However, FSO also has some limitations, most of which are caused by atmospheric turbulence, which significantly reduces its performance. In this paper [113], various limitations of FSO and the possible means to mitigate their effect are discussed.

Free Space Optics (FSO) is an optical communication method that wirelessly transfers data by disseminating light in free space, such as the air, vacuum, or celestial space. FSO communication has the potential to replace conventional means of communication in a wide range of applications and offers high data rates up to 2.5 Gbps over distances ranging from 100 meters to a few kilometres. High bandwidth and unlicensed spectrum are two of its benefits; however, interference and atmospheric turbulences have hampered its widespread use. Researchers have proposed modulation methods, channel coding, diversity, hybrid systems, and physical hardware implementation to address many of these issues. In order to examine the significant contributions, open challenges, and potential directions for FSO, a comprehensive review of current research is required. future projects for research. This paper [114] presents a state-of-the-art review of the use of FSO in important indoor and outdoor applications and identifies some of the open research problems. They are: (a) Future 5G FSO transceiver design faces the challenge of optimizing bit-error-rate and signal-to-noise ratio at the receiver, (b) cost-effective hybrid RF/FSO solutions are required to combine the benefits of RF and FSO, (c) future FSO systems would offer both illumination and communication, necessitating modulation and coding techniques for improved dimming control and efficient data communication and (d) Physical layer security remains a critical concern and must be thoroughly addressed to ensure robust and secure data transmission.

2.5 RESEARCH GAPS

Despite the growing interest and advancement in hybrid RF/FSO systems, several research gaps still persist that limit the full exploitation of such systems for high-capacity, resilient communication networks:

1. Most prior studies rely on basic statistical models like Rayleigh, Nakagami-m, or Gamma-Gamma, which offer limited accuracy in modelling real-world atmospheric and channel fading conditions, especially under strong turbulence.
2. There is a lack of comprehensive analytical expressions for performance metrics such as outage capacity, ergodic capacity, and symbol error rate (SER) for dual-hop RF/FSO systems using advanced models like Mixture Gamma and Double Generalized Gamma distribution.
3. The impact of pointing errors, which are highly relevant in practical deployments, is often simplified or overlooked in performance analysis of FSO and Ro-FSO systems.
4. While diversity techniques like MRC and SC are explored, the implementation of Equal Gain Combining (EGC) for Double GG fading channels has not been extensively analyzed, particularly using MGF-based approaches.
5. OFDM-based Ro-FSO systems are gaining popularity, but closed-form BER expressions that consider both turbulence and pointing errors are rare and often limited to specific modulation schemes or assumptions.
6. Most existing research is either simulation-based or lacks validation against mathematical closed-form results across varying turbulence regimes.

These gaps highlight the need for robust analytical modelling, generalized performance evaluation, and practical scenario consideration to advance the deployment of reliable RF/FSO communication systems.

2.6 OBJECTIVES

The primary objective of this research is to develop accurate and generalized analytical models for evaluating the performance of dual-hop RF/FSO communication systems under realistic fading scenarios and practical constraints.

The specific objectives include:

1. To model the RF and FSO channels using Mixture Gamma (MG) and Double Generalized Gamma (DGG) distributions respectively, covering weak to strong turbulence conditions.
2. To derive closed-form expressions for key performance metrics such as Outage Capacity and Ergodic Capacity for dual-hop systems using various fading scenarios including Rayleigh and Nakagami-m as special cases.
3. To analyze the Average Capacity (AC) and Symbol Error Rate (SER) for M-PSK and M-QAM modulation schemes over Double GG fading under Equal Gain Combining (EGC) scheme.
4. To develop and validate BER expressions for OFDM-based Ro-FSO systems with and without pointing errors for different modulation formats (M-QAM and K-PSK).
5. To evaluate the effect of varying turbulence conditions, diversity branches, and modulation orders on overall system performance through extensive numerical and simulation-based analysis.

2.7 SCOPE OF THE WORK

This study encompasses the theoretical modelling, analytical derivation, and simulation validation of hybrid RF/FSO communication systems. It particularly emphasizes:

- Advanced statistical channel modelling using MG and DGG distributions.
- Performance evaluation under IM/DD and heterodyne detection techniques.

- Impact assessment of practical impairments like pointing errors and non-linearity.
- Modulation and diversity schemes adapted to real-world FSO environments.
- OFDM-based Ro-FSO integration for next-generation broadband applications.

The outcomes aim to provide a generalized, scalable framework for designing reliable hybrid communication systems applicable in terrestrial, urban, satellite, and disaster-recovery environments.

CHAPTER 3

ERGODIC CAPACITY OF MIXTURE GAMMA AND DOUBLE GENERALIZED GAMMA DISTRIBUTION IN DUAL HOP RF/FSO TRANSMISSION SYSTEM

FSO communication involves transferring data between locations using an optical signal in a free space or vacuum channel. This type of system is highly efficient and reliable, with its characteristics crucial in determining its effectiveness. Researchers have been captivated by FSO due to its numerous advantages. Moreover, FSO operates at a wider bandwidth within an unlicensed spectrum than RF systems. [78].

Microwaves are typically utilized in RF systems for data transmission between a source and a destination. However, the RF communication system has several drawbacks, including reduced data security and licensed spectrum, making FSO a superior alternative. FSO is considered the best option for high-speed data communication and offers greater flexibility than fiber optics communication systems. Additionally, scattering, absorption, and pointing errors can affect FSO performance, with pointing errors resulting from receiver and transmitter misalignment caused by the vibration of transmitted beams from buildings [78].

The relaying technology helps expand the coverage area and enhances performance [79]. Relaying, along with diversity schemes, is utilized to mitigate the impact of turbulence in FSO communication. A new mathematical model, Double GG, has been developed to address turbulence in different conditions and incorporates commonly used measurable models for exceptional cases of irradiance disturbances. The exciting features of this model have made it a popular topic among researchers for performance analysis in FSO systems [78].

Due to its many advantages, including high precision and speedy creation of performance indicators like channel capacity, cooperative relay channel, cognitive radio, outage, and error rate, it is recommended to employ mixture gamma fading for the RF connection. [78] [84].

In [98], the research focuses on the performance of a dual-hop RF/FSO system using a Double Generalized Gamma fading distribution-based model. This model calculates performance parameters such as Average Symbol Error Rate (ASER/ABER), Average Capacity, and Outage Capacity (OC). In [99], the authors investigated the performance of a dual-hop RF/FSO system using a Mixed Weibull and Gamma-Gamma-based system model with the CSI-assisted Amplitude & Forward (AF) relaying protocol. They derived closed-form expressions for end-to-end SNR CDF, PDF, and ASER using heterodyne and IM/DD detection techniques and validated the results using Monte Carlo simulations. Additionally, in [100], the authors analyzed the performance of a dual-hop RF/FSO system using Rayleigh and Double Generalized Gamma fading distribution-based models.

Considering a Dual Hop RF/FSO communication system, one hop is used as RF Signal and another as an FSO channel. Here, it uses Mixture Gamma Distribution to model the RF channel and a Double Generalized Gamma distribution to model the FSO channel. Also, as a special case, of Mixture Gamma, Rayleigh and Nakagami-m distribution is modelled at RF channel. Thereby, the mathematical and graphical analysis for different turbulence conditions are performed. The system's performance is analyzed in terms of Ergodic Capacity with different threshold SNR [114].

3.1 ERGODIC CAPACITY

The equivalent PDF of the dual-hop model containing Mixture Gamma in the RF link and Double GG in the FSO link is given by [100]:

$$f_{\gamma eq}(\gamma) = \sum_{i=1}^{N} \alpha_i \, \gamma^{\beta_i - 1} \, 1 \, e^{-\zeta_i \gamma} - \sum_{i=1}^{N} \alpha_i \, \gamma^{\beta_i - 1} \, e^{-\zeta_i \gamma}$$

$$\times \frac{p^{(m_2 - 1/2)} q^{(m_1 - 1/2)} 2\pi^{\left(1 - \frac{p+q}{2}\right)}}{\Gamma m_1 \Gamma m_2}$$

$$G_{1,p+q+1}^{p+q,1}\left[\left(\left(\frac{\gamma}{\bar{\Upsilon}}\right)^{\frac{p\gamma_2}{2}}\frac{1}{I_l{}^{p\gamma_2}}\frac{m_1{}^q m_2{}^p}{p^p q^q \Omega_1{}^q \Omega_2{}^p}\middle|_{\Delta(q:m_1),\Delta(p:m_2),0}^{1}\right)\right]$$

$$+\frac{\gamma_2 p^{(m_2+1/2)} q^{(m_1-1/2)} 2\pi^{\left(1-\frac{p+q}{2}\right)}}{2\Gamma m_1 \Gamma m_2\,\gamma}$$

$$G_{0,p+q}^{p+q,0}\left[\left(\left(\frac{\gamma}{\bar{\Upsilon}}\right)^{\frac{p\gamma_2}{2}}\frac{1}{I_l{}^{p\gamma_2}}\frac{m_1{}^q m_2{}^p}{p^p q^q \Omega_1{}^q \Omega_2{}^p}\middle|_{\Delta(q:m_1),\Delta(p:m_2)}^{-}\right)\right]\frac{\gamma_2 p^{(m_2+1/2)} q^{(m_1-1/2)} 2\pi^{\left(1-\frac{p+q}{2}\right)}}{2\Gamma m_1 \Gamma m_2\,\gamma}$$

$$G_{0,p+q}^{p+q,0}\left[\left(\left(\frac{\gamma}{\bar{\Upsilon}}\right)^{\frac{p\gamma_2}{2}}\frac{1}{I_l{}^{p\gamma_2}}\frac{m_1{}^q m_2{}^p}{p^p q^q \Omega_1{}^q \Omega_2{}^p}\middle|_{\Delta(q:m_1),\Delta(p:m_2)}^{-}\right)\right]\times\sum_{i=1}^{N}\alpha_i\zeta^{-\beta_i}\,G_{1,2}^{1,1}\left(\zeta_i\gamma\middle|_{\beta_i,0}^{1}\right)\qquad(3.1)$$

This section analyzes the Ergodic Capacity, the highest data rate received without errors. It can also be said as the maximum error-free data rate. The mathematical computation for the EC of the system model under weak turbulence conditions is presented as:

On putting the values $m_1 = 4$, $m_2 = 4.5$, $p = 1$, $q = 1$, $\gamma_1 = 2.1$, $\gamma_2 = 2$, $\Omega_1 = 1.0676$, $\Omega_2 = 1.06$ in equation (3.1) given below:

$$f_{\gamma eq}(\gamma) = \sum_{i=1}^{N}\alpha_i\gamma^{\beta_i-1}\,e^{-\zeta_i\gamma} - \sum_{i=1}^{N}\alpha_i\,\gamma^{\beta_i-1}\,e^{-\zeta_i\gamma}\times\frac{1}{\Gamma m_1\Gamma m_2}\,G_{1,3}^{2,1}\left[\left(\left(\frac{\gamma}{\bar{\Upsilon}}\right)^{1}\frac{1}{I_l{}^2}\frac{m_1{}^q m_2{}^p}{\Omega_1{}^q\Omega_2{}^p}\middle|_{4,4.5,0}^{1}\right)\right]+$$

$$\frac{1}{\Gamma m_1\Gamma m_2\,\gamma}\,G_{0,2}^{2,0}\left[\left(\left(\frac{\gamma}{\bar{\Upsilon}}\right)^{1}\frac{1}{I_l{}^2}\frac{m_1{}^q m_2{}^p}{\Omega_1{}^q\Omega_2{}^p}\middle|_{4,4.5}^{-}\right)\right]-$$

$$\frac{1}{\Gamma m_1\Gamma m_2\,\gamma}\,G_{0,2}^{2,0}\left[\left(\left(\frac{\gamma}{\bar{\Upsilon}}\right)^{1}\frac{1}{I_l{}^2}\frac{m_1{}^q m_2{}^p}{\Omega_1{}^q\Omega_2{}^p}\middle|_{4,4.5}^{-}\right)\right]\sum_{i=1}^{N}\alpha_i\zeta^{-\beta_i}\,G_{1,2}^{1,1}\left(\zeta_i\gamma\middle|_{\beta_i,0}^{1}\right)\qquad(3.2)$$

From [78] the ergodic capacity is given by:

$$C = \int_0^{\infty}\log(1+\varpi\gamma)\,f_{\gamma eq}(\gamma)\,d\gamma\qquad(3.3)$$

$$
\begin{aligned}
\mathrm{C} = \int_0^{\infty} \log(1+\varpi\gamma) \sum_{\mathrm{i}=1}^{\mathrm{N}} \alpha_{\mathrm{i}} \gamma^{\beta_{\mathrm{i}}-1}\ e^{-\zeta_{\mathrm{i}}\gamma}
&- \sum_{\mathrm{i}=1}^{\mathrm{N}} \alpha_{\mathrm{i}}\, \gamma^{\beta_{\mathrm{i}}-1}\, e^{-\zeta_{\mathrm{i}}\gamma} \\
&\times \frac{1}{\Gamma m_1 \Gamma m_2}\ G_{1,3}^{2,1}\left[\left(\left(\frac{\gamma}{\bar{\Upsilon}}\right)^1 \frac{1}{{I_l}^2} \frac{{m_1}^q {m_2}^p}{{\Omega_1}^q {\Omega_2}^p}\middle|\begin{matrix}1\\ 4,4.5,0\end{matrix}\right)\right] \\
&+ \frac{1}{\Gamma m_1 \Gamma m_2\, \gamma}\ G_{0,2}^{2,0}\left[\left(\left(\frac{\gamma}{\bar{\Upsilon}}\right)^1 \frac{1}{{I_l}^2} \frac{{m_1}^q {m_2}^p}{{\Omega_1}^q {\Omega_2}^p}\middle|\begin{matrix}-\\ 4,4.5\end{matrix}\right)\right] \\
&- \frac{1}{\Gamma m_1 \Gamma m_2\, \gamma}\ G_{0,2}^{2,0}\left[\left(\left(\frac{\gamma}{\bar{\Upsilon}}\right)^1 \frac{1}{{I_l}^2} \frac{{m_1}^q {m_2}^p}{{\Omega_1}^q {\Omega_2}^p}\middle|\begin{matrix}-\\ 4,4.5\end{matrix}\right)\right] \\
&\times \sum_{\mathrm{i}=1}^{\mathrm{N}} \alpha_{\mathrm{i}} \zeta^{-\beta_{\mathrm{i}}}\, \mathrm{G}_{1,2}^{1,1}\left(\zeta_{\mathrm{i}}\gamma\middle|\begin{matrix}1\\ \beta_{\mathrm{i}},0\end{matrix}\right) d\gamma
\end{aligned}
\tag{3.4}
$$

$$
\begin{aligned}
C = &\left(\sum_{\mathrm{i}=1}^{\mathrm{N}} \alpha_{\mathrm{i}} {\zeta_{\mathrm{i}}}^{-\beta_{\mathrm{i}}}\ G_{3,2}^{1,3}\left[\left(\frac{\varpi}{\zeta_{\mathrm{i}}}\right)\middle|\begin{matrix}1-\beta_{\mathrm{i}}, 1, 1\\ 1, 0\end{matrix}\right]\right) - \sum_{\mathrm{i}=1}^{\mathrm{N}} \alpha_{\mathrm{i}} {\zeta_{\mathrm{i}}}^{-\beta_{\mathrm{i}}} \left(\frac{1}{\Gamma m_1 \Gamma m_2}\right) \\
&G_{1,0:2,2:1,3}^{0,1:1,2:2,1}\left[\begin{matrix}1-\beta_{\mathrm{i}}\\ -\end{matrix}\middle|\begin{matrix}1,1\\ 1,0\end{matrix}\middle|\begin{matrix}1\\ 4,4.5,0\end{matrix}\middle|\frac{\varpi}{\zeta_{\mathrm{i}}}, \frac{\left(\frac{1}{\bar{\Upsilon}}\right)^1 \frac{1}{{I_l}^2} \frac{{m_1}^1 {m_2}^1}{{\Omega_1}^1 {\Omega_2}^1}}{{\zeta_{\mathrm{i}}}^1}\right] \\
&+ \frac{1}{\Gamma m_1 \Gamma m_2}\ G_{2,4}^{4,1}\left(\frac{\left(\frac{1}{\bar{\Upsilon}}\right)^1 \frac{1}{{I_l}^2} \frac{{m_1}^q {m_2}^p}{{\Omega_1}^q {\Omega_2}^p}}{\varpi^1}\middle|\begin{matrix}0,1\\ 4,4.5,0,0\end{matrix}\right) \\
&- \sum_{\mathrm{i}=1}^{\mathrm{N}} \alpha_{\mathrm{i}} {\zeta_{\mathrm{i}}}^{-\beta_{\mathrm{i}}} \left(\frac{1}{\Gamma m_1 \Gamma m_2}\right) \\
&G_{2,0:2,2:1,1}^{0,2:1,2:1,1}\left[\begin{matrix}-3, -3.5\\ -\end{matrix}\middle|\begin{matrix}1,1\\ 1,0\end{matrix}\middle|\begin{matrix}1\\ \beta_{\mathrm{i}}, 0\end{matrix}\middle|\frac{\varpi}{\left(\frac{1}{\bar{\Upsilon}}\right)^1 \frac{1}{{I_l}^2} \frac{{m_1}^1 {m_2}^1}{{\Omega_1}^1 {\Omega_2}^1}}, \frac{{\zeta_{\mathrm{i}}}^1}{\left(\frac{1}{\bar{\Upsilon}}\right)^1 \frac{1}{{I_l}^2} \frac{{m_1}^1 {m_2}^1}{{\Omega_1}^1 {\Omega_2}^1}}\right]
\end{aligned}
\tag{3.5}
$$

CASE 1: For Nakagami-m:

Using the below-mentioned values as given in [84]:

$$\mathrm{N}=1,\alpha_1=\frac{\mathrm{m}^{\mathrm{m}}}{\Gamma(\mathrm{m})\bar{\gamma}^{\mathrm{m}}},\beta_1=\mathrm{m}\,,\zeta_1=\frac{\mathrm{m}}{\bar{\gamma}} \tag{3.6}$$

$$\mathrm{C}=\left(\frac{1}{\Gamma(\mathrm{m})}G_{3,2}^{1,3}\left[\left(\frac{\varpi}{\frac{\mathrm{m}}{\bar{\bar{\gamma}}}}\right)\middle|\begin{matrix}1-\mathrm{m},1,1\\1,0\end{matrix}\right]\right)-\frac{1}{\Gamma(\mathrm{m})}\left(\frac{1}{\Gamma m_1\Gamma m_2}\right)$$

$$G_{1,0:2,2:1,3}^{0,1:1,2:2,1}\left[\begin{matrix}1-\mathrm{m}\\-\end{matrix}\middle|\begin{matrix}1,1\\1,0\end{matrix}\middle|\begin{matrix}1\\4,4.5,0\end{matrix}\middle|\frac{\varpi}{\frac{\mathrm{m}}{\bar{\bar{\gamma}}}},\frac{\left(\frac{1}{\bar{\bar{\Upsilon}}}\right)^1\frac{1}{{I_l}^2}\frac{{m_1}^1{m_2}^1}{{\Omega_1}^1{\Omega_2}^1}}{\frac{\mathrm{m}}{\bar{\bar{\gamma}}}}\right]\frac{1}{\Gamma m_1\Gamma m_2}$$

$$G_{2,4}^{4,1}\left(\frac{\left(\frac{1}{\bar{\bar{\Upsilon}}}\right)^1\frac{1}{{I_l}^2}\frac{{m_1}^q{m_2}^p}{{\Omega_1}^q{\Omega_2}^p}}{\varpi^1}\middle|\begin{matrix}0,1\\4,4.5,0,0\end{matrix}\right) \tag{3.7}$$

$$-\frac{1}{\Gamma(\mathrm{m})}\left(\frac{1}{\Gamma m_1\Gamma m_2}\right)G_{2,0:2,2:1,2}^{0,2:1,2:1,1}\left[\begin{matrix}-3,-3.5\\-\end{matrix}\middle|\begin{matrix}1,1\\1,0\end{matrix}\middle|\begin{matrix}1\\\mathrm{m},0\end{matrix}\middle|\frac{\varpi}{\left(\frac{1}{\bar{\bar{\Upsilon}}}\right)^1\frac{1}{{I_l}^2}\frac{{m_1}^1{m_2}^1}{{\Omega_1}^1{\Omega_2}^1}},\frac{\frac{\mathrm{m}}{\bar{\bar{\gamma}}}}{\left(\frac{1}{\bar{\bar{\Upsilon}}}\right)^1\frac{1}{{I_l}^2}\frac{{m_1}^1{m_2}^1}{{\Omega_1}^1{\Omega_2}^1}}\right]$$

CASE 2: For Rayleigh:

$$\mathrm{N}=1,\alpha_1=\frac{1}{\bar{\gamma}}\,,\beta_1=1,\zeta_1=\frac{1}{\bar{\gamma}}\,,m=1 \tag{3.8}$$

$$\mathrm{C}=\left(G_{3,2}^{1,3}\left[\left(\frac{\varpi}{1}\gamma\right)\middle|\begin{matrix}0,1,1\\1,0\end{matrix}\right]\right)-\left(\frac{1}{\Gamma m_1\Gamma m_2}\right)$$

$$G_{1,0:2,2:1,3}^{0,1:1,2:2,1}\left[\begin{matrix}0\\-\end{matrix}\middle|\begin{matrix}1,1\\1,0\end{matrix}\middle|\begin{matrix}1\\4,4.5,0\end{matrix}\middle|\frac{\varpi}{\frac{1}{\bar{\bar{\gamma}}}},\frac{\left(\frac{1}{\bar{\bar{\Upsilon}}}\right)^1\frac{1}{{I_l}^2}\frac{{m_1}^1{m_2}^1}{{\Omega_1}^1{\Omega_2}^1}}{\frac{1}{\bar{\bar{\gamma}}}}\right]$$

$$+\frac{1}{\Gamma m_1\Gamma m_2}\;G_{2,4}^{4,1}\left(\frac{\left(\frac{1}{\bar{\bar{\Upsilon}}}\right)^1\frac{1}{{I_l}^2}\frac{{m_1}^q{m_2}^p}{{\Omega_1}^q{\Omega_2}^p}}{\varpi^1}\middle|\begin{matrix}0,1\\4,4.5,0,0\end{matrix}\right)$$

$$-\left(\frac{1}{\Gamma m_1\Gamma m_2}\right)\;G_{2,0:2,2:1,2}^{0,2:1,2:1,1}\left[\begin{matrix}-3,-3.5\\-\end{matrix}\middle|\begin{matrix}1,1\\1,0\end{matrix}\middle|\begin{matrix}1\\1,0\end{matrix}\middle|\frac{\varpi}{\left(\frac{1}{\bar{\bar{\Upsilon}}}\right)^1\frac{1}{{I_l}^2}\frac{{m_1}^1{m_2}^1}{{\Omega_1}^1{\Omega_2}^1}},\frac{\frac{1}{\bar{\bar{\gamma}}}}{\left(\frac{1}{\bar{\bar{\Upsilon}}}\right)^1\frac{1}{{I_l}^2}\frac{{m_1}^1{m_2}^1}{{\Omega_1}^1{\Omega_2}^1}}\right] \tag{3.9}$$

Using the below-mentioned values as given in [84]:

3.2 RESULTS AND DISCUSSION

Using the equation (3.7) and (3.9), the simulation results for Ergodic Capacity are obtained.

Fig 3.1 compares Ergodic Capacity vs Average electrical SNR over Rayleigh, taking different path losses at L=0.5 Km. At average electrical SNR of 30 dB, the Ergodic Capacity is 7.359, 5.363, 2.5, 1.07 for path loss of 0.4 bits/Hz, 1.5 bits/Hz, 2.7 bits/Hz, and 3.2 bits/Hz, respectively. So, in conclusion, it is observed that as the path loss values increase, there is a decrease in the corresponding Ergodic Capacity value to some extent.

Fig 3.2 compares Ergodic Capacity vs Average electrical SNR over Nakagami-m, taking different path losses at L=0.5 Km. At average electrical SNR of 30 dB, the Ergodic Capacity is 12.61, 11.76, 10.55, and 9.953 for path loss of 0.4 bits/Hz, 1.5 bits/Hz, 2.7 bits/Hz, and 3.2 bits/Hz respectively. So, in conclusion, again it is seen that as the path loss values increase, the corresponding Ergodic Capacity value decreases to some extent.

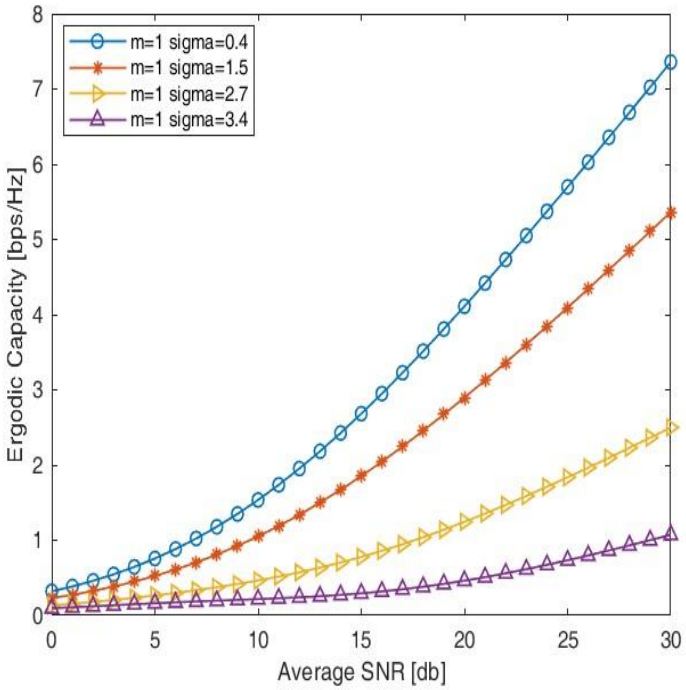

Fig. 3.1. Comparison of Ergodic Capacity for dual-hop RF/FSO system for m=1 for different path loss at L=0.5 km

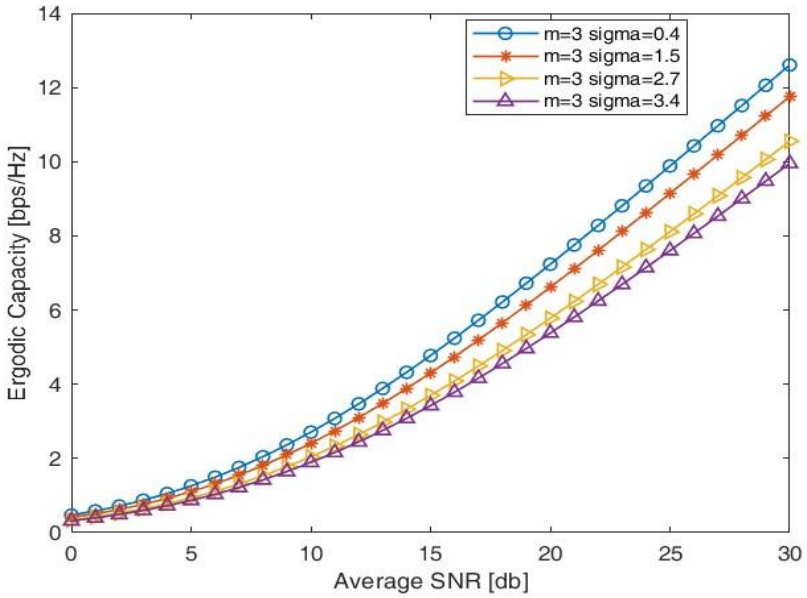

Fig. 3.2. Comparison of Ergodic Capacity for dual-hop RF/FSO system for m=3 for different path loss at L=0.5 km.

From Fig 3.1 and 3.2, it is noted that as the average electrical SNR value increases, there will be an increase in the value of Ergodic capacity. Conversely, as the value of path loss increases, there is a decrease in the value of Ergodic capacity.

Fig 3.3 compares Ergodic Capacity vs Average electrical SNR over Nakagami-m (m=3), taking different path losses at L=1 Km. At average electrical SNR of 30 dB, the Ergodic Capacity is 9.682, 8.088, 6.044, and 5.136 for path loss of 0.4 bits/Hz, 1.5 bits/Hz, 2.7 bits/Hz, and 3.2 bits/Hz, respectively. So, in conclusion, it is seen that as the path loss values increase, the corresponding Ergodic Capacity value decreases to some extent.

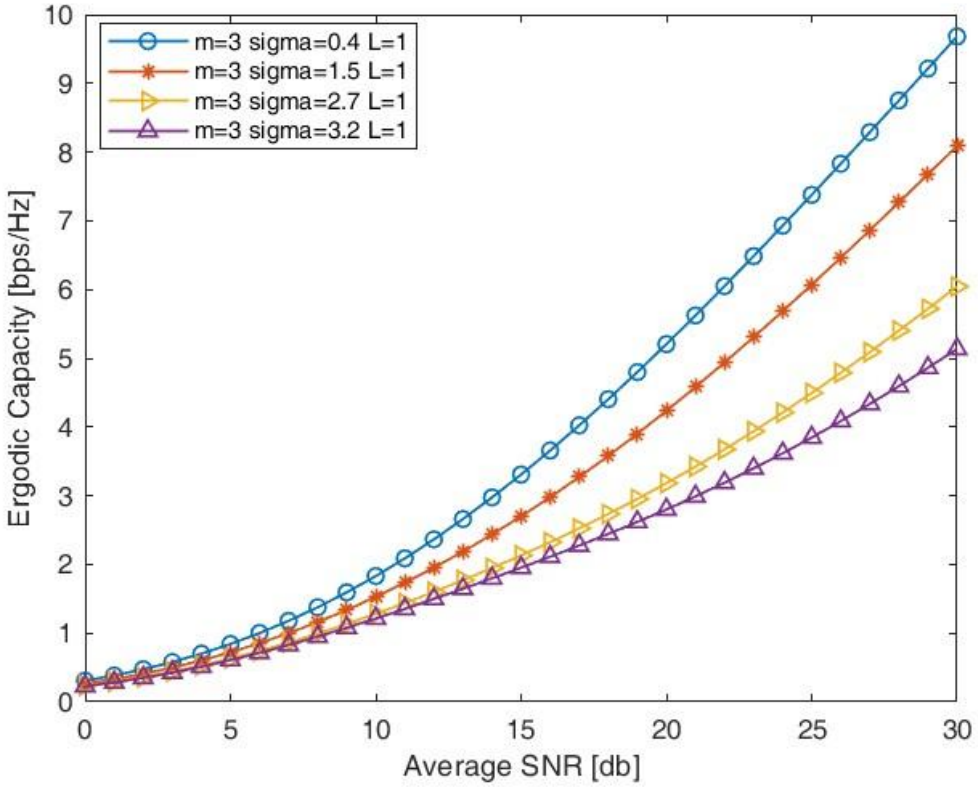

Fig. 3.3. Comparison of Ergodic Capacity for dual-hop RF/FSO system for m=3 for different path loss at L=1 km.

Fig 3.4 compares Ergodic Capacity vs Average electrical SNR over Nakagami-m (m=4), taking different path losses at L=1 Km. At average electrical SNR of 30 dB, the Ergodic Capacity is 14.53, 13.73, 12.63, and 12.11 for path loss of 0.4 bits/Hz, 1.5 bits/Hz, 2.7 bits/Hz, and 3.2 bits/Hz, respectively. So, in conclusion, it is seen that as the path loss values increase, the corresponding Ergodic Capacity value decreases to some extent.

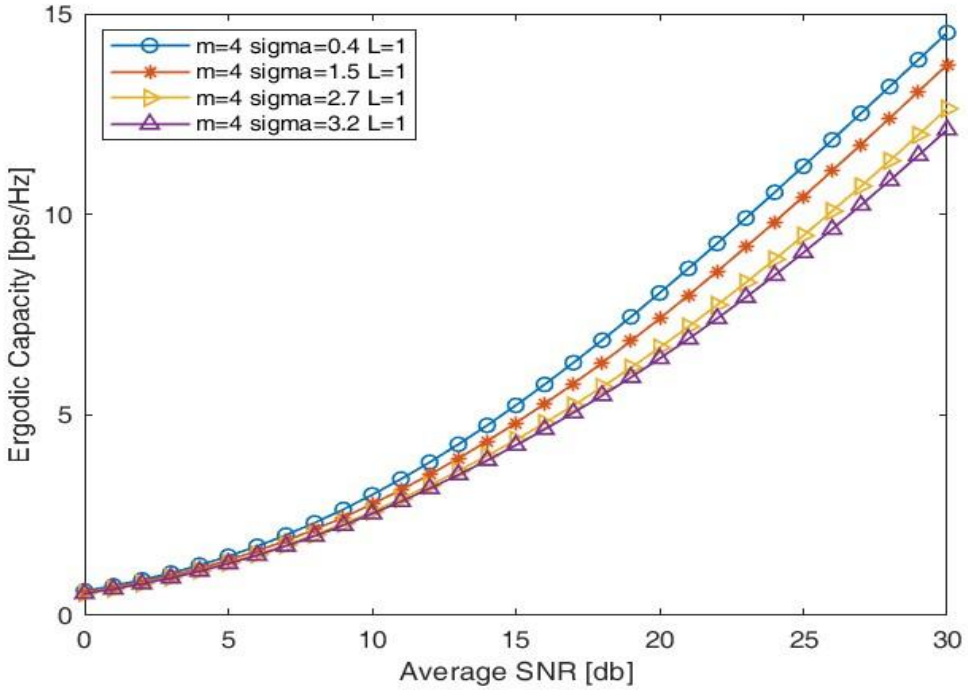

Fig. 3.4. Comparison of Ergodic Capacity for dual-hop RF/FSO system for m=4 for different path loss at L=1 km.

In Fig 3.3 and 3.4, the value of L is increased to 1 km, and it is observed that as the average electrical SNR value rises, then there will be an increase in the value of Ergodic capacity. Conversely, as the value of path loss increases, there will be a decrease in the value of Ergodic capacity. From these figures, it is seen that our model is valid for Nakagami-m at higher values of L (1, 1.5 and 2 Km).

Fig 3.5 compares Ergodic Capacity vs Average electrical SNR over Nakagami-m (m=3) taking different L= 0.5 Km, 1 Km, 1.5 Km. At average electrical SNR of 30 dB, the Ergodic Capacity is 12.61, 9.682, and 6.995 for taking L as 0.5 Km, 1 Km, and 1.5 Km, respectively. So, in conclusion, it is seen that as the value of L (propagation distance) increases, the corresponding Ergodic Capacity value decreases to some extent.

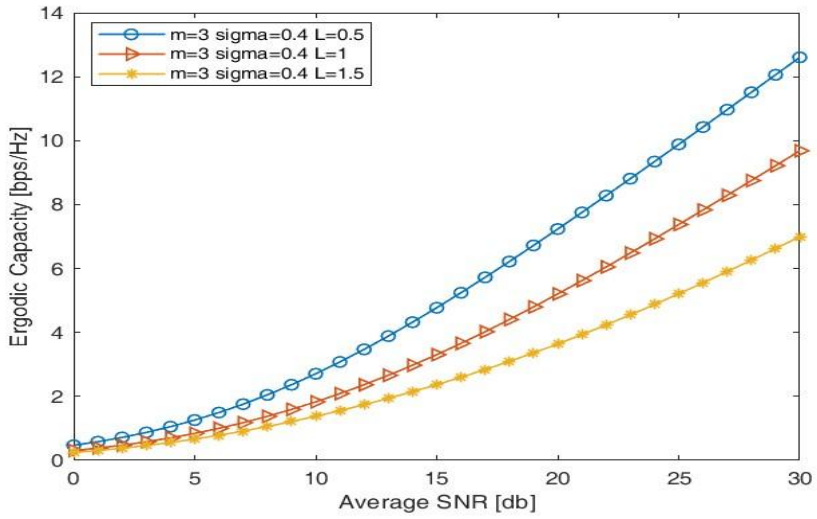

Fig. 3.5. Comparison of Ergodic Capacity for dual-hop RF/FSO system for m=3 for different values of L

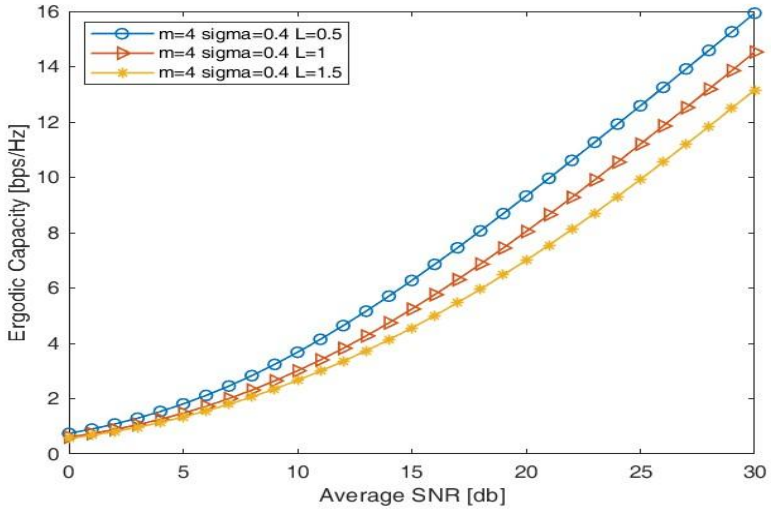

Fig. 3.6. Comparison of Ergodic Capacity for dual-hop RF/FSO system for m=4 for different values of L

Fig 3.6 compares Ergodic Capacity vs Average electrical SNR over Nakagami-m(m=4) taking different L= 0.5 Km, 1 Km, 1.5 Km. At average electrical SNR of 30 dB, the Ergodic Capacity is 15.93, 14.53, and 13.16 for taking L as 0.5 Km, 1 Km, and 1.5 Km, respectively. So, in

conclusion, it is seen that as the value of L (propagation distance) increases, the corresponding Ergodic Capacity value decreases to some extent.

In Fig 3.5 and 3.6, the value of L is increased from 0.5 km to 1 km and 1.5 km, and it is observes that as the value of L increases, there will be a slight decrease in the Ergodic Capacity for a particular average SNR. However, on the other hand, it is noted that as the average SNR increases, Ergodic capacity increases for all values of L.

Fig 3.7 compares Ergodic Capacity vs Average electrical SNR over Mixture Gamma, taking m=1, 3 and 4. At Average electrical SNR of 30 dB, the Ergodic Capacity is 15.93, 12.61, and 7.35 for m = 4, 3 and 1, respectively.

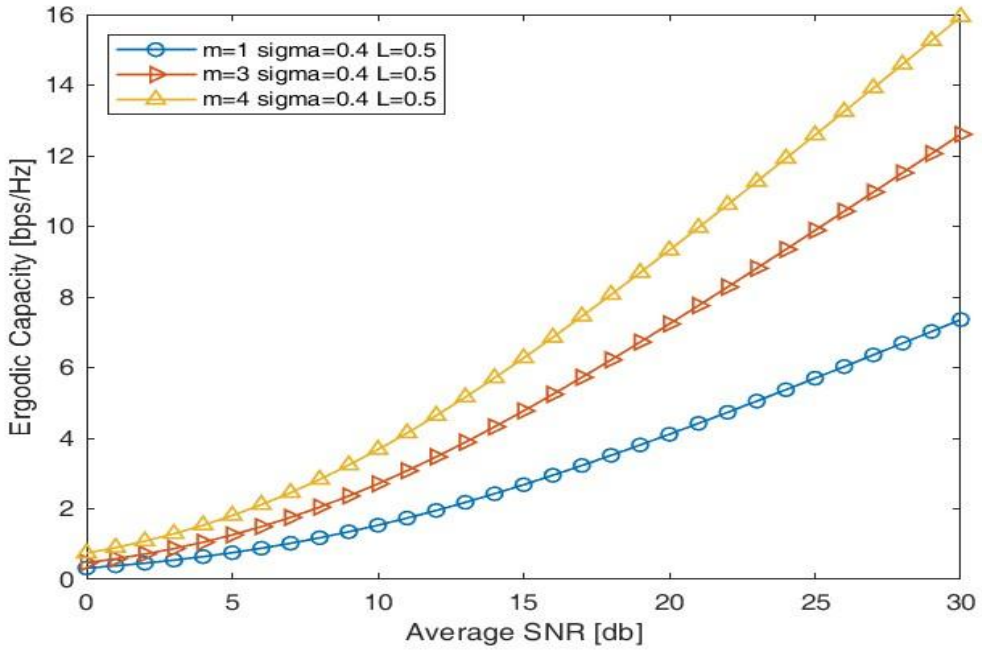

Fig. 3.7. Comparison of Ergodic Capacity for dual-hop RF/FSO system for different values of m.

3.3 SUMMARY

In this chapter, the ergodic capacity of a Mixed Dual Hop RF/FSO system is investigated. A Mixture Gamma distribution represents the RF channel, whereas the FSO channel is represented by a Double Generalised Gamma distribution. The analytical closed-form expression for the Ergodic Capacity is derived for the IM/DD detection approach to analyze the system's performance, As specific instances of the Mixture Gamma distribution, the Rayleigh and Nakagami-m distributions are employed. It is noticed that as the average electrical SNR increases, ergodic capacity increases for a specific threshold. For the ergodic capacity, it is found that when the path loss increases, the ergodic capacity reduces for a given electrical SNR.

CHAPTER 4

CLOSED FORM EXPRESSIONS OF AC AND SER FOR DOUBLE GG FADING DISTRIBUTION UNDER EGC SCHEME IN FSO COMMUNICATION SYSTEM

The impairments like, atmospheric turbulence and other nonlinear effects of optical link limits the overall system performance. To mitigate the effect of these impairments, different diversity combining schemes are implemented by different researchers. Also, it is noticeable that MGF based approach is more tractable compare to that of PDF based approach. However, performance analysis in terms of error rate and capacity under Equal Gain Combining (EGC) diversity scheme for Double Generalized Gamma fading distribution using MGF is missing from the literature of FSO. Therefore, this chapter presents closed form expressions of Average Capacity (AC) and Symbol Error Rate (SER) of M-PSK and M-QAM for Double Generalized fading distribution under EGC scheme. Further, the effect of different turbulence conditions such as weak, moderate and strong turbulences is presented. Furthermore, respective AC and SER are used to deduce those over Double Weibull and Gammagamma as special cases of Double Generalized fading distribution.

4.1 CHANNEL MODEL

Fig. 4.1 shows the FSO system under EGC diversity combining scheme, consisting of N lasers and L photodetectors. Laser diode of transmitter section emits optical signal and modulates before it transmits. At the receiver side, EGC (first co-phased and then weighted equally to form resultant output) scheme is applied after the signal is detected by the photodetector. Out of EGC, MRC and SC schemes, it is noticeable that EGC is least complex whereas MRC is

most complex. With this view, the authors implement EGC scheme in the FSO communication system.

Scintillation also known as atmospheric turbulence-induced fading, hinders the performance of FSO system. It is primarily because of variations in the refractive index by virtue of inhomogeneities of the temperature and pressure. This manifests itself as random fluctuations in the received signal. Various statistical models are proposed in the literature in an effort to model the fading in FSO. Further, it is classified into weak, moderate and strong turbulence fading depending on the severity of turbulence.

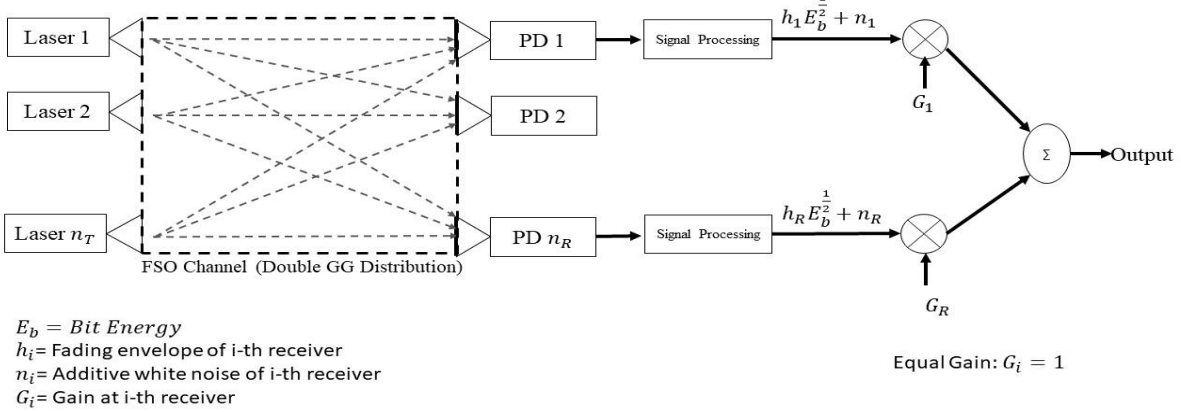

Fig.4.1 System Model for Free space Communication System under EGC Diversity [115]

However, Double GG distribution includes the entire range from weak to strong turbulence condition. The PDF of Double GG distribution is given as [8]

$$f_I(I) = \frac{\gamma_1}{I\Gamma(m_1)\Gamma(m_2)} H_{2,0}^{0,2}\left[\frac{\Omega_1}{m_1 I^{\gamma_1}}\left(\frac{\Omega_2}{m_2}\right)^{\frac{\gamma_1}{\gamma_2}}\middle|(1-m_1,1),\left(1-m_2,\frac{\gamma_1}{\gamma_2}\right)\right] \quad (4.1)$$

where, $H_{2,0}^{0,2}[\ ]$ represents Fox H function and $\gamma_i > 0$, $m_i > 0.5$ *and* Ω_i, $i = 1,2$ are the parameters of the generalized gamma distribution.

With [116], MGF is given as

$$M_y(s) = \int_0^\infty e^{-sI} f_I(I) dI \quad (4.2)$$

Putting the value of PDF in Eq. (4.2) and following simple mathematical steps [117], we get

$$M_y(s) = \frac{\gamma_1}{\Gamma(m_1)\Gamma(m_2)} H_{3\ 0}^{0\ 3}\left(\frac{m_1 s^{\gamma_1}}{\Omega_1}\left(\frac{m_2}{\Omega_2}\right)^{\frac{\gamma_1}{\gamma_2}} \middle| \begin{matrix} (1,-\gamma_1),(1-m_1,1),\left(1-m_2,\frac{\gamma_1}{\gamma_2}\right) \\ - \end{matrix}\right) \quad (4.3)$$

4.2 PROPOSED ANALYTICAL EXPRESSION OF PERFORMANCE MEASURES

4.2.1 Closed form expression of Average Capacity under EGC scheme

Average Capacity (AC) of L-branch diversity combiner over neither mutually not necessarily independent nor identically distributed fading channel having bandwidth W given by [1, Eq. (4.8)]

$$C_{avg} = \frac{w}{log2} \int_0^\infty C_q(s)\left[\frac{\partial}{\partial s} M_y(\emptyset_{p,q} s)\right] \text{ds} \quad (4.4)$$

where, $\emptyset_{p,q} = \sqrt[q]{E_s/N_o L^{(p-q-1)/2}}$ and where the auxiliary function $C_q(s)$ is given by

$C_q(s) = \frac{-1}{\sqrt{q(2\pi)^{1-q}}} G_{q+2,2}^{1,2}\left(\frac{q^q}{2^q} \middle| \begin{matrix} 1,1,\Delta_q^1 \\ 1,0 \end{matrix}\right)$, where $\Delta_n^x = \frac{x}{n}, \frac{x+1}{n}, \ldots\ldots, \frac{x+n-1}{n}$ with x€C and n€N

Also, for (p, q) as (1,2) Eq. (4.4) represents EGC combining scheme.

Therefore, the auxiliary function for EGC is given as

$$C_{EGC}(s) = C_q(s)|_{q\to 2} = -\sqrt{\pi} G_{3,1}^{0,2}\left(\frac{4}{s^2} \middle| \begin{matrix} 1,1,\frac{1}{2} \\ 0 \end{matrix}\right) \quad (4.5)$$

Substituting Eq. (4.5) in Eq. (4.4), we get

$$C_{avg}^{EGC} = \frac{w}{log2} \int_0^\infty -\sqrt{\pi} G_{3,1}^{0,2}\left(\frac{4}{s^2} \middle| \begin{matrix} 1,1,\frac{1}{2} \\ 0 \end{matrix}\right)\left[\frac{\partial}{\partial s} M_y(\emptyset_{p,q} s)\right] \quad (4.6)$$

Also, for EGC, $\emptyset_{p,q}$ is written as

$$\emptyset_{p,q} = \sqrt{\frac{E_S L}{N_o}} \quad (4.7)$$

where, $\frac{E_S}{N_o}$ is transmitted SNR per symbol. With Eq. (4.3), Eq. (4.6) and Eq. (4.7), we get

$$M_y(\emptyset_{p,q}s) = \frac{\gamma_1}{\Gamma(m_1)\Gamma(m_2)} H_{3\ 0}^{0\ 3}\left(\frac{m_1\left(\sqrt{\frac{E_S L}{N_o}}s\right)^{\gamma_1}}{\Omega_1}\left(\frac{m_2}{\Omega_2}\right)^{\frac{\gamma_1}{\gamma_2}}\middle|\begin{matrix}(1,-\gamma_1),(1-m_1,1),\left(1-m_2,\frac{\gamma_1}{\gamma_2}\right)\\ -\end{matrix}\right) \tag{4.8}$$

With [33, Eq (2.2.1)]

$$\left(\frac{d}{dz}\right)^K\left[z^w H_{pq}^{mn}\left(cz^\sigma\middle|\begin{matrix}(aj,Aj)_p\\(bj,Bj)_q\end{matrix}\right)\right] = (-1)^K z^{w-K} H_{p+1,q+1}^{m+1,n}\left(cz^\sigma\middle|\begin{matrix}(aj,Aj)p,(-w,\sigma)\\(K-w,\sigma),(bj,Bj)q\end{matrix}\right) \tag{4.9}$$

$$\frac{\partial}{\partial s}M_y(\emptyset_{p,q}s) = -s^{-1}\frac{\gamma_1}{\Gamma(m_1)\Gamma(m_2)} H_{4\ 1}^{1\ 3}\left(\frac{m_1\left(\sqrt{\frac{E_S L}{N_o}}s\right)^{\gamma_1}}{\Omega_1}\left(\frac{m_2}{\Omega_2}\right)^{\frac{\gamma_1}{\gamma_2}}\middle|\begin{matrix}(1,-\gamma_1),(1-m_1,1),\left(1-m_2,\frac{\gamma_1}{\gamma_2}\right),(0,\gamma_1)\\(1,\gamma_1)\end{matrix}\right) \tag{4.10}$$

Converting Meijer G into Fox H [118], Eq (1.23)], we get

$$G_{3,1}^{0,2}\left(\frac{4}{s^2}\middle|\begin{matrix}1,1,\frac{1}{2}\\0\end{matrix}\right) = H_{3,1}^{0,2}\left(\frac{4}{s^2}\middle|\begin{matrix}(1,1),(1,1),(\frac{1}{2},1)\\(0,1)\end{matrix}\right) \tag{4.11}$$

Substituting Eq. (4.10) and Eq. (4.11) into Eq.(4.6), we get

$$C_{avg}^{EGC} = \frac{w\sqrt{\pi}}{log2}\frac{\gamma_1}{\Gamma(m_1)\Gamma(m_2)} *$$

$$\int_0^\infty s^{-1} H_{3,1}^{0,2}\left(\frac{4}{s^2}\middle|\begin{matrix}(1,1),(1,1),\left(\frac{1}{2},1\right)\\(0,1)\end{matrix}\right) H_{4\ 1}^{1\ 3}\left(\frac{m_1\left(\sqrt{\frac{E_S L}{N_o}}s\right)^{\gamma_1}}{\Omega_1}\left(\frac{m_2}{\Omega_2}\right)^{\frac{\gamma_1}{\gamma_2}}\middle|\begin{matrix}(1,-\gamma_1),(1-m_1,1),\left(1-m_2,\frac{\gamma_1}{\gamma_2}\right),(0,\gamma_1)\\(1,\gamma_1)\end{matrix}\right) \text{ds} \tag{4.12}$$

Let $\frac{1}{s^2} = t \quad => ds = \frac{-1}{2}t^{-3/2}$ dt, Eq. (4.12) yields

$$C_{avg}^{EGC} = \frac{w\sqrt{\pi}}{log2}\frac{\gamma_1}{\Gamma(m_1)\Gamma(m_2)} *$$

$$\int_0^\infty t^{-1} H_{3,1}^{0,2}\left(4t\middle|\begin{matrix}(1,1),(1,1),\left(\frac{1}{2},1\right)\\(0,1)\end{matrix}\right) H_{4\ 1}^{1\ 3}\left(\frac{m_1\left(\sqrt{\frac{E_S L}{N_o}}\right)^{\gamma_1} t^{-\frac{\gamma_1}{2}}}{\Omega_1}\left(\frac{m_2}{\Omega_2}\right)^{\frac{\gamma_1}{\gamma_2}}\middle|\begin{matrix}(1,-\gamma_1),(1-m_1,1),\left(1-m_2,\frac{\gamma_1}{\gamma_2}\right),(0,\gamma_1)\\(1,\gamma_1)\end{matrix}\right) dt \tag{4.13}$$

But we have, [119]

$$\int_0^\infty x^{\alpha-1} H_{uv}^{st}\left(\sigma x \middle| \begin{matrix} c_u, C_u \\ d_v, D_v \end{matrix}\right) H_{pq}^{mn}\left(w x^r \middle| \begin{matrix} a_p, A_p \\ b_q, B_q \end{matrix}\right) dx$$

$$= \sigma^{-\alpha} H_{p+v,q+u}^{m+t,n+s}\left(\frac{w}{\sigma^r} \middle| \begin{matrix} (a_n, A_n), (1-d_v-\alpha D_v, r D_v), (a_{n+1}, A_{n+1}) - - - (a_p, A_P) \\ (b_m, B_m), (1-c_u-\alpha C_u, r C_u), (b_{m+1}, B_{m+1}) - - - (b_q, B_q) \end{matrix}\right) \tag{4.14}$$

By comparing Eq. (4.13) with Eq. (4.14), we get

$$\alpha = C_{avg}^{EGC} =$$

$$\frac{w\sqrt{\pi}}{log2} \frac{\gamma_1}{\Gamma(m_1)\Gamma(m_2)} H_{5\,4}^{3\,3}\left(\frac{m_1\left(\sqrt{\frac{E_S L}{N_o}}\right)^{\gamma_1} 4^{\frac{\gamma_1}{2}}}{\Omega_1}\left(\frac{m_2}{\Omega_2}\right)^{\frac{\gamma_1}{\gamma_2}} \middle| \begin{matrix} (1,-\gamma_1),(1-m_1,1),\left(1-m_2,\frac{\gamma_1}{\gamma_2}\right),\left(1,\frac{-\gamma_1}{2}\right),(0,\gamma_1) \\ (1,\gamma_1),\left(0,\frac{-\gamma_1}{2}\right),\left(0,\frac{-\gamma_1}{2}\right),\left(\frac{1}{2},\frac{-\gamma_1}{2}\right) \end{matrix}\right) \tag{4.15}$$

Eq. (4.15) represents channel capacity of FSO systems over Double Generalized Gamma distribution under ECG scheme. Different atmospheric turbulence conditions are analysed using Eq. (4.15). Also, by inserting γ_i= 1 and Ω_i = 1/ m_i = 1, capacity over Gamma-Gamma and Double Weibull fading respectively is realized.

4.2.2 Closed form expression of SER of MPSK scheme under EGC

The PDF of Double GG distribution is given as [8]

$$f_I(I) = \frac{\gamma_1}{I\Gamma(m_1)\Gamma(m_2)} H_{2,0}^{0,2}\left[\frac{\Omega_1}{m_1 I^{\gamma_1}}\left(\frac{\Omega_2}{m_2}\right)^{\frac{\gamma_1}{\gamma_2}} \middle| (1-m_1,1),\left(1-m_2,\frac{\gamma_1}{\gamma_2}\right)\right] \tag{4.16}$$

where I is the normalized irradiance at the receiver and the instantaneous electrical SNR is defined as $\gamma = \frac{(\eta I)^2}{N_0}$with η as effective photo current conversion ratio and N_0 as Double sided power spectral density Gaussian noise. Also, the average electrical SNR is given as $\mu = \frac{(\eta\langle I\rangle)^2}{N_0}$ with ⟨I⟩ as Mean value of the irradiance.

With random variable transformation in Eq. (4.16), we get

$$f_\gamma(\gamma) = \frac{\gamma_1}{2\gamma\Gamma(m_1)\Gamma(m_2)} H_{2,0}^{0,2}\left[\frac{\Omega_1}{m_1}\left(\frac{\Omega_2}{m_2}\right)^{\frac{\gamma_1}{\gamma_2}}\left(\frac{\gamma}{\mu}\right)^{\frac{-\gamma_1}{2}}\middle|(1-m_1,1),\left(1-m_2,\frac{\gamma_1}{\gamma_2}\right)\right] \quad (4.17)$$

Using Eq. (4.2) along with [4], we get

$$M_y(s) = \frac{\gamma_1}{2\Gamma(m_1)\Gamma(m_2)} H_{3\,0}^{0\,3}\left(\frac{m_1 s^{\frac{\gamma_1}{2}}}{\Omega_1\,\mu^{\frac{-\gamma_1}{2}}}\left(\frac{m_2}{\Omega_2}\right)^{\frac{\gamma_1}{\gamma_2}}\middle|\begin{matrix}\left(1,\frac{-\gamma_1}{2}\right),(1-m_1,1),\left(1-m_2,\frac{\gamma_1}{\gamma_2}\right)\\ -\end{matrix}\right) \quad (4.19)$$

With [120], Symbol Error Rate (SER) for M-PSK is given as

$$P_e = \left(\frac{\Omega}{2\Pi}-\frac{1}{6}\right)M_\gamma\left(Sin^2\left(\frac{\Pi}{L}\right)\right)+\left(\frac{1}{4}\right)M_\gamma\left(\frac{4}{3}*Sin^2\left(\frac{\Pi}{L}\right)\right)+\left(\frac{\Omega}{2\Pi}-\frac{1}{4}\right)M_\gamma\left(\frac{4}{3}*\left(\frac{Sin^2\left(\frac{\Pi}{L}\right)}{Sin^2(\Omega)}\right)\right) \quad (4.20)$$

where $\Omega = \frac{\Pi(L-1)}{L}$

Substituting Eq. (4.19) into Eq. (4.20), we get

$$P_e = \frac{\gamma_1}{2\Gamma(m_1)\Gamma(m_2)}\left[\left(\frac{\Omega}{2\Pi}-\frac{1}{6}\right)H_{3\,0}^{0\,3}\left(\frac{m_1\left(Sin^2\left(\frac{\Pi}{L}\right)\right)^{\frac{\gamma_1}{2}}}{\Omega_1\,\mu^{\frac{-\gamma_1}{2}}}\left(\frac{m_2}{\Omega_2}\right)^{\frac{\gamma_1}{\gamma_2}}\middle|\begin{matrix}\left(1,\frac{-\gamma_1}{2}\right),(1-m_1,1),\left(1-m_2,\frac{\gamma_1}{\gamma_2}\right)\\ -\end{matrix}\right)+\right.$$

$$\left(\frac{1}{4}\right)H_{3\,0}^{0\,3}\left(\frac{m_1\left(\frac{4}{3}*Sin^2\left(\frac{\Pi}{L}\right)\right)^{\frac{\gamma_1}{2}}}{\Omega_1\,\mu^{\frac{-\gamma_1}{2}}}\left(\frac{m_2}{\Omega_2}\right)^{\frac{\gamma_1}{\gamma_2}}\middle|\begin{matrix}\left(1,\frac{-\gamma_1}{2}\right),(1-m_1,1),\left(1-m_2,\frac{\gamma_1}{\gamma_2}\right)\\ -\end{matrix}\right)+\left(\frac{\Omega}{2\Pi}-\right.$$

$$\left.\left.\frac{1}{4}\right)H_{3\,0}^{0\,3}\left(\frac{m_1\left(\frac{4}{3}*\left(\frac{Sin^2\left(\frac{\Pi}{L}\right)}{Sin^2(\Omega)}\right)\right)^{\frac{\gamma_1}{2}}}{\Omega_1\,\mu^{\frac{-\gamma_1}{2}}}\left(\frac{m_2}{\Omega_2}\right)^{\frac{\gamma_1}{\gamma_2}}\middle|\begin{matrix}\left(1,\frac{-\gamma_1}{2}\right),(1-m_1,1),\left(1-m_2,\frac{\gamma_1}{\gamma_2}\right)\\ -\end{matrix}\right)\right] \quad (4.21)$$

4.2.3 Closed form expression of SER of MQAM scheme under EGC

Again, with [120], Symbol Error Rate (SER) for M-QAM is given as

$$P_e = 4\Omega\left(\frac{1}{12}M_\gamma\left(\varepsilon_{qam}\right) + \frac{1}{4}M_\gamma\left(\frac{4}{3}\varepsilon_{qam}\right)\right) - 4\Omega^2\frac{1}{8}M_\gamma\left(2\varepsilon_{qam}\right) \tag{4.22}$$

where $\Omega = 1 - \frac{1}{\sqrt{M}}$ and $\varepsilon_{qam} = \frac{3}{2(M-1)}$, $M_\gamma(.)$ denotes MGF as in Eq. (4.19).

Substituting Eq. (4.19) into Eq. (4.22), we get

$$P_e = \frac{2\gamma_1\left(1-\frac{1}{\sqrt{M}}\right)}{\Gamma(m_1)\Gamma(m_2)}\left(\left(\frac{1}{12}H_{3\ 0}^{0\ 3}\left(\frac{m_1\left(\frac{3}{2(M-1)}\right)^{\frac{\gamma_1}{2}}}{\Omega_1\ \mu^{\frac{-\gamma_1}{2}}}\left(\frac{m_2}{\Omega_2}\right)^{\frac{\gamma_1}{\gamma_2}}\middle|\begin{matrix}\left(1,\frac{-\gamma_1}{2}\right),(1-m_1,1),\left(1-m_2,\frac{\gamma_1}{\gamma_2}\right)\\ -\end{matrix}\right) + \right.\right.$$

$$\left.\left.\frac{1}{4}H_{3\ 0}^{0\ 3}\left(\frac{m_1\left(\frac{2}{(M-1)}\right)^{\frac{\gamma_1}{2}}}{\Omega_1\ \mu^{\frac{-\gamma_1}{2}}}\left(\frac{m_2}{\Omega_2}\right)^{\frac{\gamma_1}{\gamma_2}}\middle|\begin{matrix}\left(1,\frac{-\gamma_1}{2}\right),(1-m_1,1),\left(1-m_2,\frac{\gamma_1}{\gamma_2}\right)\\ -\end{matrix}\right)\right) - \frac{1}{8}\left(1 - \right.\right.$$

$$\left.\left.\frac{1}{\sqrt{M}}\right)H_{3\ 0}^{0\ 3}\left(\frac{m_1\left(\frac{3}{(M-1)}\right)^{\frac{\gamma_1}{2}}}{\Omega_1\ \mu^{\frac{-\gamma_1}{2}}}\left(\frac{m_2}{\Omega_2}\right)^{\frac{\gamma_1}{\gamma_2}}\middle|\begin{matrix}\left(1,\frac{-\gamma_1}{2}\right),(1-m_1,1),\left(1-m_2,\frac{\gamma_1}{\gamma_2}\right)\\ -\end{matrix}\right)\right) \tag{4.23}$$

Again, it is noticeable that Eq. (4.21) and Eq. (4.23) are used to calculate the SER of M-PSK and MQAM modulation schemes respectively under different turbulence conditions. Also, Eq. (4.21) and Eq. (4.23) are used to achieve SER over other fading models like Gamma-Gamma fading channel and Double Weibull fading channel as a special case.

4.3 RESULTS AND DISCUSSION

This section presents the numerical analysis of the proposed analytical expressions for performance metrics such as average capacity and symbol error rate (SER), carried out using MATLAB. Specifically, we present the average capacity over Double Generalized fading channel under EGC scheme. In addition, we present SER of MPSK and MQAM modulation schemes for the same scenario. It is worthful to mention that all the possible turbulence conditions namely, weak, moderate and strong turbulence conditions are included in the

analysis. However, simulation parameters used in the numerical analysis are given in Table 4.1.

Table 4.1 Simulation Parameters

S. No	Distribution Parameter	Weak Turbulence	Moderate Turbulence	Strong Turbulence
1	m_1	4	0.55	0.5
2	m_2	4.5	2.35	1.8
3	γ_1	2.1	2.1690	1.8621
4	γ_2	2.1	0.8530	0.7638
5	Ω_1	1.06	1.5793	1.5074
6	Ω_2	1.06	0.9671	0.9280
7	$\sigma Rytov2$	0.1	2	25

In Fig. 4.2, AC is depicted under EGC scheme from L=1 to L=4 considering both weak and strong turbulence conditions. Over strong turbulence condition, it is observed that as number of diversity branches increases, the capacity increases. The improvement of capacity is more as it increases from L=1 to L=2 than L=2 to L=3 which is found in agreement with [115]. Also, the same trend is observed over weak turbulence condition. Similarly, it is observed that as the fading severity increases from weak to strong, the capacity for L=1 decreases from 9.81bits/Hz to 7.543 bits/Hz which is approximately 23%.

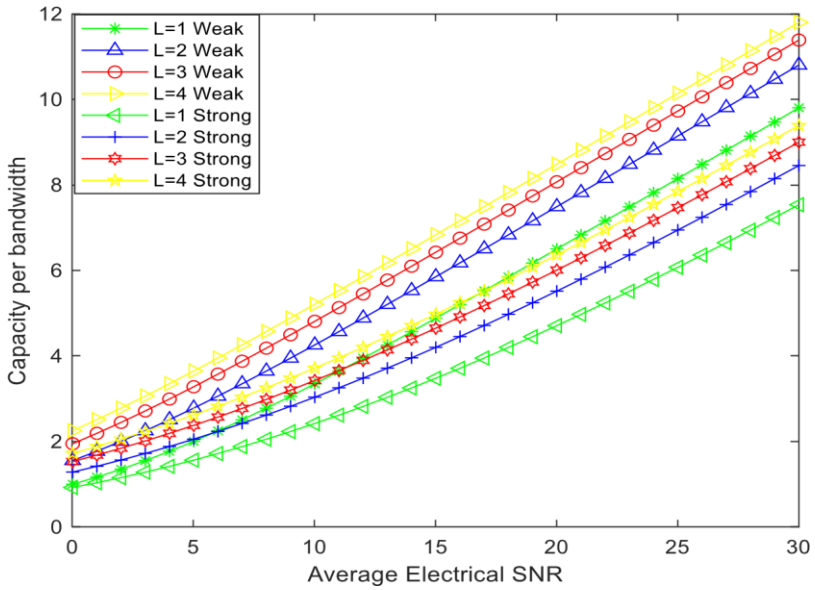

Fig. 4.2 AC over Double GG fading under EGC scheme over weak and strong turbulence conditions

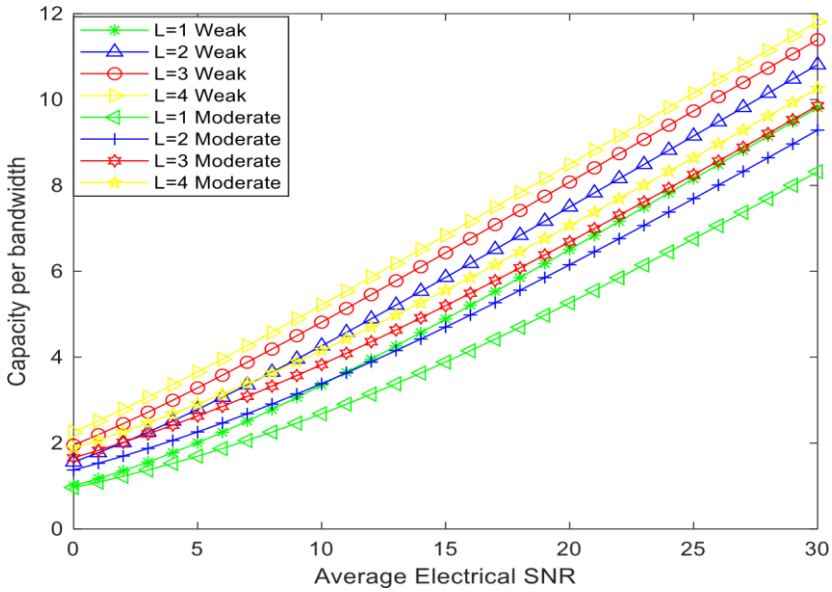

Fig. 4.3 AC over Double GG fading under EGC scheme over weak and moderate turbulence conditions

In Fig. 4.3, AC is depicted under EGC scheme for variation of diversity branches from L=1 to L=4 considering weak and moderate turbulence conditions. Like Fig. 1, for variation of L, the

same results are obtained over moderate turbulence condition. Similarly, it is found that the capacity for L=1 decreases by 15.3% as fading severity increases from weak to moderate. Also, for the given value of L, as fading severity increases, the capacity decreases. So, the same performance is obtained by increasing the number of diversity branches. This result shows the perfect agreement with [120]. This trend is valid over all turbulence conditions.

In Fig. 4.4, AC is depicted under EGC scheme from L=1 to L=4 considering moderate and strong turbulence conditions. It is observed that the effect of fading severity is more at higher values of electrical SNR in comparison with lower values of electrical SNR. Also, it is evident that the effect of fading severity is less at L=4 as compared to L=1. This trend is valid over all turbulence conditions.

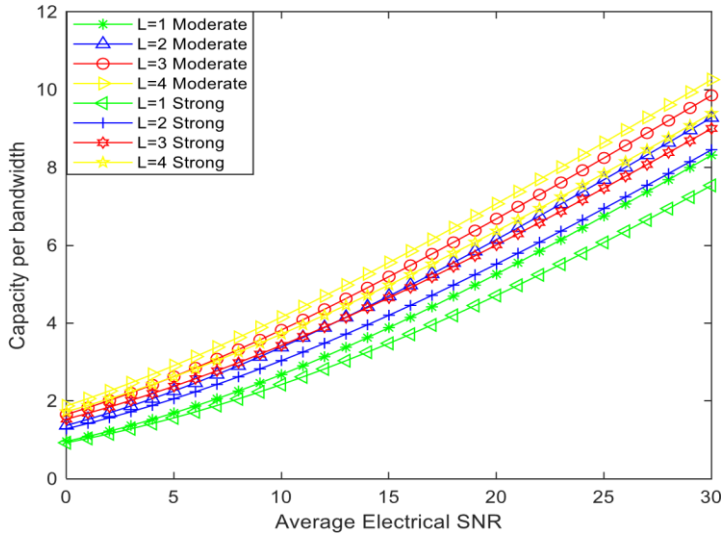

Fig. 4.4 AC over Double GG fading with EGC scheme for L= 1, 2, 3 and 4 over moderate and strong turbulence conditions

Fig. 4.5 shows AC under EGC scheme for different fading channel conditions such as Double Generalized Gamma, Gamma-Gamma and Double Weibull fading distributions. Also, both weak and strong turbulence conditions are considered. It is noticeable that AC for Double GG distribution is better than that of Gamma-Gamma fading distribution over weak turbulence

condition. However, over strong turbulence condition, AC for Double GG distribution is almost equal to that of Gamma-Gamma fading distribution.

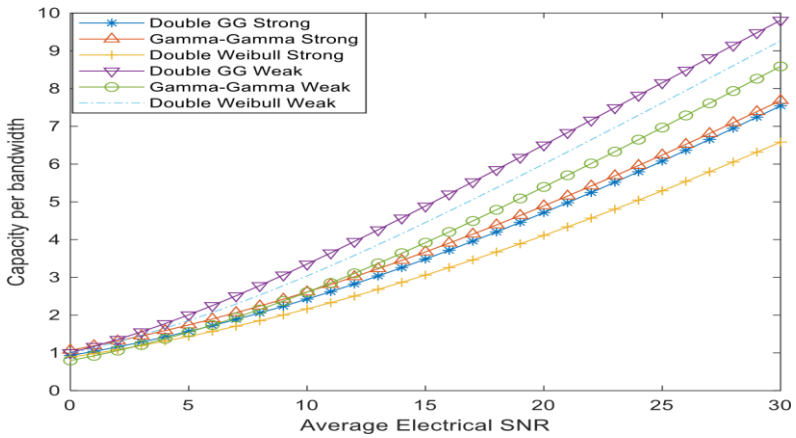

Fig. 4.5 AC for various fading distribution under EGC scheme over weak and strong turbulence conditions

Fig. 4.6, shows the comparison of AC under EGC scheme for Double Generalized Gamma, GammaGamma and Double Weibull fading distributions over weak and moderate turbulence conditions. Over moderate turbulence condition, it is seen that AC for Double GG distribution is superior compared to that of Gamma-Gamma and Double Weibull distributions.

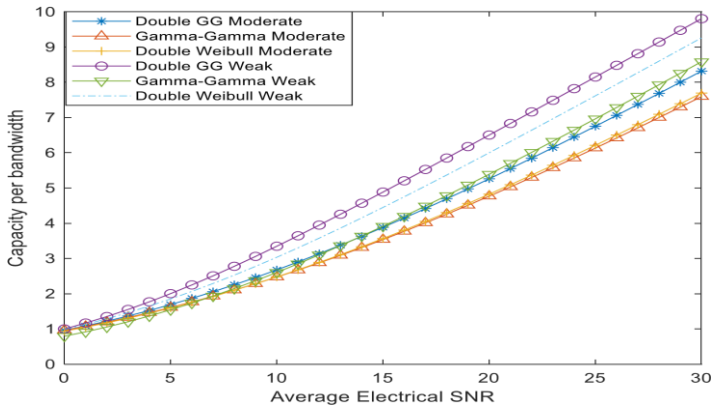

Fig. 4.6 AC for various fading distribution under EGC scheme over weak and moderate turbulence conditions

Fig. 4.7 the comparison of AC under EGC scheme for Double Generalized Gamma, Gamma-Gamma and Double Weibull fading distributions over moderate and strong turbulence conditions. The findings that AC for Gamma-Gamma distribution overestimates Double GG distribution by 1.8% at average SNR of 30 dB over strong turbulence condition.

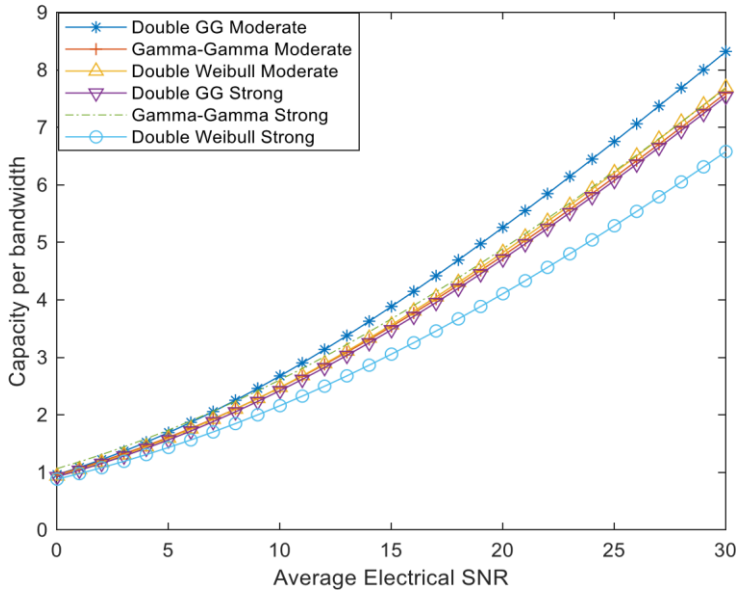

Fig. 4.7 AC over various fading distribution under EGC scheme moderate and strong turbulence conditions

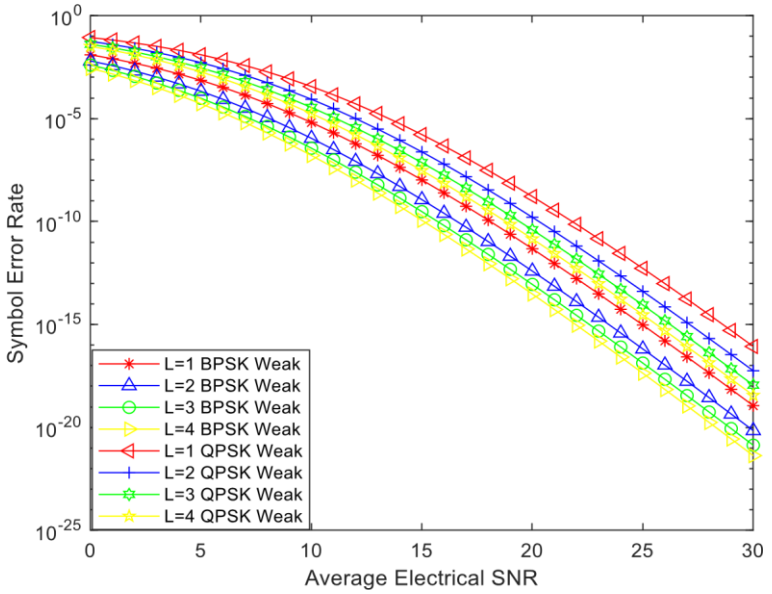

Fig. 4.8 SER of BPSK and QPSK for Double GG fading under EGC scheme over weak turbulence condition for L= 1, 2, 3 and 4

Fig. 4.7shows SER of BPSK and QPSK for L=1 to L=4 under weak turbulence condition. It is observed that as the number of diversity branches increases from L=1 to L=4, SER improves. The improvement is more as it increases from L=1 to L=2 than L=2 to L=3 which is found in agreement with [115].

Fig. 4.9 shows SER of BPSK and QPSK from L=1 to L=4 considering moderate turbulence condition. It is observed that increase in SNR reflects reduction in SER. Also, SER of BPSK with L=1 is reduced by several magnitude as compared to SER of QPSK with L=1 over a given turbulence condition. This is again well-established theoretical background. This trend is valid over all turbulence conditions.

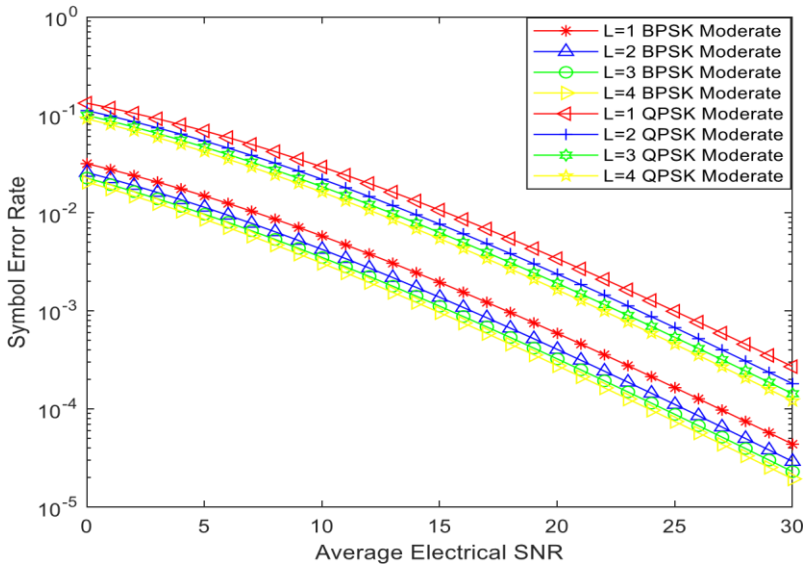

Fig. 4.9 SER of BPSK and QPSK for Double GG fading under EGC scheme over moderate turbulence condition for L= 1, 2, 3 and 4

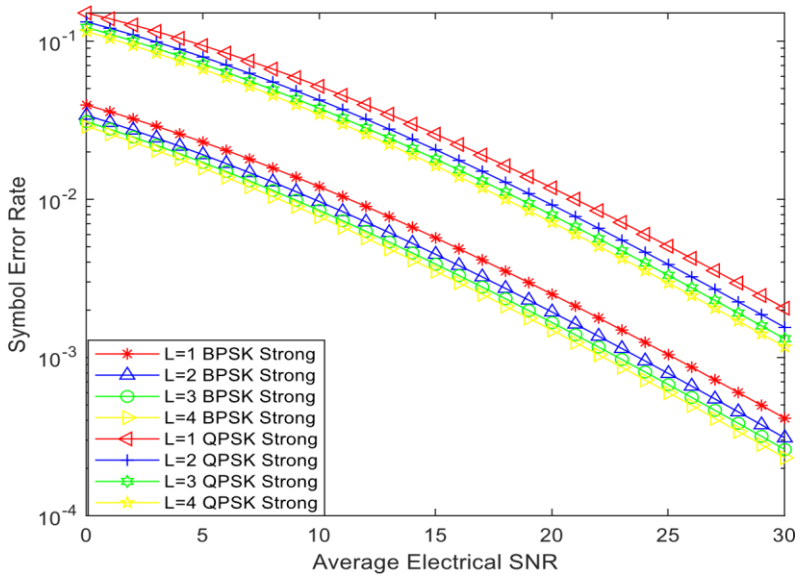

Fig. 4.10 SER of BPSK and QPSK for Double GG fading under EGC scheme over strong turbulence condition for L= 1, 2, 3 and 4

Fig. 4.10 shows SER of BPSK and QPSK from L=1 to L=4 considering strong turbulence condition. It is observed that SER of QPSK is $3.7\text{x}10^{-19}$, $1.2\text{x}10^{-4}$ and $1.1\text{x}10^{-3}$ for an average electrical SNR of 30dB over weak, moderate and strong turbulence conditions respectively. It is clearly seen that SNR requirement increases as fading severity increases for a particular value of L. This trend is valid over all turbulence conditions.

Fig. 4.11 shows SER of 4QAM and 8QAM from L=1 to L=4 considering weak turbulence condition. It is observed that increase in SNR reflects reduction in SER. Also, SER of 4QAM with L=1 is reduced by several magnitude as compared to SER of 8QAM with L=1 over a given turbulence condition. This is again well-established theoretical background. This trend is valid over all turbulence conditions.

Fig. 4.12 shows SER of 4QAM and 8QAM from L=1 to L=4 considering moderate turbulence condition. It is observed that SER of 10^{-3} is obtained at an average electrical SNR of 14 dB for 4QAM over moderate turbulence condition whereas the same performance is achieved at SER

of 19 dB over strong turbulence condition. It is clearly observed that SNR requirement increases as fading severity increases for a particular value of L. This trend is valid over all turbulence conditions.

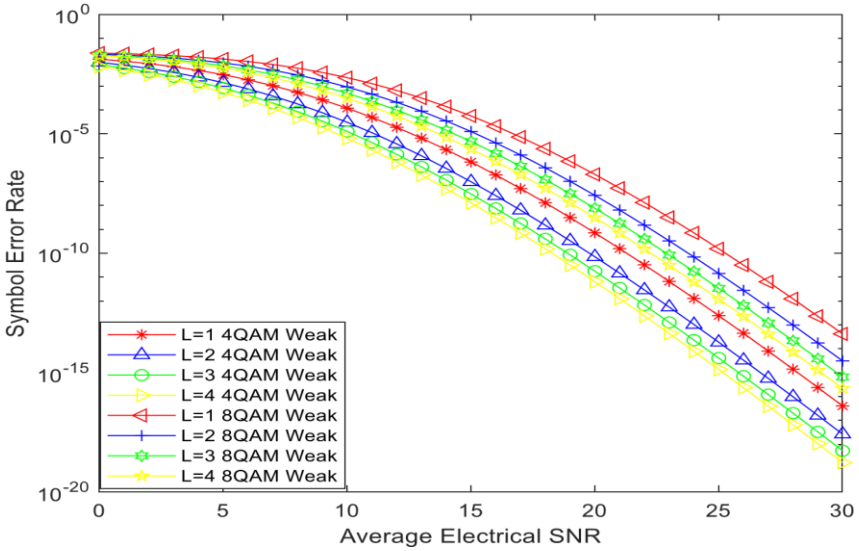

Fig. 4.11 SER of 4QAM and 8QAM for Double GG fading under EGC scheme over weak turbulence condition for L= 1, 2, 3 and 4

Fig. 4.13 shows SER of 4QAM and 8QAM from L=1 to L=4 considering strong turbulence condition. It is seen that SER of 4QAM is 0.001442, 0.001133, 0.0009805 and 0.0008841 for L=1, L=2, L=3 and L=4 respectively at an average electrical SNR of 20 dB. So, it is concluded that that as the number of diversity branches increases from L=1 to L=4, SER improves. The improvement is more for L=1 to L=2 as compared to L=2 to L=3, shows perfect agreement with [115].

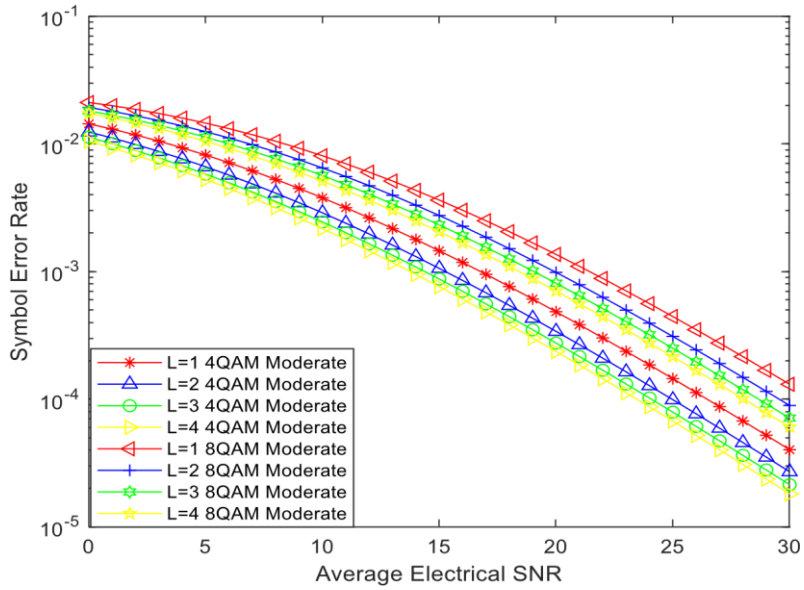

Fig. 4.12 SER of 4QAM and 8QAM for Double GG fading under EGC scheme over moderate turbulence condition for L= 1, 2, 3 and 4

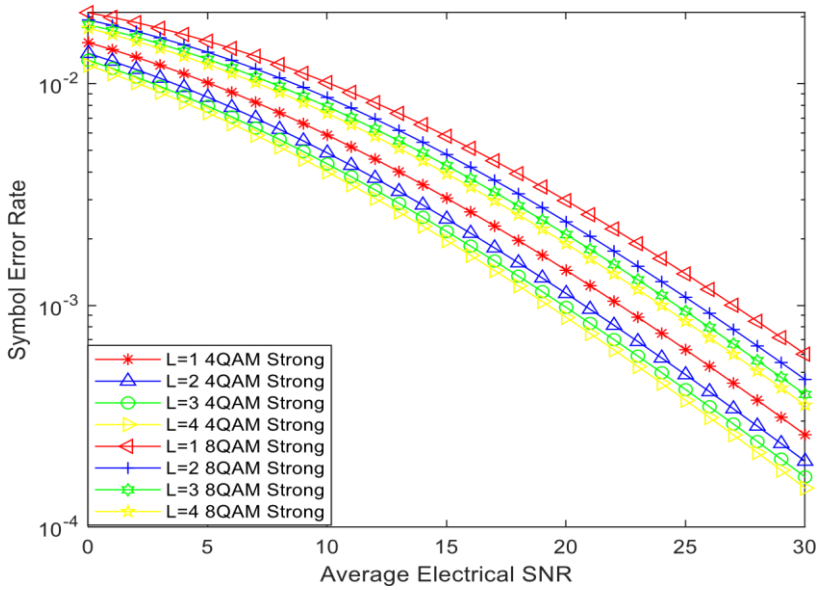

Fig. 4.13 SER of 4QAM and 8QAM for Double GG fading under EGC scheme over strong turbulence condition for L= 1, 2, 3 and 4

Fig. 4.14 shows SER of BPSK under EGC scheme for different fading distributions such as Double Generalized Gamma, Gamma-Gamma and Double Weibull over moderate and strong turbulence

conditions. It is found that SER of BPSK for Double GG is lowest over moderate and strong turbulence conditions.

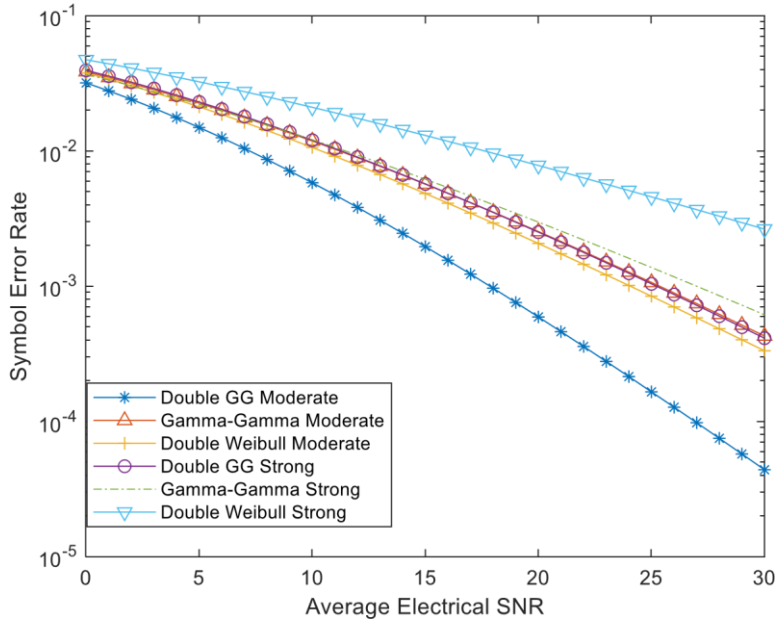

Fig. 4.14 SER of BPSK for various fading distributions under EGC scheme over moderate and strong turbulence conditions

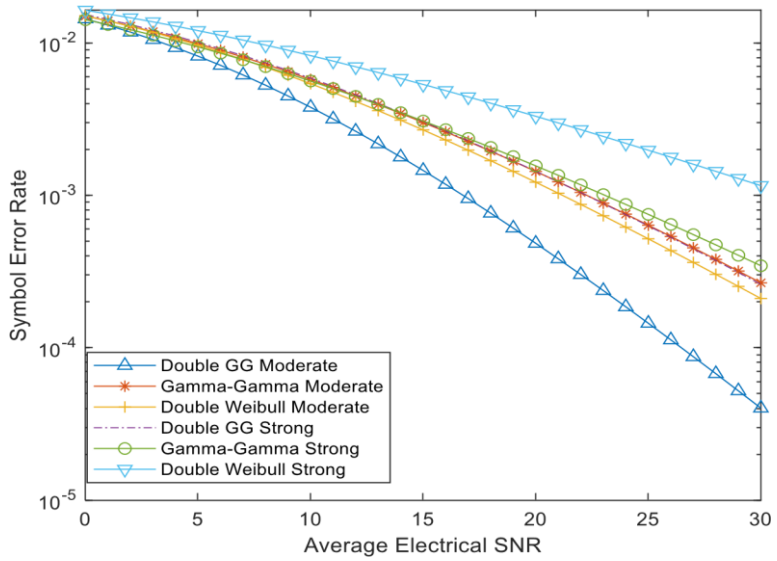

Fig. 4.15 SER of 4QAM over various fading distributions under EGC scheme over moderate and strong turbulence conditions

Fig. 4.15 shows SER of 4QAM under EGC scheme for different fading distributions such as Double Generalized Gamma, Gamma-Gamma and Double Weibull over moderate and strong turbulence conditions. Similar conclusion as shown in fig. 4.14 for BPSK is arrived for 4QAM from fig. 15 over moderate and strong turbulence conditions.

4.4 Summary

In this chapter, the performance improvement of FSO system is analyzed in terms of AC and SER. Specifically, analytical expression of AC for Double Generalized Gamma fading distribution under Equal Gain Combining (EGC) is presented. In addition, MGF based analytical expression of Symbol Error Rate (SER) of M-PSK and M-QAM for Double Generalized Gamma fading distribution under EGC scheme in terms of Fox-H is presented. Various special cases of proposed expressions are deduced for different fading distributions such as Double Weibull and Gamma-Gamma. It is evident from the results that increasing the diversity branches improve the performance in terms of AC and SER. However, the capacity improvement is more as it increases from L=1 to L=2 than L=2 to L=3 which is found in agreement with the literature. Further, at SNR of 30 dB, SER of QPSK are $3.7\text{x}10^{-19}$, $1.2\text{x}10^{-4}$ and $1.1\text{x}10^{-3}$ over weak, moderate and strong turbulence conditions respectively. Similarly, SER of BPSK, 4QAM and 8QAM is analyzed over weak, moderate and strong turbulence conditions. This implies that irrespective of fading scenario and/modulation scheme, the effect of moderate turbulence lies in between strong and weak turbulence conditions. This shows perfect agreement with the theoretical background. Performance analysis under different diversity schemes for generic fading distribution can be the future scope of this research work.

CHAPTER 5

OUTAGE AND ERGODIC CAPACITY OF MIXTURE GAMMA AND DOUBLE GENERALIZED GAMMA DISTRIBUTION IN DUAL HOP RF/FSO TRANSMISSION SYSTEM

In this two-hop paradigm, the first hop is the RF connection (from the transmitter to the relay), and the second is the FSO link (from the relay to the receiver). The model is based on the Double Generalised Gamma distribution in the FSO link and the Mixture Gamma distribution in the RF link. We evaluate the effectiveness of our mathematical model for outage capacity and finally, we evaluate the effectiveness of our mathematical model for Ergodic Capacity.

5.1 Outage and Ergodic Capacity

The equivalent PDF of the dual-hop model containing Mixture Gamma in the RF link and Double GG in the FSO link is given by [100]:

$$f_{\gamma eq}(\gamma) = \sum_{i=1}^{N} \alpha_i \gamma^{\beta_i - 1} 1\, e^{-\zeta_i \gamma} - \sum_{i=1}^{N} \alpha_i \gamma^{\beta_i - 1} e^{-\zeta_i \gamma}$$

$$\times \frac{p^{(m_2 - 1/2)} q^{(m_1 - 1/2)} 2\pi^{\left(1 - \frac{p+q}{2}\right)}}{\Gamma m_1 \Gamma m_2}$$

$$G_{1,p+q+1}^{p+q,1}\left[\left(\left(\frac{\gamma}{\bar{\Upsilon}}\right)^{\frac{p\gamma_2}{2}} \frac{1}{I_l^{p\gamma_2}} \frac{{m_1}^q {m_2}^p}{p^p q^q {\Omega_1}^q {\Omega_2}^p}\middle|_{\Delta(q:m_1),\Delta(p:m_2),0}^{1}\right)\right] + \frac{\gamma_2 p^{(m_2 + 1/2)} q^{(m_1 - 1/2)} 2\pi^{\left(1 - \frac{p+q}{2}\right)}}{2\Gamma m_1 \Gamma m_2\, \gamma}$$

$$G_{0,p+q}^{p+q,0}\left[\left(\left(\frac{\gamma}{\bar{\Upsilon}}\right)^{\frac{p\gamma_2}{2}} \frac{1}{I_l^{p\gamma_2}} \frac{{m_1}^q {m_2}^p}{p^p q^q {\Omega_1}^q {\Omega_2}^p}\middle|_{\Delta(q:m_1),\Delta(p:m_2)}^{-}\right)\right] - \frac{\gamma_2 p^{(m_2 + 1/2)} q^{(m_1 - 1/2)} 2\pi^{\left(1 - \frac{p+q}{2}\right)}}{2\Gamma m_1 \Gamma m_2\, \gamma}$$

$$G_{0,p+q}^{p+q,0}\left[\left(\left(\frac{\gamma}{\bar{\Upsilon}}\right)^{\frac{p\gamma_2}{2}} \frac{1}{I_l^{p\gamma_2}} \frac{{m_1}^q {m_2}^p}{p^p q^q {\Omega_1}^q {\Omega_2}^p}\middle|_{\Delta(q:m_1),\Delta(p:m_2)}^{-}\right)\right]$$

$$\times \sum_{i=1}^{N} \alpha_i \zeta^{-\beta_i} G_{1,2}^{1,1}\left(\zeta_i \gamma \middle|_{\beta_i,0}^{1}\right) \tag{5.1}$$

5.1.1 Outage Capacity

Outage capacity is one of the most extensive and vital communication system and network design metrics. In short, it specifies the upper limit of the amount of data wired or can be properly received by a wireless device. Therefore, knowledge of Outage capacity allows communication system designers to predict the number of possible users and share the transmission band by specifying the destination data Rate and type of data that can be sent, depending on the quality of service.

Outage capacity is the probability of specified failure, the likelihood that the signal is not decoded correctly. But the value of outage capacity depends mainly on it. The possibility of failure and the Signal to Noise Ratio (SNR) are expressed as the product of the two functions of outage probability. When one of the two functions increases, the other decreases, and vice versa.

Outage Capacity is defined as:

$$\bar{C} = B \log_2(1 + \gamma_{eq}) \tag{5.2}$$

So, taking B=1

$$\gamma_{eq} = \frac{2^{\bar{C}}-1}{\varpi} = x \tag{5.3}$$

Outage capacity is obtained by putting γ_{th} with x in equations (4.17) & (4.18) of [114] for the outage probability of double GG with Nakagami-m and Rayleigh, respectively.

CASE 1: For Nakagami-m:

The parameter values are given from [79] as:

$$\mathrm{N} = 1, \quad \alpha_1 = \frac{\mathrm{m}^{\mathrm{m}}}{\Gamma(\mathrm{m})\bar{\gamma}^{\mathrm{m}}}, \quad \beta_1 = \mathrm{m}, \quad \zeta_1 = \frac{\mathrm{m}}{\bar{\gamma}} \tag{5.4}$$

$$F_{outage}(x) = \frac{1}{\Gamma(\mathrm{m})} \mathrm{G}_{1,2}^{1,1}\left(\frac{\mathrm{m}}{\bar{\Upsilon}} x \middle|_{\mathrm{m},0}^{1}\right) + \frac{p^{(m_2-1/2)} q^{(m_1-1/2)} 2\pi^{\left(1-\frac{p+q}{2}\right)}}{\Gamma m_1 \Gamma m_2} G_{1,p+q+1}^{p+q,1}$$

$$\left[\left(\left(\frac{x}{\bar{\Upsilon}}\right)^{\frac{p\gamma_2}{2}} \frac{1}{{I_l}^{p\gamma_2}} \frac{{m_1}^q {m_2}^p}{p^p q^q {\Omega_1}^q {\Omega_2}^p} \middle|_{\Delta(q:m_1),\Delta(p:m_2),0}^{1}\right)\right] \tag{5.5}$$

$$- \frac{1}{\Gamma(\mathrm{m})} \mathrm{G}_{1,2}^{1,1}\left(\frac{\mathrm{m}}{\bar{\Upsilon}} x \middle|_{\mathrm{m},0}^{1}\right)$$

$$\times \frac{p^{(m_2-1/2)} q^{(m_1-1/2)} 2\pi^{\left(1-\frac{p+q}{2}\right)}}{\Gamma m_1 \Gamma m_2} G_{1,p+q+1}^{p+q,1}\left[\left(\left(\frac{\mathrm{x}}{\bar{\Upsilon}}\right)^{\frac{p\gamma_2}{2}} \frac{1}{{I_l}^{p\gamma_2}} \frac{{m_1}^q {m_2}^p}{p^p q^q {\Omega_1}^q {\Omega_2}^p} \middle|_{\Delta(q:m_1),\Delta(p:m_2),0}^{1}\right)\right]$$

CASE 2: For Rayleigh:

$$\mathrm{N} = 1, \alpha_1 = \frac{1}{\bar{\Upsilon}}, \beta_1 = 1, \zeta_1 = \frac{1}{\bar{\Upsilon}}, m = 1 \tag{5.6}$$

$$F_{outage}(\mathrm{x}) = \mathrm{G}_{1,2}^{1,1}\left(\frac{1}{\bar{\Upsilon}} x \middle|_{1,0}^{1}\right) +$$

$$\frac{p^{(m_2-1/2)} q^{(m_1-1/2)} 2\pi^{\left(1-\frac{p+q}{2}\right)}}{\Gamma m_1 \Gamma m_2} G_{1,p+q+1}^{p+q,1}\left[\left(\left(\frac{x}{\bar{\Upsilon}}\right)^{\frac{p\gamma_2}{2}} \frac{1}{{I_l}^{p\gamma_2}} \frac{{m_1}^q {m_2}^p}{p^p q^q {\Omega_1}^q {\Omega_2}^p} \middle|_{\Delta(q:m_1),\Delta(p:m_2),0}^{1}\right)\right] - \mathrm{G}_{1,2}^{1,1}\left(\frac{1}{\bar{\Upsilon}} x \middle|_{1,0}^{1}\right) \times$$

$$\frac{p^{(m_2-1/2)} q^{(m_1-1/2)} 2\pi^{\left(1-\frac{p+q}{2}\right)}}{\Gamma m_1 \Gamma m_2} G_{1,p+q+1}^{p+q,1}\left[\left(\left(\frac{x}{\bar{\Upsilon}}\right)^{\frac{p\gamma_2}{2}} \frac{1}{{I_l}^{p\gamma_2}} \frac{{m_1}^q {m_2}^p}{p^p q^q {\Omega_1}^q {\Omega_2}^p} \middle|_{\Delta(q:m_1),\Delta(p:m_2),0}^{1}\right)\right] \tag{5.7}$$

5.1.2 Ergodic Capacity

This section analyzes the Ergodic Capacity, the highest data rate received without errors. It can also be said as the maximum error-free data rate. The mathematical computation for the EC of the system model under weak turbulence conditions is presented as:

On putting the values $m_1 = 4$, $m_2 = 4.5$, $p = 1$, $q = 1$, $\gamma_1 = 2.1$, $\gamma_2 = 2$, $\Omega_1 = 1.0676$, $\Omega_2 =$

1.06 in equation (5.1) given below:

$$f_{\gamma eq}(\gamma) = \sum_{i=1}^{N} \alpha_i \gamma^{\beta_i - 1} \quad e^{-\zeta_i \gamma} - \sum_{i=1}^{N} \alpha_i \gamma^{\beta_i - 1} e^{-\zeta_i \gamma} \frac{1}{\Gamma m_1 \Gamma m_2} G_{1,3}^{2,1}\left[\left(\left(\frac{\gamma}{\bar{\Upsilon}}\right)^1 \frac{1}{I_l^{\,2}} \frac{m_1^{\,q} m_2^{\,p}}{\Omega_1^{\,q} \Omega_2^{\,p}} \middle|_{4,4.5,0}^{1}\right)\right]$$

$$+ \frac{1}{\Gamma m_1 \Gamma m_2 \gamma} G_{0,2}^{2,0}\left[\left(\left(\frac{\gamma}{\bar{\Upsilon}}\right)^1 \frac{1}{I_l^{\,2}} \frac{m_1^{\,q} m_2^{\,p}}{\Omega_1^{\,q} \Omega_2^{\,p}} \middle|_{4,4.5}^{-}\right)\right] \tag{5.8}$$

$$- \frac{1}{\Gamma m_1 \Gamma m_2 \gamma} G_{0,2}^{2,0}\left[\left(\left(\frac{\gamma}{\bar{\Upsilon}}\right)^1 \frac{1}{I_l^{\,2}} \frac{m_1^{\,q} m_2^{\,p}}{\Omega_1^{\,q} \Omega_2^{\,p}} \middle|_{4,4.5}^{-}\right)\right] \times \sum_{i=1}^{N} \alpha_i \zeta^{-\beta_i} G_{1,2}^{1,1}\left(\zeta_i \gamma \middle|_{\beta_i,0}^{1}\right)$$

From [88] the ergodic capacity is given by:

$$C = \int_0^{\infty} \log(1 + \varpi\gamma)\, f_{\gamma eq}(\gamma) d\gamma \tag{5.9}$$

$$C = \int_0^{\infty} \log(1 + \varpi\gamma) \sum_{i=1}^{N} \alpha_i \gamma^{\beta_i - 1} \; e^{-\zeta_i \gamma}$$

$$- \sum_{i=1}^{N} \alpha_i \gamma^{\beta_i - 1} e^{-\zeta_i \gamma} \times \frac{1}{\Gamma m_1 \Gamma m_2} G_{1,3}^{2,1}\left[\left(\left(\frac{\gamma}{\bar{\Upsilon}}\right)^1 \frac{1}{I_l^{\,2}} \frac{m_1^{\,q} m_2^{\,p}}{\Omega_1^{\,q} \Omega_2^{\,p}} \middle|_{4,4.5,0}^{1}\right)\right]$$

$$+ \frac{1}{\Gamma m_1 \Gamma m_2 \gamma} G_{0,2}^{2,0}\left[\left(\left(\frac{\gamma}{\bar{\Upsilon}}\right)^1 \frac{1}{I_l^{\,2}} \frac{m_1^{\,q} m_2^{\,p}}{\Omega_1^{\,q} \Omega_2^{\,p}} \middle|_{4,4.5}^{-}\right)\right] \tag{5.10}$$

$$- \frac{1}{\Gamma m_1 \Gamma m_2 \gamma} G_{0,2}^{2,0}\left[\left(\left(\frac{\gamma}{\bar{\Upsilon}}\right)^1 \frac{1}{I_l^{\,2}} \frac{m_1^{\,q} m_2^{\,p}}{\Omega_1^{\,q} \Omega_2^{\,p}} \middle|_{4,4.5}^{-}\right)\right] \times \sum_{i=1}^{N} \alpha_i \zeta^{-\beta_i} G_{1,2}^{1,1}\left(\zeta_i \gamma \middle|_{\beta_i,0}^{1}\right) d\gamma$$

$$C$$

$$= \left(\sum_{i=1}^{N} \alpha_i \zeta_i^{-\beta_i} \; G_{3,2}^{1,3} \left[\left(\frac{\varpi}{\zeta_i} \right) \middle| \begin{matrix} 1-\beta_i, 1,1 \\ 1,0 \end{matrix} \right] \right)$$

$$- \sum_{i=1}^{N} \alpha_i \zeta_i^{-\beta_i} \left(\frac{1}{\Gamma m_1 \Gamma m_2} \right) G_{1,0:2,2:1,3}^{0,1:1,2:2,1} \left[\begin{matrix} 1-\beta_i \\ - \end{matrix} \middle| \begin{matrix} 1,1 \\ 1,0 \end{matrix} \middle| \begin{matrix} 1 \\ 4,4.5,0 \end{matrix} \middle| \frac{\varpi}{\zeta_i}, \frac{\left(\frac{1}{\bar{\Upsilon}}\right)^1 \frac{1}{{I_l}^2} \frac{{m_1}^1 {m_2}^1}{{\Omega_1}^1 {\Omega_2}^1}}{{\zeta_i}^1} \right]$$

$$+ \frac{1}{\Gamma m_1 \Gamma m_2} \; G_{2,4}^{4,1} \left(\left. \frac{\left(\frac{1}{\bar{\Upsilon}}\right)^1 \frac{1}{{I_l}^2} \frac{{m_1}^q {m_2}^p}{{\Omega_1}^q {\Omega_2}^p}}{\varpi^1} \right|_{4,4.5,0,0}^{0,1} \right) \tag{5.11}$$

$$- \sum_{i=1}^{N} \alpha_i \zeta_i^{-\beta_i} \left(\frac{1}{\Gamma m_1 \Gamma m_2} \right) G_{2,0:2,2:1,2}^{0,2:1,2:1,1} \left[\begin{matrix} -3, -3.5 \\ - \end{matrix} \middle| \begin{matrix} 1,1 \\ 1,0 \end{matrix} \middle| \begin{matrix} 1 \\ \beta_i, 0 \end{matrix} \middle| \frac{\varpi}{\left(\frac{1}{\bar{\Upsilon}}\right)^1 \frac{1}{{I_l}^2} \frac{{m_1}^1 {m_2}^1}{{\Omega_1}^1 {\Omega_2}^1}}, \frac{{\zeta_i}^1}{\left(\frac{1}{\bar{\Upsilon}}\right)^1 \frac{1}{{I_l}^2} \frac{{m_1}^1 {m_2}^1}{{\Omega_1}^1 {\Omega_2}^1}} \right]$$

CASE 1: For Nakagami-m:

Using the below-mentioned values as given in [84]:

$$\mathrm{N} = 1, \alpha_1 = \frac{\mathrm{m}^{\mathrm{m}}}{\Gamma(\mathrm{m}) \bar{\gamma}^{\mathrm{m}}}, \beta_1 = \mathrm{m}\,, \zeta_1 = \frac{\mathrm{m}}{\bar{\gamma}} \tag{5.12}$$

$$
\begin{aligned}
\mathrm{C} &= \left(\frac{1}{\Gamma(\mathrm{m})} G_{3,2}^{1,3}\left[\left(\frac{\varpi}{\frac{\mathrm{m}}{\bar{\Upsilon}}}\right)\middle|\begin{matrix}1-\mathrm{m},1,1\\1,0\end{matrix}\right]\right) \\
&- \frac{1}{\Gamma(\mathrm{m})}\left(\frac{1}{\Gamma m_1 \Gamma m_2}\right) G_{1,0:2,2:1,3}^{0,1:1,2:2,1}\left[\begin{matrix}1-\mathrm{m}\\-\end{matrix}\middle|\begin{matrix}1,1\\1,0\end{matrix}\middle|\begin{matrix}1\\4,4.5,0\end{matrix}\middle|\frac{\varpi}{\frac{\mathrm{m}}{\bar{\Upsilon}}}, \frac{\left(\frac{1}{\bar{\Upsilon}}\right)^1 \frac{1}{{I_l}^2}\frac{{m_1}^1{m_2}^1}{{\Omega_1}^1{\Omega_2}^1}}{\frac{\mathrm{m}}{\bar{\Upsilon}}}\right] \\
&+ \frac{1}{\Gamma m_1 \Gamma m_2}\, G_{2,4}^{4,1}\left(\frac{\left(\frac{1}{\bar{\Upsilon}}\right)^1 \frac{1}{{I_l}^2}\frac{{m_1}^q{m_2}^p}{{\Omega_1}^q{\Omega_2}^p}}{\varpi^1}\middle|\begin{matrix}0,1\\4,4.5,0,0\end{matrix}\right) \\
&- \frac{1}{\Gamma(\mathrm{m})}\left(\frac{1}{\Gamma m_1 \Gamma m_2}\right) G_{2,0:2,2:1,2}^{0,2:1,2:1,1}\left[\begin{matrix}-3,-3.5\\-\end{matrix}\middle|\begin{matrix}1,1\\1,0\end{matrix}\middle|\begin{matrix}1\\\mathrm{m},0\end{matrix}\middle|\frac{\varpi}{\left(\frac{1}{\bar{\Upsilon}}\right)^1 \frac{1}{{I_l}^2}\frac{{m_1}^1{m_2}^1}{{\Omega_1}^1{\Omega_2}^1}}, \frac{\frac{\mathrm{m}}{\bar{\Upsilon}}}{\left(\frac{1}{\bar{\Upsilon}}\right)^1 \frac{1}{{I_l}^2}\frac{{m_1}^1{m_2}^1}{{\Omega_1}^1{\Omega_2}^1}}\right]
\end{aligned}
\tag{5.13}
$$

CASE 2: For Rayleigh:

Using the below-mentioned values as given in [84]:

$$
\mathrm{N} = 1, \alpha_1 = \frac{1}{\bar{\gamma}}, \beta_1 = 1, \zeta_1 = \frac{1}{\bar{\gamma}}, m = 1 \tag{5.14}
$$

$$
\mathrm{C} = \left(G_{3,2}^{1,3}\left[\left(\frac{\varpi}{1}\gamma\right)\middle|\begin{matrix}0,1,1\\1,0\end{matrix}\right]\right) - \left(\frac{1}{\Gamma m_1 \Gamma m_2}\right) G_{1,0:2,2:1,3}^{0,1:1,2:2,1}\left[\begin{matrix}0\\-\end{matrix}\middle|\begin{matrix}1,1\\1,0\end{matrix}\middle|\begin{matrix}1\\4,4.5,0\end{matrix}\middle|\frac{\varpi}{\frac{1}{\bar{\Upsilon}}}, \frac{\left(\frac{1}{\bar{\Upsilon}}\right)^1 \frac{1}{{I_l}^2}\frac{{m_1}^1{m_2}^1}{{\Omega_1}^1{\Omega_2}^1}}{\frac{1}{\bar{\Upsilon}}}\right]
$$

$$
+ \frac{1}{\Gamma m_1 \Gamma m_2}\, G_{2,4}^{4,1}\left(\frac{\left(\frac{1}{\bar{\Upsilon}}\right)^1 \frac{1}{{I_l}^2}\frac{{m_1}^q{m_2}^p}{{\Omega_1}^q{\Omega_2}^p}}{\varpi^1}\middle|\begin{matrix}0,1\\4,4.5,0,0\end{matrix}\right) - \tag{5.15}
$$

$$
\left(\frac{1}{\Gamma m_1 \Gamma m_2}\right) G_{2,0:2,2:1,2}^{0,2:1,2:1,1}\left[\begin{matrix}-3,-3.5\\-\end{matrix}\middle|\begin{matrix}1,1\\1,0\end{matrix}\middle|\begin{matrix}1\\1,0\end{matrix}\middle|\frac{\varpi}{\left(\frac{1}{\bar{\Upsilon}}\right)^1 \frac{1}{{I_l}^2}\frac{{m_1}^1{m_2}^1}{{\Omega_1}^1{\Omega_2}^1}}, \frac{\frac{1}{\bar{\Upsilon}}}{\left(\frac{1}{\bar{\Upsilon}}\right)^1 \frac{1}{{I_l}^2}\frac{{m_1}^1{m_2}^1}{{\Omega_1}^1{\Omega_2}^1}}\right]
$$

5.2. Simulation Results

In this work, performance of Mixed Dual hop RF/FSO system in terms of Outage and Ergodic capacity is studied. RF channel is modelled with Mixture Gamma distribution and FSO channel is modelled using Double Generalized Gamma distribution. The analytical closed form expressions for the cumulative CDF and Outage probability are derived for heterodyne detection techniques. Rayleigh and Nakagami-m distribution is used as special cases of Mixture Gamma distribution. MATLAB is used to simulate the obtained mathematical results. Simulation parameters used are given below in Tables 5.1 and 5.2

Table 5.1: Parameter Values.

Parameter	**Weak Turbulence**	**Moderate Turbulence**	**Strong Turbulence**
γ_1	2.1	2.1690	1.8621
γ_2	2	0.8530	0.7638
Ω_1	1.0676	1.5793	1.5074
Ω_2	1.06	0.9671	0.9280
m_1	4	0.55	0.5
m_2	4.5	2.35	1.8
p	1	28	13
q	1	11	2

Table 5.2: Modulation Parameter Values.

Modulation Scheme	$\boldsymbol{\delta}$	$\boldsymbol{\tau}$
CBFSK	0.5	0.5
NBFSK	0.5	1
CBPSK	1	0.5

DBPSK	1	1

5.2.1 Results of Outage Capacity

Using the equation (5.5) and (5.7), we get the simulation results for Outage Capacity. The average electrical SNR through Rayleigh fading and double GG is compared with the outage capacity in Fig. 5.1. The comparison is performed at a 1 dB outage threshold. Under mild, moderate, and heavy turbulence circumstances, the Outage Capacity values are 0.00321, 0.05598, and 0.1253 at an average electrical SNR of 30 dB.

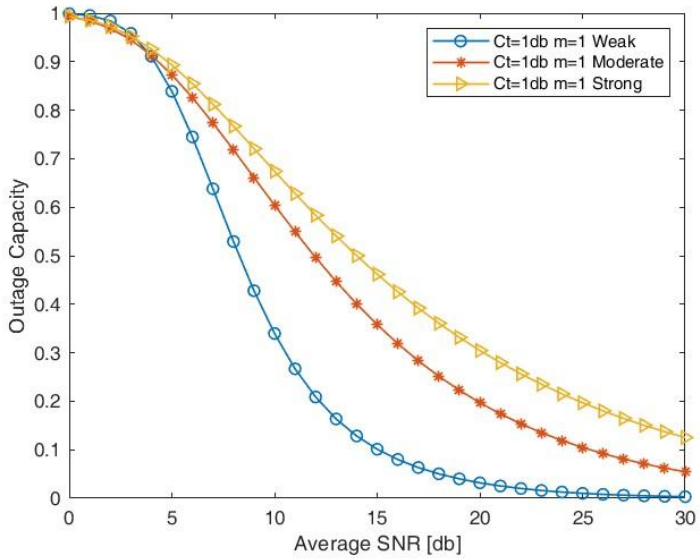

Fig. 5.1 Comparison of Outage Capacity over Rayleigh distribution under dual-hop RF/FSO system at different turbulence conditions

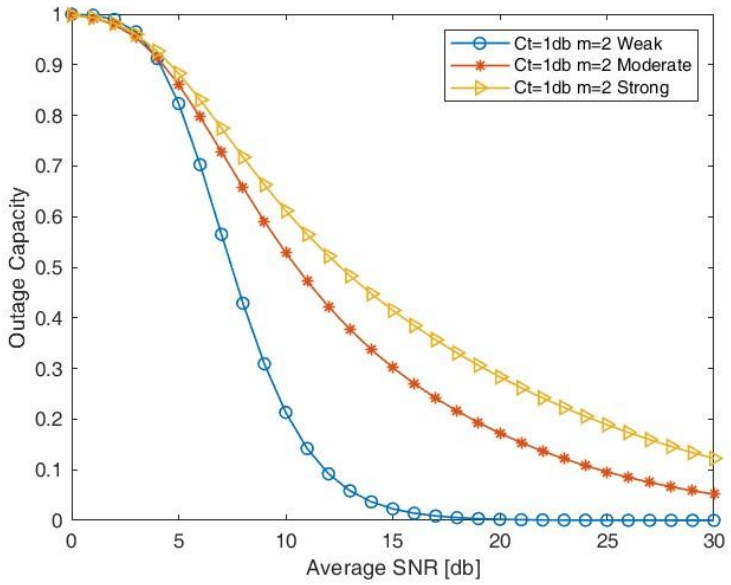

Fig. 5.2 Comparison of Outage Capacity over Nakagami-m distribution at m=2 under dualhop RF/FSO system at different turbulence conditions

Fig. 5.2 compares the average electrical SNR over Nakagami-m fading and Double GG with the outage capacity. The outage threshold used for this comparison is 1 dB. Under light, moderate, and heavy turbulence circumstances, the Outage Capacity values are 0.00002, 0.05295, and 0.12243, respectively, at an average electrical SNR of 30 dB. The outage capacity and average electrical SNR at a 1 dB outage threshold are compared in Fig. 5.3. The outage capacity at an average electrical SNR of 30 dB for light, moderate, and high turbulence circumstances is 0.00002, 0.05293, and 0.12243, respectively.

In Fig. 5.4, the average electrical SNR for weak turbulence with various m values is compared with outage capacity. The threshold for outages is set at 1 dB. The outage capacity for m=1, 2, and 3 is 0.101, 0.2276, and 0.00845 respectively, for an average electrical SNR of 15 dB.

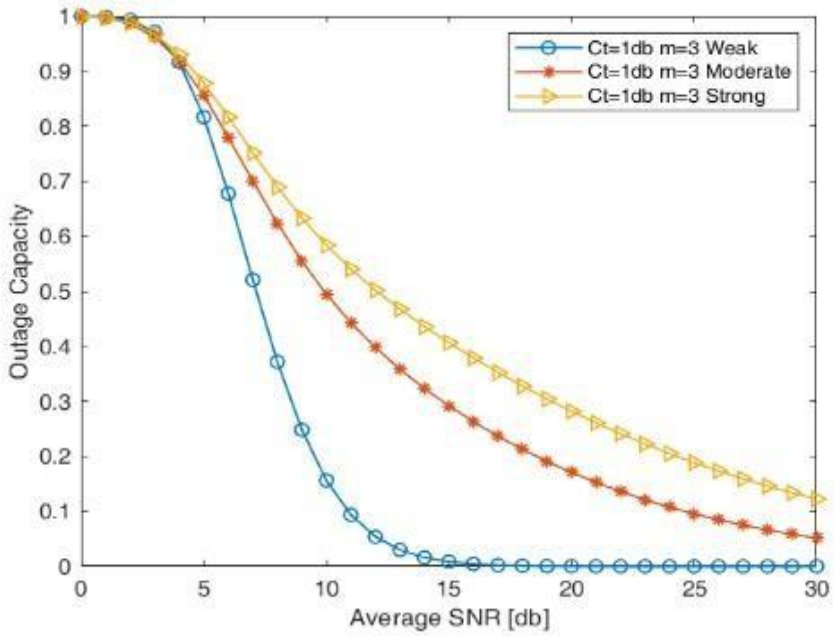

Fig. 5.3 Comparison of Outage Capacity over Nakagami-m distribution at m=3 under dualhop RF/FSO system at different turbulence conditions

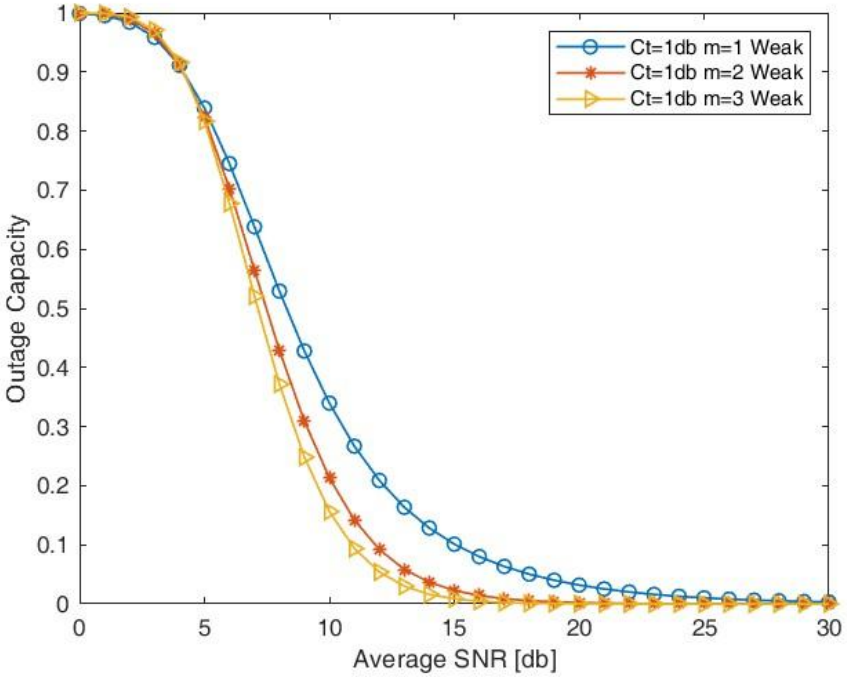

Fig. 5.4 Comparison of Outage Capacity for dual-hop RF/FSO system at different m values considering weak turbulence condition

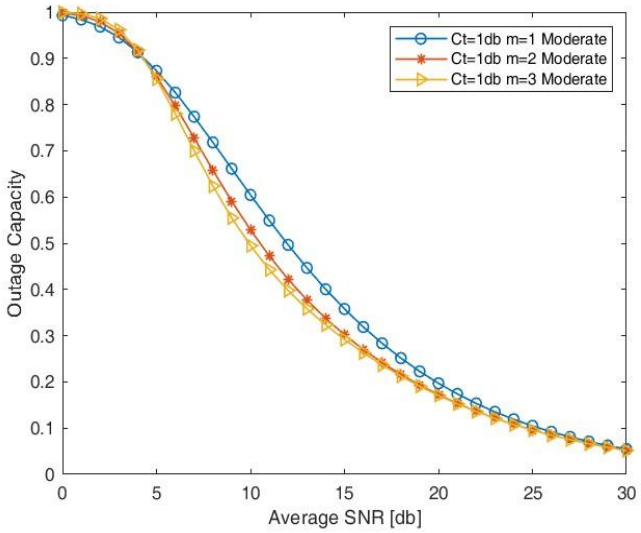

Fig. 5.5 Comparison of Outage Capacity for dual-hop RF/FSO system at different m values considering moderate turbulence condition

In Fig. 5.5, different m values for moderate turbulence are compared against outage capacity and average electrical SNR. The threshold for outages is set at 1 dB. The outage capacity for m=1, 2, and 3 is 0.3632, 0.3077, and 0.2976, respectively, for an average electrical SNR of 15 dB.

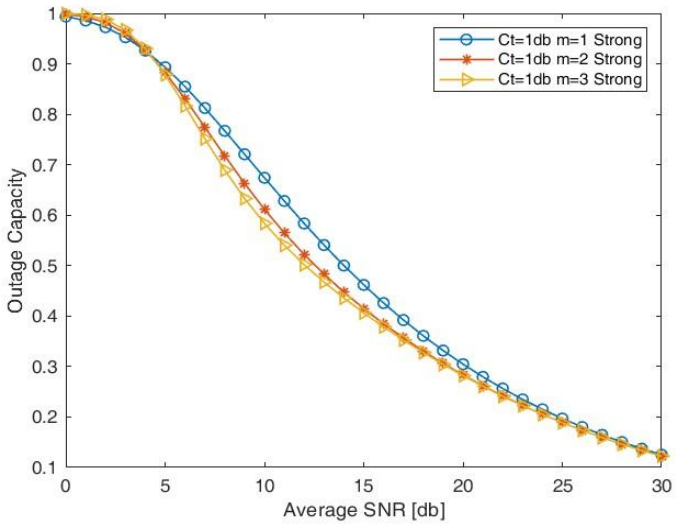

Fig. 5.6 Comparison of Outage Capacity for dual-hop RF/FSO system at different m values considering strong turbulence condition.

Fig. 5.6 compares outage capacity and average electrical SNR for heavy turbulence at various m values. The threshold for outages is set at 1 dB. The outage capacity is 0.461, 0.4149, and 0.4064 for m=1, 2, and 3 at an average electrical SNR of 15 dB.

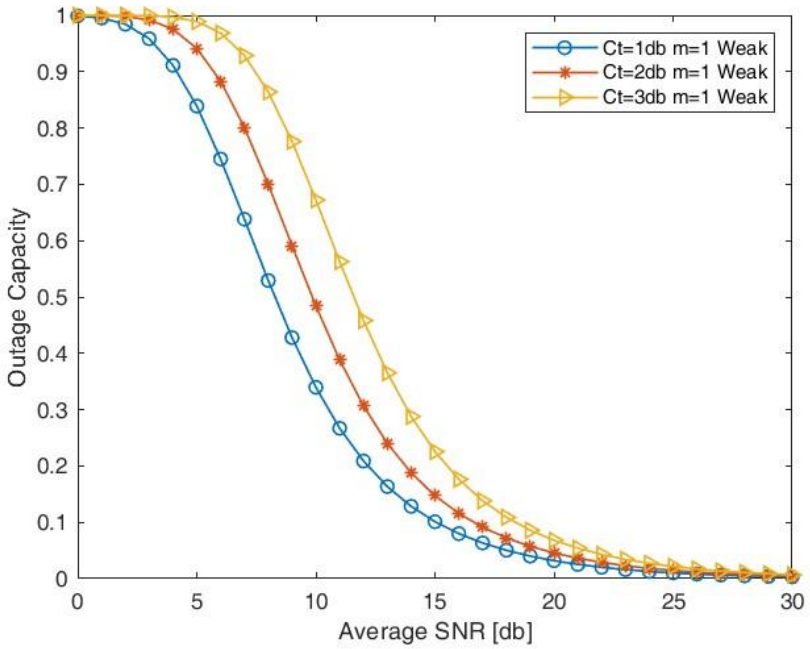

Fig. 5.7 Comparison of Outage Capacity for dual-hop RF/FSO system for Rayleigh considering weak turbulence condition.

Considering outage threshold values of 1, 2, and 3 dB, Fig. 5.7 relates outage capacity to Average Electrical SNR over Rayleigh for Weak Turbulence. For outage threshold values of 1, 2, and 3 dB, respectively, the outage capacity is 0.00321, 0.0046, and 0.0068 for an average electrical SNR of 30 dB.

Considering outage threshold values of 1, 2, and 3 dB, Fig. 5.8 relates outage capacity to Average Electrical SNR over Rayleigh for Weak Turbulence. For instance, the outage capacity for outage threshold values of 1, 2, and 3 dB, respectively, is 0.05, 0.06, and 0.07 for an average electrical SNR of 30 dB.

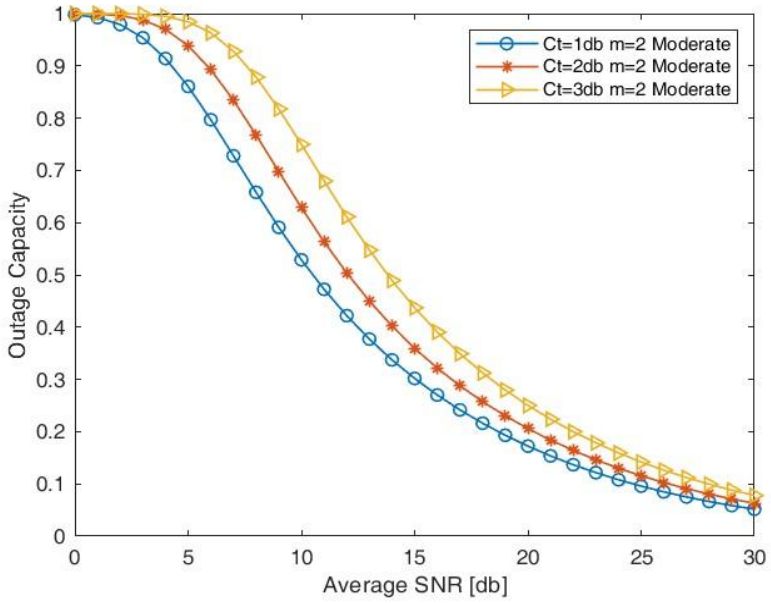

Fig. 5.8 Comparison of Outage Capacity for dual-hop RF/FSO system for m=2 considering moderate turbulence condition.

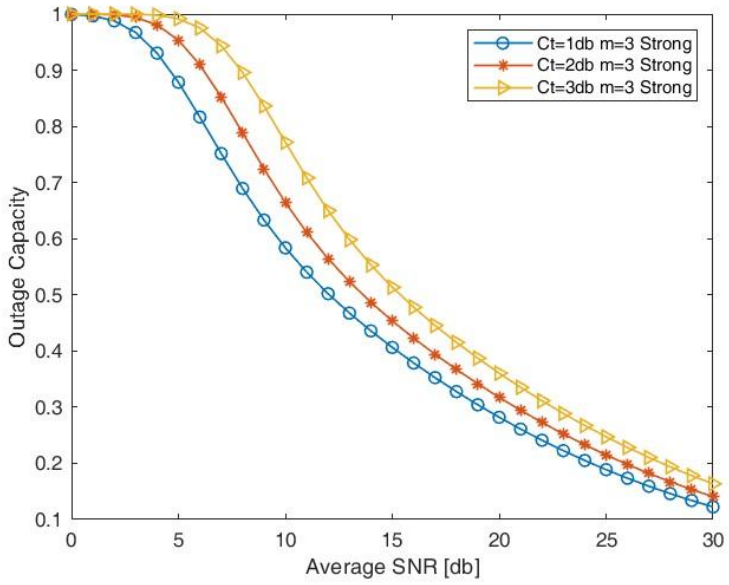

Fig 5.9 Comparison of Outage Capacity for dual-hop RF/FSO system for m=3 considering moderate turbulence condition.

Fig. 5.9 compares the outage capacity and average electrical SNR across Rayleigh fading for weak turbulence while considering outage thresholds of 1, 2, and 3 dB. For instance, the outage capacity values for outage thresholds of 1, 2, and 3 dB, respectively, are 0.12243, 0.1406, and

0.16358 for an average electrical SNR of 30 dB.

5.2.2 Results of Ergodic Capacity

Using the equation (5.13) and (5.15), we get the simulation results for Ergodic Capacity. Fig 5.10 compares Ergodic Capacity vs Average electrical SNR over Rayleigh, taking different path losses at L=0.5 Km. At average electrical SNR of 30 dB, the Ergodic Capacity is 7.359, 5.363, 2.5, 1.07 for path loss of 0.4 bits/Hz, 1.5 bits/Hz, 2.7 bits/Hz, and 3.2 bits/Hz, respectively. So, in conclusion, we can say that as the path loss values increase, there is a decrease in the corresponding Ergodic Capacity value to some extent.

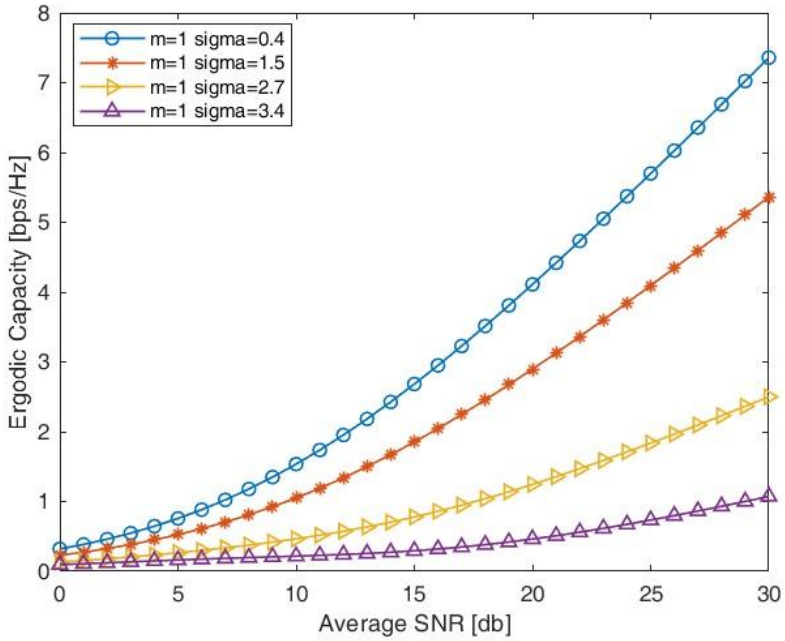

Fig. 5.10 Comparison of Ergodic Capacity for dual-hop RF/FSO system for m=1 for different path loss at L=0.5 km

Fig 5.11 compares Ergodic Capacity vs Average electrical SNR over Nakagami-m, taking different path losses at L=0.5 Km. At average electrical SNR of 30 dB, the Ergodic Capacity is 12.61, 11.76, 10.55, and 9.953 for path loss of 0.4 bits/Hz, 1.5 bits/Hz, 2.7 bits/Hz, and 3.2

bits/Hz respectively. So, in conclusion, we can say that as the path loss values increase, the corresponding Ergodic Capacity value decreases to some extent.

From figs. 5.10 and 5.11, we can conclude that as the average electrical SNR value increases, there will be an increase in the value of Ergodic capacity. Conversely, as we increase the value of path loss, there is a decrease in the value of Ergodic capacity.

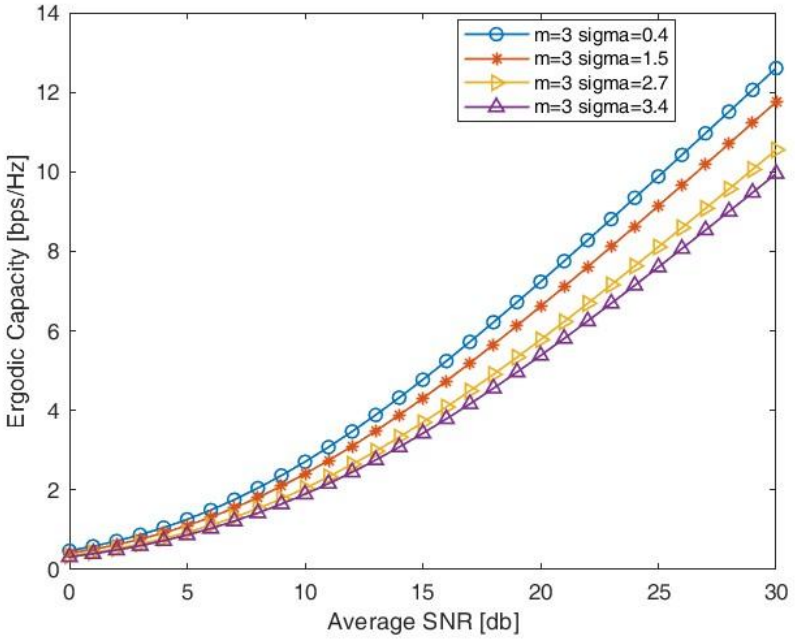

Fig. 5.11 Comparison of Ergodic Capacity for dual-hop RF/FSO system for m=3 for different path loss at L=0.5 km.

Fig 5.12 compares Ergodic Capacity vs Average electrical SNR over Nakagami-m (m=3), taking different path losses at L=1 Km. At average electrical SNR of 30 dB, the Ergodic Capacity is 9.682, 8.088, 6.044, and 5.136 for path loss of 0.4 bits/Hz, 1.5 bits/Hz, 2.7 bits/Hz, and 3.2 bits/Hz, respectively. So, in conclusion, we can say that as the path loss values increase, the corresponding Ergodic Capacity value decreases to some extent.

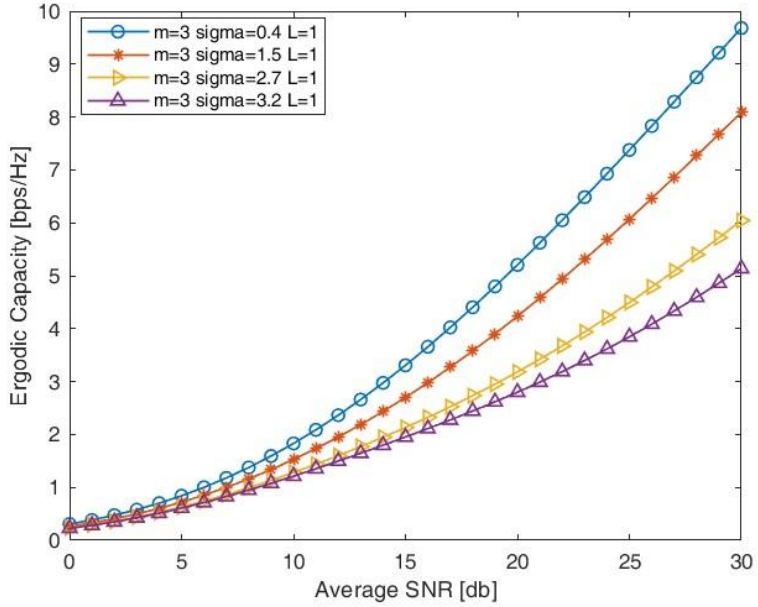

Fig. 5.12 Comparison of Ergodic Capacity for dual-hop RF/FSO system for m=3 for different path loss at L=1 km.

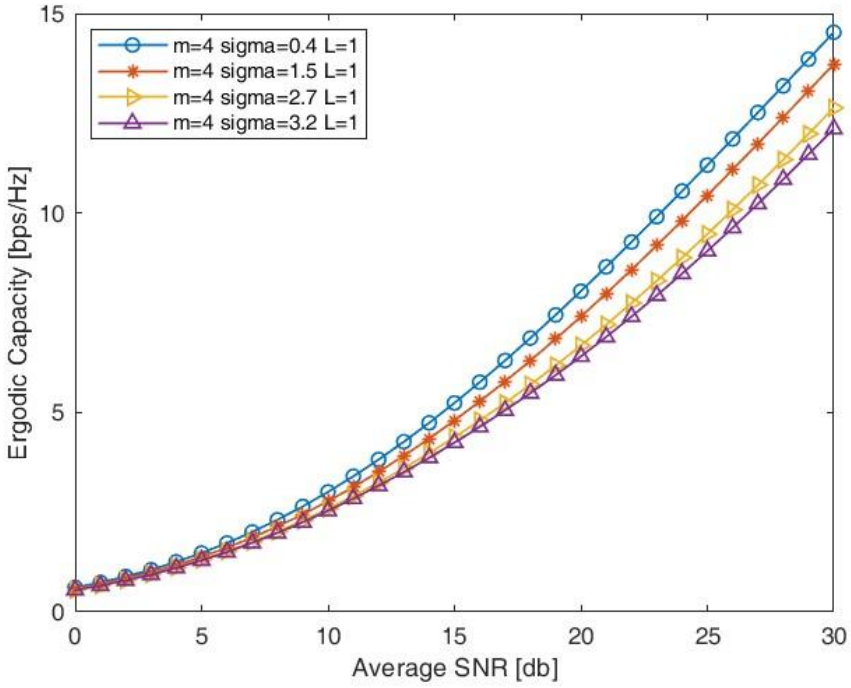

Fig. 5.13 Comparison of Ergodic Capacity for dual-hop RF/FSO system for m=4 for different path loss at L=1 km.

Fig 5.13 compares Ergodic Capacity vs Average electrical SNR over Nakagami-m (m=4), taking different path losses at L=1 Km. At average electrical SNR of 30 dB, the Ergodic Capacity is 14.53, 13.73, 12.63, and 12.11 for path loss of 0.4 bits/Hz, 1.5 bits/Hz, 2.7 bits/Hz, and 3.2 bits/Hz, respectively. So, in conclusion, we can say that as the path loss values increase, the corresponding Ergodic Capacity value decreases to some extent.

In figs. 5.12 and 5.13, we have increased the value of L to 1 km, and we observe that as the average electrical SNR value rises, then there will be an increase in the value of Ergodic capacity. Conversely, as we increase the value of path loss, there will be a decrease in the value of Ergodic capacity. From these figures, we can say that our model is valid for Nakagami-m at higher values of L (1, 1.5 and 2 Km).

Fig 5.14 compares Ergodic Capacity vs Average electrical SNR over Nakagami-m (m=3) taking different L= 0.5 Km, 1 Km, 1.5 Km. At average electrical SNR of 30 dB, the Ergodic Capacity is 12.61, 9.682, and 6.995 for taking L as 0.5 Km, 1 Km, and 1.5 Km, respectively. So, in conclusion, we can say that as the value of L (propagation distance) increases, the corresponding Ergodic Capacity value decreases to some extent.

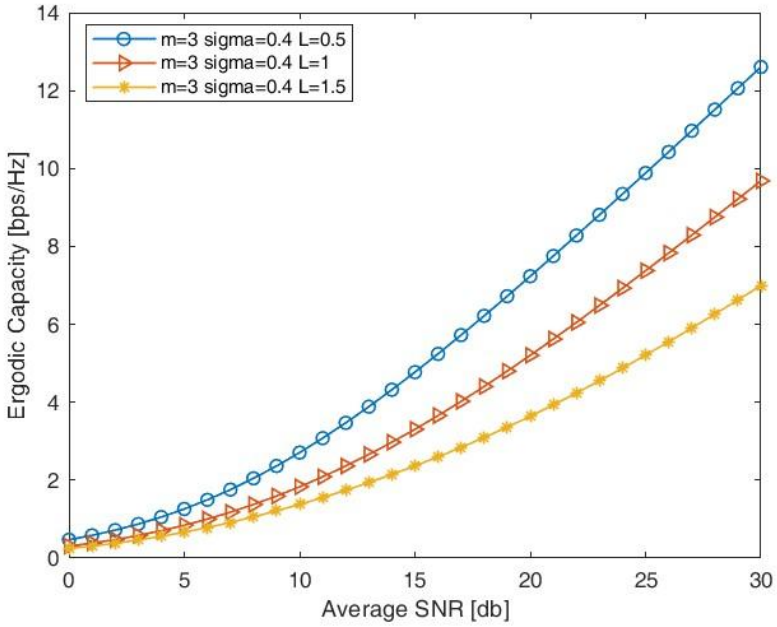

Fig. 5.14 Comparison of Ergodic Capacity for dual-hop RF/FSO system for m=3 for different values of L

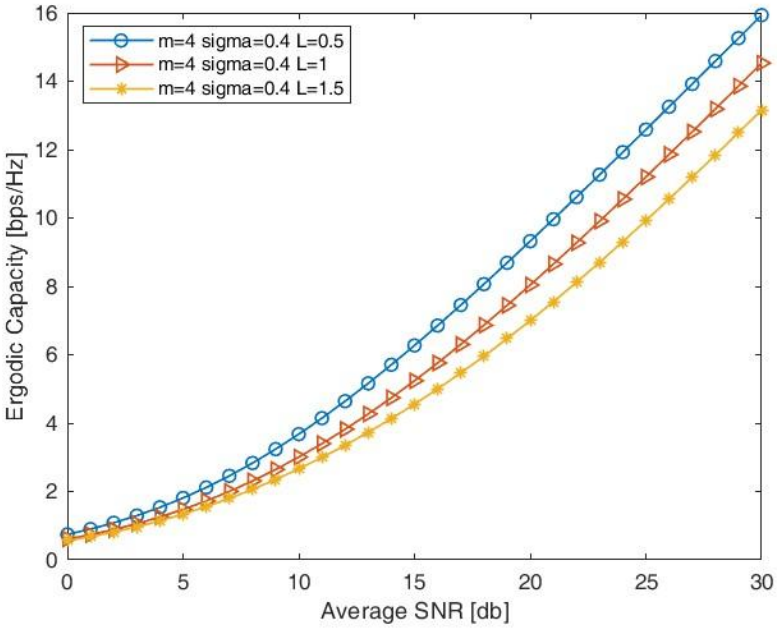

Fig. 5.15 Comparison of Ergodic Capacity for dual-hop RF/FSO system for m=4 for different values of L

In figs. 5.14 and 5.15, we have increased the value of L from 0.5 km to 1 km and 1.5 km, and we observe that as the value of L increases, there will be a slight decrease in the Ergodic Capacity for a particular average SNR. However, on the other hand, we also observe that as the average SNR increases, Ergodic capacity increases for all values of L.

Fig 5.16 compares Ergodic Capacity vs Average electrical SNR over Mixture Gamma, taking m=1, 3 and 4. At Average electrical SNR of 30 dB, the Ergodic Capacity is 15.93, 12.61, and 7.35 for m = 4, 3 and 1, respectively.

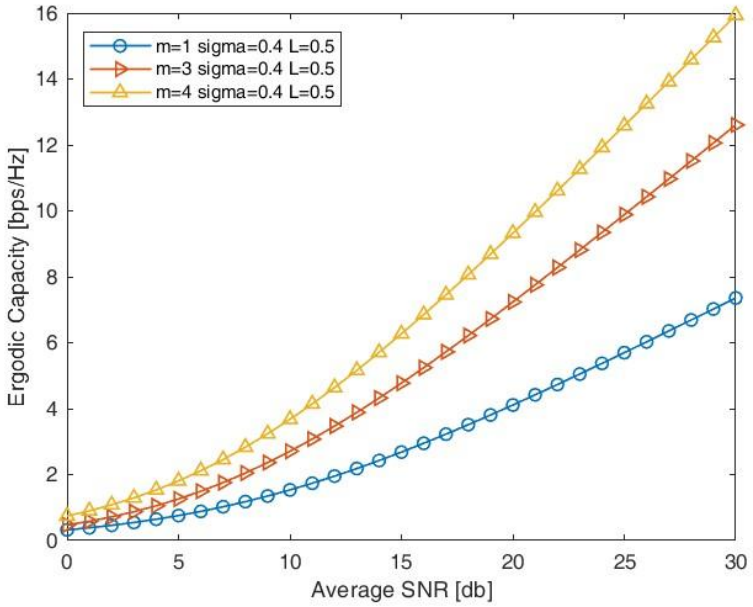

Fig. 5.16 Comparison of Ergodic Capacity for dual-hop RF/FSO system for different values of m.

5.3 Summary

In this chapter, we investigated the Outage and the Ergodic Capacity of a Mixed Dual Hop RF/FSO system. A Mixture Gamma distribution represented the RF channel, whereas the FSO channel was represented by a Double Generalised Gamma distribution. The analytical closedform expression for the Outage and Ergodic Capacity was derived for the IM/DD detection approach to analyze the system's performance. As specific instances of the Mixture Gamma distribution, the Rayleigh and Nakagami-m distributions were employed. The study

found that, given a particular threshold, the outage capacity decreases when the average electrical SNR rises and increases with the outage rate value rises. Also, it was noticed that as the average electrical SNR increases, Ergodic capacity increases for a specific threshold. For the ergodic capacity, it was found that when the path loss increases, the ergodic capacity reduces for a given electrical SNR.

CHAPTER 6

PHASE-JITTER PDF BASED ERROR RATE ANALYSIS OF COHERENT-MPSK MODULATED SIGNALS OVER MIXER GAMMA FADING CHANNEL – UNIFIED AND IMPROVED

Here, we present OFDM based Ro-FSO system over Double Generalized Gamma distribution with and without pointing error. Basically, novel closed form expressions for BER of MQAM and KPSK modulation scheme over Double Generalized Gamma distribution are derived for OFDM Ro-FSO system.

6.1 System and Channel Model:

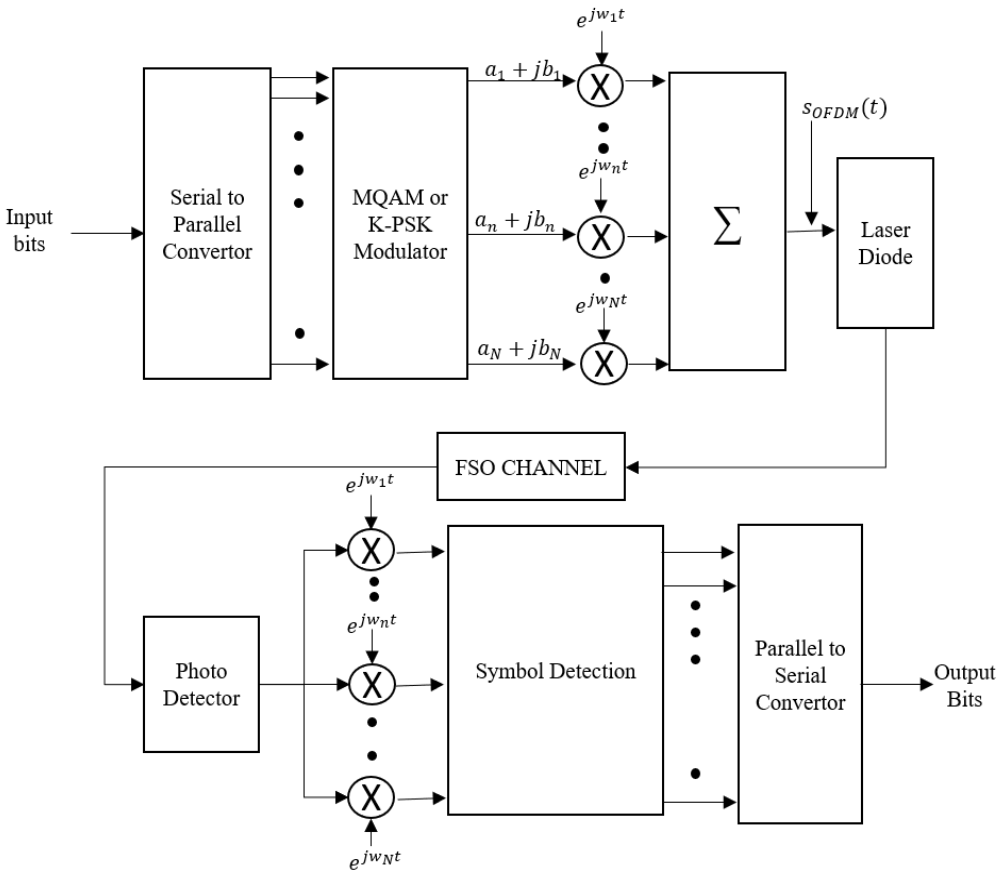

Fig: 6.1 OFDM RoFSO system [121]

Figure 6.1 shows the Orthogonal Frequency Division Multiple Access (OFDM) RoFSO system. Here, OFDM signal is transmitted by Laser diode and propagate through FSO channel where it gets attenuated due to atmospheric turbulences and received by a photodetector at the receiver. It is noticeable that OFDM is a special multicarrier modulation scheme in which parallel subcarriers convey the information sign. Specifically, in OFDM system, streams of high data rate are split into the streams of lower data rate and then transmitted over several narrow band subcarriers. Further, different modulation (in our case, Phase shift keying (PSK) or Quadrature amplitude modulation (QAM) modulation) techniques are used to modulate these subcarriers on a high-frequency carrier [121]. At the transmitter end, Inverse Fast Fourier Transform (IFFT) and at the receiving end, Fast Fourier Transform (FFT) is done to retrieve data. However, OFDM signal, after up converted to carrier frequency, is given as [122]

$$s_{OFDM}(t) = \sum_{n=0}^{N-1} s_n(t), \qquad for\ 0 \le t \le T_s \tag{6.1}$$

Also, n^{th} subcarrier $s_n(t)$ is given as

$$s_n(t) = X_n e^{[i(w_n + 2\pi f_c)t]} \tag{6.2}$$

where, T_s is the OFDM duration, and X_n is the complex data of n_{th} subcarrier. As output after IFFT becomes bipolar, so in order to maintain OFDM unipolar a dc bias is added to it. Further, the OFDM signal, $s_{OFDM}(t)$ modulates the optical signal from Laser diode. However, non-linearity of laser diode, results in inter-modulation distortion (IMD) with generated harmonics.

However, the transmitted output optical power as a nonlinear function is expressed as [122]

$$p(t) = p_t \left[1 + \sum_{n=0}^{N-1} m_n s_n(t) + a_3 \left(\sum_{n=0}^{N-1} m_n s_n(t) \right)^3 \right] \tag{6.3}$$

where, p_t is the average transmitted power, $a_3$represents the third order non linearity coefficient and $m_n$is the optical modulation index (OMI) for each OFDM frequency. Now, as OFDM signal travels through free space where it gets attenuated, and noise is added to it. Therefore, optical power received at Photodetector is expresses as

$$P_r(t) = Ip(t) + n_{opt}(t) \tag{6.4}$$

where I represent channel attenuation due to atmospheric turbulence and pointing errors. n_{opt} is the optical AWGN power having zero mean and variance equal to half of noise power i.e. $N_o/2$.

Using Equation (6.3) & Equation (6.4), the output current of photo-detector (receiver) is expressed as,

$$i(t, I) = I_0 \left[1 + \sum_{n=0}^{N-1} m_n s_n(t) + a_3 \left(\sum_{n=0}^{N-1} m_n s_n(t) \right)^3 \right] + n_{opt}(t) \tag{6.5}$$

where, $I_0 = \rho L_{tot} p_t I$ represents the dc value of $i(t, I)$, ρ is the photodetector responsivity, and noise power N_0 expresses as

$$N_0 = \frac{4K_B TF}{R_L} + 2qI_0 + I_0^2(R_{IN}) \tag{6.6}$$

Where, K_B, T and F are the Boltzmann's constant, temperature and the noise figure of the receiver respectively. Whereas, R_L is the load resistor at the photodetector's side, q is the electron charge and R_{IN} is the relative intensity noise.

The IMD which affects the carrier w_n among N equally spaced subcarriers is given as [123]

$$\sigma_{IMD}^2 = \frac{9a_3^2 m_n^6}{8}\left(\frac{D_2(N,n)}{2} + D_3(N,n)\right)\rho L_{tot} p_t I \tag{6.7}$$

Where, the values of intermodulation distortion products D_2 and D_3 are

$$D_2(n,N) = 0.5[N - 2 - 0.5(1-(-1)^N)(-1)^N] \tag{6.8}$$

$$\begin{aligned} D_3(n,N) = {} & 0.5n(N-n-1) + 0.25[(N-3)^2 - 5] \\ & - 0.125[(1-(-1)^N)(-1)^{N+n}] \end{aligned} \tag{6.9}$$

The instantaneous carrier-to-noise plus distortion ratio($CNDR_n(I)$), by considering optical noise and IMD, for particular subcarrier at output of receiver is expressed as,

$$CNDR_n(I) = \frac{(m_n \rho L_{tot} p_t I)^2}{2\left(\frac{N_0}{T_s} + \sigma_{IMD}^2\right)} \tag{6.10}$$

Finally, the average $CNDR_n$ per OFDM subcarrier is approximated as [122]

$$[CNDR_n]_{AV} = \frac{(m_n \rho L_{tot} p_t)^2}{2\left(\left[\frac{N_0}{T_s}\right]_{AV} + [\sigma_{IMD}^2]_{AV}\right)} \tag{6.11}$$

Where, subscript n and AV are the n^{th} OFDM subcarrier and average value of each quantity respectively.

Further, in the proposed system FSO channel is modelled using Double Generalized Gamma distribution. It is noteworthy to mention that Double GG distribution includes all the turbulence condition from weak to strong in addition

it includes various channel models like lognormal, Gamma-Gamma, Double Weibull and K distribution as it special cases.

However, intensity, I is represented as [121]

$$I = I_a I_p \tag{6.12}$$

Where, I_a shows atmospheric turbulences & I_p represents pointing errors

However, PDF of Double generalized Gamma distribution is given as [8]

$$f_{I_a}(I_a) = \frac{\Upsilon_1}{I_a \Gamma(m_1)\Gamma(m_2)} H_{2,0}^{0,2}\left[\frac{\Omega_1}{m_1 I_a^{\Upsilon_1}}\left(\frac{\Omega_2}{m_2}\right)^{\frac{\Upsilon_1}{\Upsilon_2}}\middle|\begin{matrix}(1-m_1,1),\\ \_\end{matrix}\left(1-m_2,\frac{\Upsilon_1}{\Upsilon_2}\right)\right] \tag{6.13}$$

Where, $H_{2,0}^{0,2}$ represents Fox H function. Also,$\Upsilon_i > 0, m_i > 0.5 \; and \; \Omega_i, i = 1,2$ are the parameters of the generalized gamma distribution.

Υ_1 and Υ_2 are the distribution parameters.

m_1 and m_2 are the shaping parameters.

Ω_1 and Ω_2 are the average power of the distribution parameters.

On the other hand, PDF of I_P pointing error is given as [122]:

$$f_{I_P}(I_P) = \frac{\xi^2}{A_0^{\xi^2}} I_P^{\xi^2-1}; \;\; 0 \le I_P \le A_0 \tag{6.14}$$

Where,I_P represents effect of pointing error.

$\xi = \frac{w_{eq}}{2\sigma_s^2}$ is the ratio between equivalent beam width and pointing error displacement standard deviation.

Also,

$$w_{eq}{}^2 = \frac{\sqrt{\pi}\,\mathrm{erf}(V_m) w_z{}^2}{2V_m\, e^{(-V_m^2)}} \tag{6.15}$$

Parameter $A_o = [\mathrm{erf}(V_m)]^2$ is a fraction of collected power

with $V_m = \frac{\sqrt{\pi}a}{\sqrt{2}w_z}$ (6.16)

where a is aperture radius and w_z is beam radius

The combined probability distribution function of Double Generalized Gamma distribution under influence of pointing errors is evaluated as [122]:

$$f_I(I) = \int_0^{A_0} f_{I/I_P}\left(\frac{I}{I_P}\right) \times f_{I_P}(I_P) dI_P \tag{6.17}$$

$$where\ f(I/I_p) = \frac{1}{I_p} f_{I_a}\left(\frac{I}{I_p}\right), \qquad 0 \le I_P \le A_0 I_0 \tag{6.18}$$

By substituting Equation (6.13) and Equation (6.14) in Equation (6.17) and after solving it using identity from [119] we get the PDF of Double GG Distribution with pointing errors as:

$$f_I(I) = \frac{\Upsilon_1 \xi^2}{I\Gamma(m_1)\Gamma(m_2)} \times$$
$$H_{4,1}^{0,4}\left[\left(\frac{\Omega_1}{m_1}\right)\left(\frac{\Omega_2}{m_2}\right)^{\frac{\Upsilon_1}{\Upsilon_2}} \frac{1}{I^{\Upsilon_1}} A_0^{\Upsilon_1} \middle| \begin{matrix}(1-\xi^2, \Upsilon_1), (0,0), (1-m_1, 1), \left(1-m_2, \frac{\Upsilon_1}{\Upsilon_2}\right) \\ (-\xi^2, \Upsilon_1)\end{matrix}\right] \tag{6.19}$$

6.2. Proposed Analytical BER Expressions for OFDM RoFSO Link:

6.2.1 M-QAM OFDM Link

BER expression of M-QAM modulation, is given as [121]

$$P_{b,M-QAM} = \frac{N^{-1}}{log_2(M)} \sum_{n=0}^{N-1} \left\{ 1 - \left[1 - \left(1 - \sqrt{M^{-1}} \right) erfc \left(\sqrt{\frac{3CNDR_n(I)}{2(M-1)}} \right) \right]^2 \right\} \quad (6.20)$$

where, $erfc(.)$ is the complementary error function, and M is given as $M = 2^{\xi}$and ξ is an even number.

The average BER estimation of M-QAM modulation over Double Generalized Gamma is expressed as

$$P_{b,M-QAM,AV} = \frac{\left(1-\sqrt{M^{-1}}\right)N^{-1}}{log_2(M)} \sum_{n=0}^{N-1} \int_0^{\infty} \left\{ 2erfc \left(\sqrt{\frac{3CNDR_n(I)}{2(M-1)}} \right) \right. \quad (6.21)$$

$$\left. - \left(1 - \sqrt{M^{-1}} \right) erfc^2 \left(\sqrt{\frac{3CNDR_n(I)}{2(M-1)}} \right) \right\} f_I(I) dI$$

where, $f_I(I)$ is the PDF of the channel distribution

Now $erfc^2(.)$ is simplified as [119],

$$erfc^2(x) = \frac{1}{36} \left[exp(-x^2) + 3exp\left(-\frac{4x^2}{3} \right) \right]^2 \quad (6.22)$$

Expressing $erfc(.)$ and exponential into Fox H function using [119]

$$erfc(x) = \frac{1}{\sqrt{\pi}} H_{1,2}^{2,0} \left[x^2 \middle| \begin{matrix} (1,1) \\ (0,1), (\frac{1}{2}, 1) \end{matrix} \right] \quad (6.23)$$

$$exp(-x) = H_{0,1}^{1,0} \left[x \middle| \begin{matrix} . \\ (0,1) \end{matrix} \right] \quad (6.24)$$

By substituting Equation (6.22), (6.23) & (6.24) in Equation (6.21) we obtained

$$P_{b,M-QAM,AV} = \quad (6.25)$$

$$\frac{2\left(1-\sqrt{M^{-1}}\right)N^{-1}}{log_2(M)}\sum_{n=0}^{N-1}\int_0^{\infty}\left\{\frac{1}{\sqrt{\pi}}H_{1,2}^{2,0}\left[\frac{3CNDR_n(I)}{2(M-1)}\middle|\begin{matrix}(1,1)\\(0,1),\left(\frac{1}{2},1\right)\end{matrix}\right]\right.$$

$$-\frac{\left(1-\sqrt{M^{-1}}\right)}{72}\times$$

$$\left(H_{0,1}^{1,0}\left[\frac{3CNDR_n(I)}{(M-1)}\middle|_{(0,1)}^{\cdot}\right]+9H_{0,1}^{1,0}\left[\frac{4CNDR_n(I)}{(M-1)}\middle|_{(0,1)}^{\cdot}\right]\right.$$

$$\left.\left.+6H_{0,1}^{1,0}\left[\frac{7CNDR_n(I)}{2(M-1)}\middle|_{(0,1)}^{\cdot}\right]\right)\right\}f_I(I)dI$$

Now from Equation (6.10) & (6.11) we get

$$CNDR_n(I)=[CNDR_n(I)]_{AV}I^2 \tag{6.26}$$

By substituting it in equation (6.26) we get

$$P_{b,M-QAM,AV}=$$

$$\frac{2\left(1-\sqrt{M^{-1}}\right)N^{-1}}{log_2(M)}\sum_{n=0}^{N-1}\int_0^{\infty}\left\{\frac{1}{\sqrt{\pi}}H_{1,2}^{2,0}\left[\frac{3[CNDR_n(I)]_{AV}I^2}{2(M-1)}\middle|\begin{matrix}(1,1)\\(0,1),\left(\frac{1}{2},1\right)\end{matrix}\right]\right.$$

$$-\frac{\left(1-\sqrt{M^{-1}}\right)}{72}\times \tag{6.27}$$

$$\left(H_{0,1}^{1,0}\left[\frac{3[CNDR_n(I)]_{AV}I^2}{(M-1)}\middle|_{(0,1)}^{\cdot}\right]+9H_{0,1}^{1,0}\left[\frac{4[CNDR_n(I)]_{AV}I^2}{(M-1)}\middle|_{(0,1)}^{\cdot}\right]\right.$$

$$\left.\left.+6H_{0,1}^{1,0}\left[\frac{7[CNDR_n(I)]_{AV}I^2}{2(M-1)}\middle|_{(0,1)}^{\cdot}\right]\right)\right\}f_I(I)dI$$

6.2.1.1 Without Pointing Errors

Now by substituting the PDF of Double Generalized Gamma distribution without pointing errors from Equation (6.13) in Equation (6.27), we obtain

$$P_{b,M-QAM,AV} = \frac{2\left(1-\sqrt{M^{-1}}\right)N^{-1}}{log_2(M)} \sum_{n=0}^{N-1} \int_0^{\infty} \left\{ \frac{1}{\sqrt{\pi}} H_{1,2}^{2,0} \left[\frac{3[CNDR_n(I)]_{AV} I^2}{2(M-1)} \middle| \begin{matrix} (1,1) \\ (0,1), \left(\frac{1}{2}, 1\right) \end{matrix} \right] \right.$$

$$- \frac{\left(1-\sqrt{M^{-1}}\right)}{72} \times \left(H_{0,1}^{1,0} \left[\frac{3[CNDR_n(I)]_{AV} I^2}{(M-1)} \middle| \begin{matrix} . \\ (0,1) \end{matrix} \right] \right.$$

$$\left. \left. + 9H_{0,1}^{1,0} \left[\frac{4[CNDR_n(I)]_{AV} I^2}{(M-1)} \middle| \begin{matrix} . \\ (0,1) \end{matrix} \right] + 6H_{0,1}^{1,0} \left[\frac{7[CNDR_n(I)]_{AV} I^2}{2(M-1)} \middle| \begin{matrix} . \\ (0,1) \end{matrix} \right] \right) \right\} \times$$

$$\frac{\Upsilon_1}{I\Gamma(m_1)\Gamma(m_2)} H_{2,0}^{0,2} \left[\frac{\Omega_1}{m_1 I^{\Upsilon_1}} \left(\frac{\Omega_2}{m_2}\right)^{\frac{\Upsilon_1}{\Upsilon_2}} \middle| \begin{matrix} (1-m_1,1), \left(1-m_2, \frac{\Upsilon_1}{\Upsilon_2}\right) \\ \_ \end{matrix} \right] dI \tag{6.28}$$

By solving and simplifying the Equation (6.28) using [119] we obtained the finalized expression as

$$P_{b,M-QAM,AV} = \frac{2\left(1-\sqrt{M^{-1}}\right)N^{-1}}{log_2(M)} \frac{\Upsilon_1}{\Gamma(m_1)\Gamma(m_2)} \times$$

$$\sum_{n=0}^{N-1} \left\{ \frac{1}{2\sqrt{\pi}} H_{3,2}^{2,2} \left[\frac{\Omega_1}{m_1} \left(\frac{\Omega_2}{m_2}\right)^{\frac{\Upsilon_1}{\Upsilon_2}} \left(\frac{3[CNDR_n(I)]_{AV}}{2(M-1)} \right)^{\frac{\Upsilon_1}{2}} \middle| \begin{matrix} (1-m_1,1), \left(1-m_2, \frac{\Upsilon_1}{\Upsilon_2}\right), \left(1, \frac{\Upsilon_1}{2}\right) \\ \left(0, \frac{\Upsilon_1}{2}\right), \left(\frac{1}{2}, \frac{\Upsilon_1}{2}\right) \end{matrix} \right] \right.$$

$$- \frac{\left(1-\sqrt{M^{-1}}\right)}{72} \left(\frac{1}{2} H_{2,1}^{1,2} \left[\frac{\Omega_1}{m_1} \left(\frac{\Omega_2}{m_2}\right)^{\frac{\Upsilon_1}{\Upsilon_2}} \left(\frac{3[CNDR_n(I)]_{AV}}{(M-1)} \right)^{\frac{\Upsilon_1}{2}} \middle| \begin{matrix} (1-m_1,1), \left(1-m_2, \frac{\Upsilon_1}{\Upsilon_2}\right) \\ \left(0, \frac{\Upsilon_1}{2}\right) \end{matrix} \right] \right. \tag{6.29}$$

$$+ \frac{9}{2} H_{2,1}^{1,2} \left[\frac{\Omega_1}{m_1} \left(\frac{\Omega_2}{m_2}\right)^{\frac{\Upsilon_1}{\Upsilon_2}} \left(\frac{4[CNDR_n(I)]_{AV}}{(M-1)} \right)^{\frac{\Upsilon_1}{2}} \middle| \begin{matrix} (1-m_1,1), \left(1-m_2, \frac{\Upsilon_1}{\Upsilon_2}\right) \\ \left(0, \frac{\Upsilon_1}{2}\right) \end{matrix} \right]$$

$$\left. \left. + \frac{6}{2} H_{2,1}^{1,2} \left[\frac{\Omega_1}{m_1} \left(\frac{\Omega_2}{m_2}\right)^{\frac{\Upsilon_1}{\Upsilon_2}} \left(\frac{7[CNDR_n(I)]_{AV}}{2(M-1)} \right)^{\frac{\Upsilon_1}{2}} \middle| \begin{matrix} (1-m_1,1), \left(1-m_2, \frac{\Upsilon_1}{\Upsilon_2}\right) \\ \left(0, \frac{\Upsilon_1}{2}\right) \end{matrix} \right] \right) \right\}$$

6.2.1.2 With Pointing Errors

Now by substituting the PDF of Double Generalized Gamma distribution with pointing errors from Equation (6.19) in Equation (6.27), we obtained

$$P_{b,M-QAM,AV} =$$

$$\frac{2\left(1-\sqrt{M^{-1}}\right)N^{-1}}{log_2(M)}\sum_{n=0}^{N-1}\int_0^{\infty}\left\{\frac{1}{\sqrt{\pi}}H_{1,2}^{2,0}\left[\frac{3[CNDR_n(I)]_{AV}I^2}{2(M-1)}\middle|\begin{matrix}(1,1)\\(0,1),\left(\frac{1}{2},1\right)\end{matrix}\right]\right.$$

$$-\frac{\left(1-\sqrt{M^{-1}}\right)}{72}\times$$

$$\left(H_{0,1}^{1,0}\left[\frac{3[CNDR_n(I)]_{AV}I^2}{(M-1)}\middle|\begin{matrix}.\\(0,1)\end{matrix}\right]\right.$$

$$+9H_{0,1}^{1,0}\left[\frac{4[CNDR_n(I)]_{AV}I^2}{(M-1)}\middle|\begin{matrix}.\\(0,1)\end{matrix}\right]$$

$$\left.\left.+6H_{0,1}^{1,0}\left[\frac{7[CNDR_n(I)]_{AV}I^2}{2(M-1)}\middle|\begin{matrix}.\\(0,1)\end{matrix}\right]\right)\right\}\times\frac{\Upsilon_1\xi^2}{I\Gamma(m_1)\Gamma(m_2)}\times$$

$$H_{4,1}^{0,4}\left[\left(\frac{\Omega_1}{m_1}\right)\left(\frac{\Omega_2}{m_2}\right)^{\frac{\Upsilon_1}{\Upsilon_2}}\frac{1}{I^{\Upsilon_1}}A_0^{\Upsilon_1}\middle|\begin{matrix}(1-\xi^2,\Upsilon_1),(0,0),(1-m_1,1),\left(1-m_2,\frac{\Upsilon_1}{\Upsilon_2}\right)\\(-\xi^2,\Upsilon_1)\end{matrix}\right]dI \quad (6.30)$$

By solving and simplifying the Equation (6.30) using [119] we obtained the finalized expression as

$$P_{b,M-QAM,AV}$$

$$=\frac{2\left(1-\sqrt{M^{-1}}\right)N^{-1}}{log_2(M)}\frac{\Upsilon_1\xi^2}{\Gamma(m_1)\Gamma(m_2)}\sum_{n=0}^{N-1}\frac{1}{2\sqrt{\pi}}H_{5,3}^{2,4}\left[\frac{\Omega_1}{m_1}\left(\frac{\Omega_2}{m_2}\right)^{\frac{\Upsilon_1}{\Upsilon_2}}\left(\frac{3[CNDR_n(I)]_{AV}}{2(M-1)}\right)^{\frac{\Upsilon_1}{2}}\right.$$

$$\left.A_0^{\Upsilon_1}\middle|\begin{matrix}(1-\xi^2,\Upsilon_1),(0,0),(1-m_1,1),\left(1-m_2,\frac{\Upsilon_1}{\Upsilon_2}\right),\left(1,\frac{\Upsilon_1}{2}\right)\\\left(0,\frac{\Upsilon_1}{2}\right),\left(\frac{1}{2},\frac{\Upsilon_1}{2}\right),(-\xi^2,\Upsilon_1)\end{matrix}\right]-\frac{\left(1-\sqrt{M^{-1}}\right)}{72}\left(\frac{1}{2}\times\right. \quad (6.31)$$

$$H_{4,2}^{1,4}\left[\frac{\Omega_1}{m_1}\left(\frac{\Omega_2}{m_2}\right)^{\frac{\Upsilon_1}{\Upsilon_2}}\left(\frac{3[CNDR_n(I)]_{AV}}{(M-1)}\right)^{\frac{\Upsilon_1}{2}}A_0^{\Upsilon_1}\left|\begin{matrix}(1-\xi^2,\Upsilon_1),(0,0),(1-m_1,1),\left(1-m_2,\frac{\Upsilon_1}{\Upsilon_2}\right)\\ \left(0,\frac{\Upsilon_1}{2}\right),(-\xi^2,\Upsilon_1)\end{matrix}\right.\right]+$$

$$\frac{9}{2}H_{4,2}^{1,4}\left[\frac{\Omega_1}{m_1}\left(\frac{\Omega_2}{m_2}\right)^{\frac{\Upsilon_1}{\Upsilon_2}}\left(\frac{4[CNDR_n(I)]_{AV}}{(M-1)}\right)^{\frac{\Upsilon_1}{2}}A_0^{\Upsilon_1}\left|\begin{matrix}(1-\xi^2,\Upsilon_1),(0,0),(1-m_1,1),\left(1-m_2,\frac{\Upsilon_1}{\Upsilon_2}\right)\\ \left(0,\frac{\Upsilon_1}{2}\right),(-\xi^2,\Upsilon_1)\end{matrix}\right.\right]$$

$$+3H_{4,2}^{1,4}\left[\frac{\Omega_1}{m_1}\left(\frac{\Omega_2}{m_2}\right)^{\frac{\Upsilon_1}{\Upsilon_2}}\left(\frac{7[CNDR_n(I)]_{AV}}{2(M-1)}\right)^{\frac{\Upsilon_1}{2}}A_0^{\Upsilon_1}\left|\begin{matrix}(1-\xi^2,\Upsilon_1),(0,0),(1-m_1,1),\left(1-m_2,\frac{\Upsilon_1}{\Upsilon_2}\right)\\ \left(0,\frac{\Upsilon_1}{2}\right),(-\xi^2,\Upsilon_1)\end{matrix}\right.\right]\Bigg)$$

Equation (6.29) and (6.30) represents the finalized closed form BER expression of OFDM RoFSO link with MQAM modulation over Double Generalized Gamma distribution without and with pointing errors respectively. Also, it is used to achieve BER over other fading models like Gamma-Gamma fading channel and Double Weibull fading channel as a special case by inserting γ_i= 1 and Ω_i= 1/ m_i = 1 over Gamma-Gamma and Double Weibull fading respectively.

6.2.2 K-PSK OFDM Link

BER expression of K-PSK modulation is given as [121],

$$P_{b,K-PSK} = \frac{N^{-1}}{log_2(K)}\sum_{n=0}^{N-1}\left\{erfc\left[\sqrt{CNDR_n(I)}sin\left(\frac{\pi}{k}\right)\right]\right\} \quad (6.32)$$

The average BER estimation of K-PSK modulation over Double Generalized Gamma is expressed as

$$P_{b,K-PSK} = \frac{N^{-1}}{log_2(K)}\sum_{n=0}^{N-1}\int_0^{\infty}\left\{erfc\left[\sqrt{CNDR_n(I)}sin\left(\frac{\pi}{k}\right)\right]f_I(I)dI\right\} \quad (6.33)$$

where, $f_I(I)$ is the PDF of the channel distribution

Now by expressing $erfc(.)$ into Fox H function using Equation (6.23) and also substituting Equation (6.26) into Equation (6.33) and by simplifying we get

$$P_{b,K-PSK} = \frac{N^{-1}}{log_2(K)} \sum_{n=0}^{N-1} \int_0^{\infty} \frac{1}{\sqrt{\pi}} H_{1,2}^{2,0}\left[[CNDR_n(I)]_{AV} I^2 sin^2\left(\frac{\pi}{k}\right) \middle| \begin{matrix} (1,1) \\ (0,1), \left(\frac{1}{2}, 1\right) \end{matrix} \right] \times f_I(I) dI \quad (6.34)$$

6.2.2.1 Without Pointing Errors

Now by substituting the PDF of Double Generalized Gamma distribution without pointing errors from Equation (6.13) in Equation (6.34) we obtained

$$P_{b,K-PSK} = \frac{N^{-1}}{log_2(K)} \sum_{n=0}^{N-1} \int_0^{\infty} \frac{1}{\sqrt{\pi}} H_{1,2}^{2,0}\left[[CNDR_n(I)]_{AV} I^2 sin^2\left(\frac{\pi}{k}\right) \middle| \begin{matrix} (1,1) \\ (0,1), \left(\frac{1}{2}, 1\right) \end{matrix} \right]$$

$$\times \frac{\Upsilon_1}{I\Gamma(m_1)\Gamma(m_2)} H_{2,0}^{0,2}\left[\frac{\Omega_1}{m_1 I^{\Upsilon_1}} \left(\frac{\Omega_2}{m_2}\right)^{\frac{\Upsilon_1}{\Upsilon_2}} \middle| \begin{matrix} \\ (1-m_1,1), \left(1-m_2, \frac{\Upsilon_1}{\Upsilon_2}\right) \end{matrix} \right] dI \quad (6.35)$$

By solving and simplifying the Equation (6.35) using [119] we obtained the finalized expression as

$$P_{b,K-PSK} = \frac{\Upsilon_1 N^{-1}}{2\sqrt{\pi}\Gamma(m_1)\Gamma(m_2) log_2(K)}$$

$$\sum_{n=0}^{N-1} H_{3,2}^{2,2}\left[\frac{\Omega_1}{m_1} \left(\frac{\Omega_2}{m_2}\right)^{\frac{\Upsilon_1}{\Upsilon_2}} \left([CNDR_n(I)]_{AV} sin^2\left(\frac{\pi}{k}\right) \right)^{\frac{\Upsilon_1}{2}} \middle| \begin{matrix} (1-m_1,1), \left(1-m_2, \frac{\Upsilon_1}{\Upsilon_2}\right), \left(1, \frac{\Upsilon_1}{2}\right) \\ \left(0, \frac{\Upsilon_1}{2}\right), \left(\frac{1}{2}, \frac{\Upsilon_1}{2}\right) \end{matrix} \right] \quad (6.36)$$

6.2.2.2 With Pointing Errors

Now by substituting the PDF of Double Generalized Gamma distribution with pointing errors from Equation (6.19) in Equation (6.34) we obtained

$$P_{b,K-PSK} = \frac{N^{-1}}{log_2(K)} \sum_{n=0}^{N-1} \int_0^{\infty} \frac{1}{\sqrt{\pi}} H_{1,2}^{2,0}\left[[CNDR_n(I)]_{AV} I^2 sin^2\left(\frac{\pi}{k}\right) \middle| \begin{matrix} (1,1) \\ (0,1), \left(\frac{1}{2}, 1\right) \end{matrix} \right] \times$$

$$\frac{\Upsilon_1 \xi^2}{I\Gamma(m_1)\Gamma(m_2)} H_{4,1}^{0,4}\left[\left(\frac{\Omega_1}{m_1}\right) \left(\frac{\Omega_2}{m_2}\right)^{\frac{\Upsilon_1}{\Upsilon_2}} \frac{1}{I^{\Upsilon_1}} A_0^{\Upsilon_1} \middle| \begin{matrix} (1-\xi^2, \Upsilon_1), (0,0), (1-m_1, 1), \left(1-m_2, \frac{\Upsilon_1}{\Upsilon_2}\right) \\ (-\xi^2, \Upsilon_1) \end{matrix} \right] dI \qquad (6.37)$$

By solving and simplifying the Equation (6.37) using [119] we obtained the finalized expression as

$$P_{b,K-PSK} = \frac{\Upsilon_1 N^{-1} \xi^2}{2\sqrt{\pi}\Gamma(m_1)\Gamma(m_2) log_2(K)} \sum_{n=0}^{N-1} H_{5,3}^{2,4}\left[\frac{\Omega_1}{m_1} \left(\frac{\Omega_2}{m_2}\right)^{\frac{\Upsilon_1}{\Upsilon_2}} \times \right.$$

$$\left. \left([CNDR_n(I)]_{AV} sin^2\left(\frac{\pi}{k}\right) \right)^{\frac{\Upsilon_1}{2}} A_0^{\Upsilon_1} \middle| \begin{matrix} (1-\xi^2, \Upsilon_1), (0,0), (1-m_1, 1), \left(1-m_2, \frac{\Upsilon_1}{\Upsilon_2}\right), \left(1, \frac{-\Upsilon_1}{2}\right) \\ \left(0, \frac{\Upsilon_1}{2}\right), \left(\frac{1}{2}, \frac{\Upsilon_1}{2}\right), (-\xi^2, \Upsilon_1) \end{matrix} \right] \qquad (6.38)$$

Equation (6.36) and (6.38) represents the finalized closed form BER expression of OFDM RoFSO link with K-PSK modulation over Double Generalized Gamma distribution without and with pointing errors respectively. Also, it is used to achieve BER over other fading models like Gamma-Gamma fading channel and Double Weibull fading channel as a special case by inserting γ_i= 1 and Ω_i= 1/ m_i = 1 over Gamma-Gamma and Double Weibull fading respectively.

6.3 Numerical Results

In this section the proposed analytical expressions of BER for different modulation schemes, in OFDM RoFSO system, are analyzed numerically. Specifically, BER of

MQAM and K-PSK modulation schemes over Double Generalized Gamma distribution, with and without Pointing errors under different turbulence conditions, are presented numerically. Also, as special cases, BER of different modulation schemes over GammaGamma and Double Weibull fading are presented numerically. The simulations are performed in MATLAB. However, the simulation parameters are given in Table 6.1 & Table 6.2.

Table 6.1 Parameters for Double Generalized Gamma Distribution

Double GG Parameters	**Weak**	**moderate**	**Strong**
Υ_1	2.1	2.1690	1.8621
Υ_2	2.1	0.8530	0.7638
m_1	4	0.55	0.5
m_2	4.5	2.35	1.8
Ω 1	1.0676	1.5793	1.507
Ω_2	1.06	0.9671	0.9280
$\sigma 2_{Rytov}$	0.1	2	25

Table 6.2: Parameters for OFDM System

PARAMETER	SYMBOL	VALUE
No of OFDM subcarriers	N	1000
OFDM symbol duration	T_s	1ms
Operating Wavelength	λ	1550 nm
Transmitted optical Power	p_t	20dbm
Atmospheric losses	L_{tot}	-20db
Detector Responsivity	ρ	0.9 A/W
Detector Load Resistance	R_L	50Ω
Relative Intensity Noise	R_{IN}	-130 dB/Hz
Absolute Temperature	T	300K
Third order non-linear parameter	a_3	9 x 10^{-4}

Also, for M-QAM and K-PSK modulation schemes, the order of modulation, M & K are 4, 8 and 16 respectively.

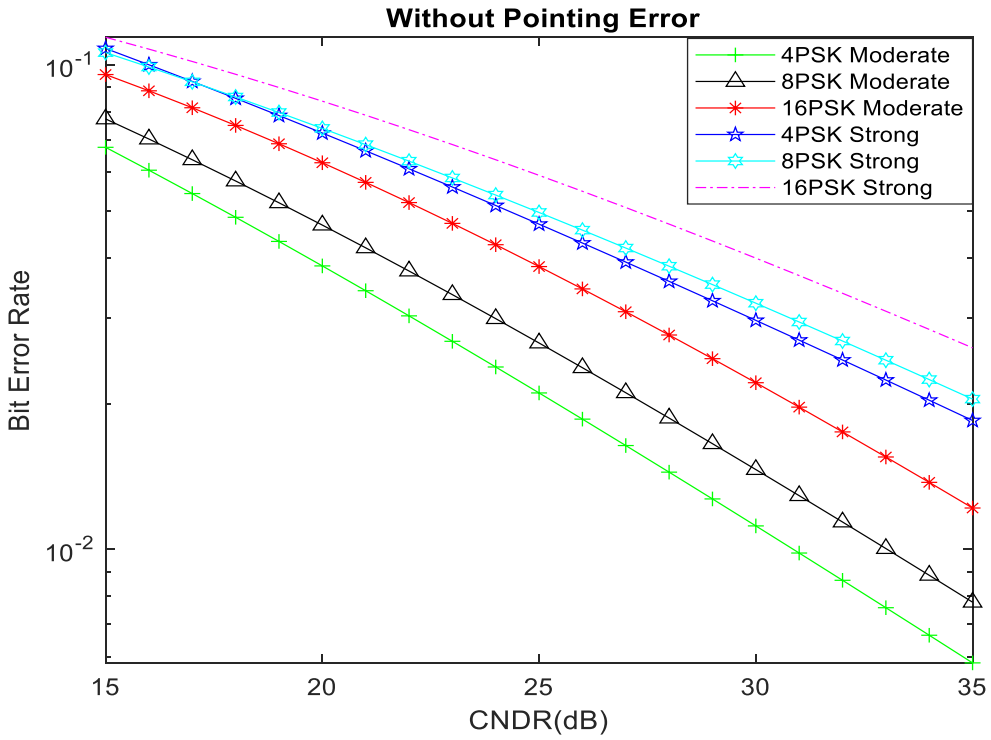

Fig.6.2: BER of K-PSK (K=4, 8 and 16) Modulation Scheme under Moderate and Strong Turbulence Conditions.

Fig.6.2 shows the BER of K-PSK modulation scheme without pointing errors under moderate and strong turbulence conditions. It is observed that at CNDR of 35 dB under moderate turbulence condition, BER of 4PSK, 8PSK & 16PSK modulation schemes, is 0.005828, 0.007778 & 0.01217, respectively. Whereas, at same CNDR, BER for 4PSK, 8PSK & 16PSK modulation scheme is 0.01845, 0.02043 & 0.02607 respectively under strong turbulence conditions. This shows that as the severity of turbulence is increased from moderate to strong, BER increases. Also, irrespective of severity of turbulence be it strong or be it moderate an increase in order of modulation causes in an increase in BER. Observed results shows perfect agreement with theoretical background.

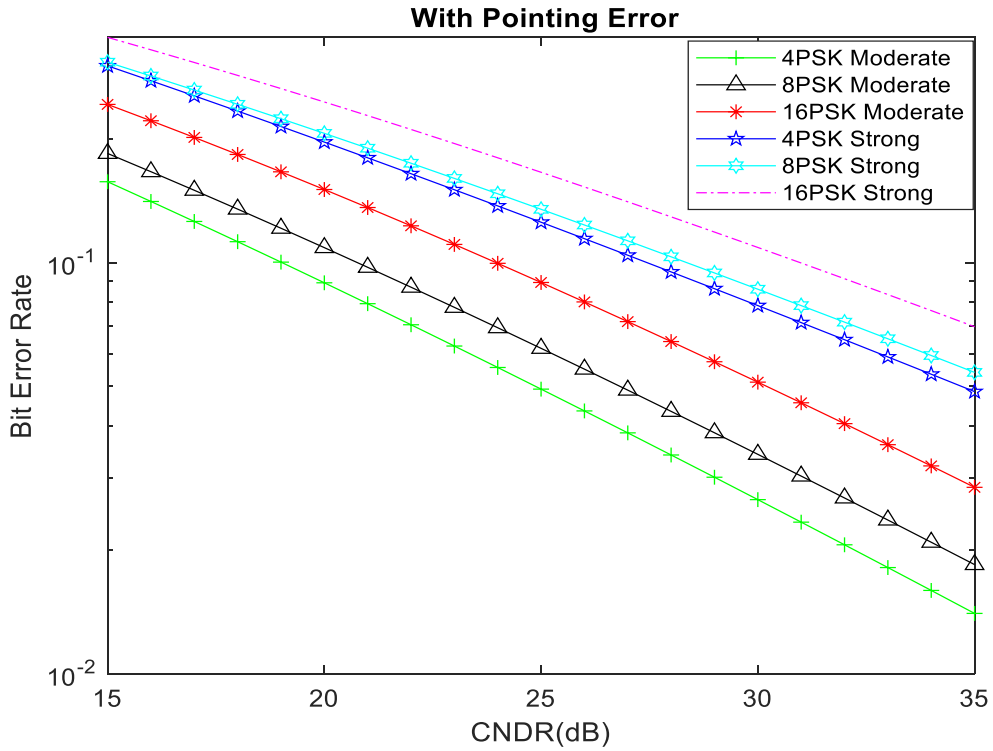

Fig.6.3: BER of KPSK (K=4, 8 and 16) Modulation Scheme with pointing errors under Moderate and Strong Turbulence Conditions.

Fig.6.3 shows the BER of K-PSK modulation scheme with pointing errors under moderate and strong turbulence conditions. It is observed that at CNDR of 35 dB, under moderate turbulence condition, BER of 4PSK, 8PSK & 16PSK modulation schemes, is 0.01403, 0.01844& 0.01403 respectively. Whereas, at same CNDR, BER for 4PSK, 8PSK & 16PSK modulation scheme is 0.04855, 0.05407& 0.06982 respectively under strong turbulence condition. With respect to both turbulence condition and order of modulation, a similar observation is made from Fig.6.3 with pointing error that has been observed from Fig.6.2 without pointing error. However, it is most important to mention that BER performance degrades significantly with pointing errors.

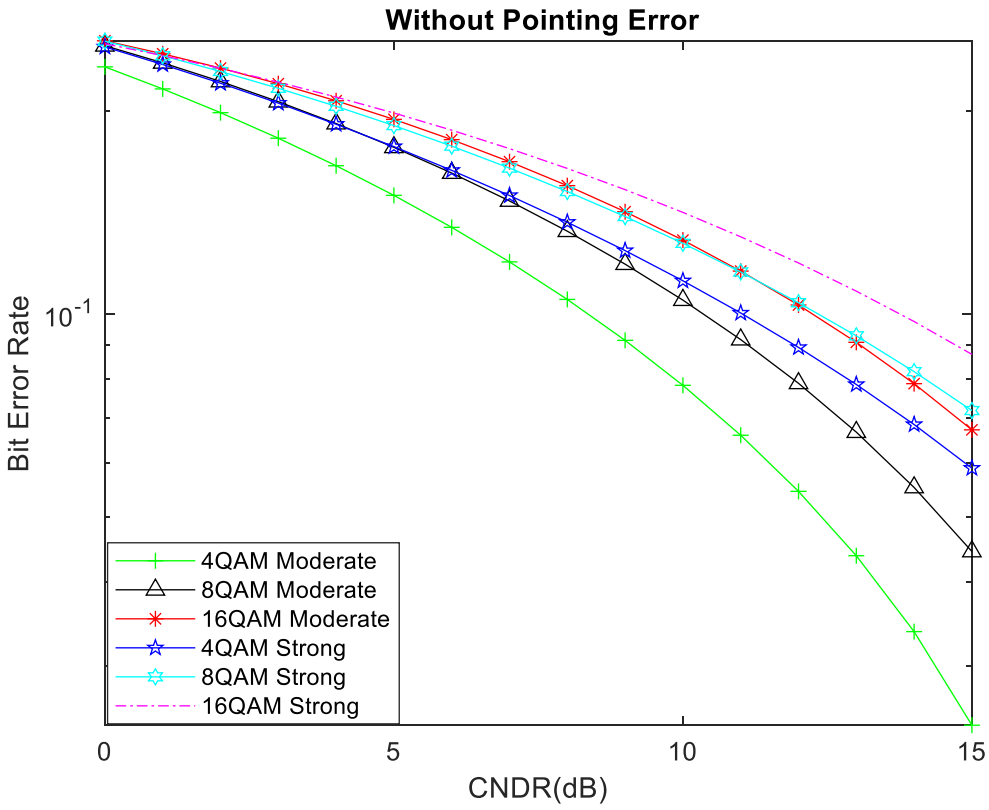

Fig.6.4: BER of MQAM (M=4, 8 and 16) Modulation scheme under Moderate and Strong turbulence conditions.

Fig.6.4 shows the BER of M-QAM modulation scheme without pointing errors under moderate and strong turbulence conditions. It is observed that at CNDR of 15 dB BER obtained is0.02452, 0.04439 & 0.06725 for 4QAM, 8QAM& 16QAM modulation scheme respectively under moderate turbulence condition. Whereas BER obtained is 0.05899, 0.07183 & 0.08703 for 4QAM, 8QAM& 16QAM modulation scheme respectively under strong turbulence condition. With respect to both turbulence condition

and order of modulation, same trend is observed in case of M-QAM modulation as observed in case of K-PSK modulation in Fig.6.2 and Fig.6.3. However, for 8QAM modulation CNDR required is 10.3 dB and 12.3dB for moderate and strong turbulence respectively to achieve a BER of 10^{-1}. Similarly, for 16QAM modulation CNDR required is 12.3 dB and 13.7dB for moderate and strong turbulence respectively. Also, it is observed that if order of modulation is increased form Q =4 to Q =16 BER is increased with an increased from in spectral efficiency. Also, with increased severity, from moderate to strong causes an increase in BER.

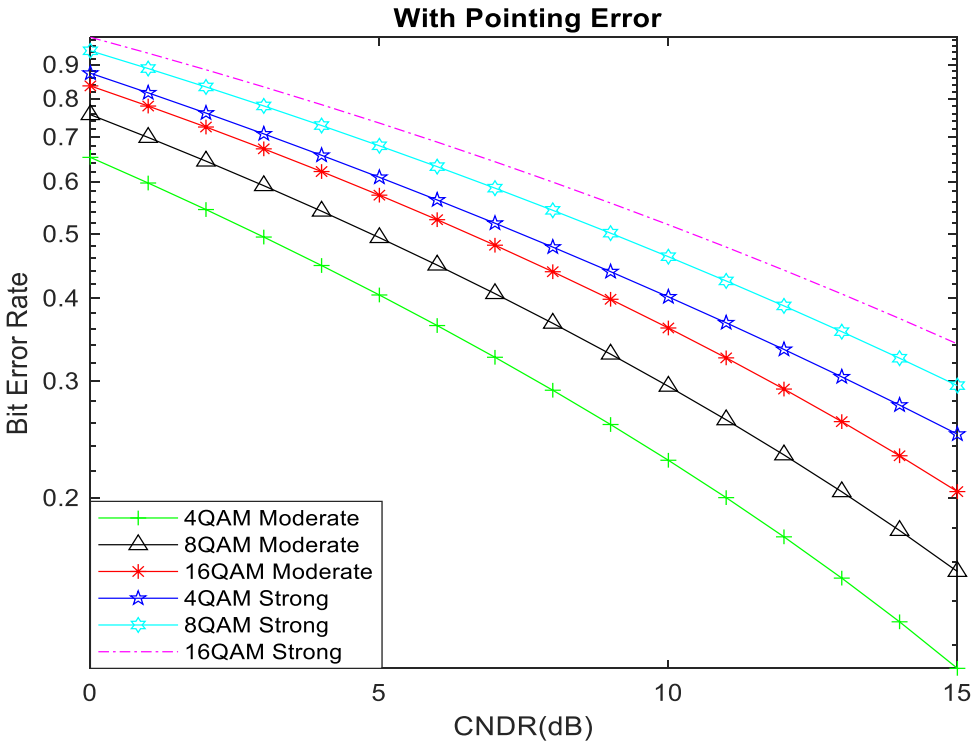

Fig.6.5: BER of MQAM (M=4, 8 and 16) Modulation Scheme with pointing errors under Moderate and Strong Turbulence Conditions.

Fig.6.5 shows the BER of M-QAM modulation scheme with pointing errors subject to moderate and strong turbulence conditions. Much the same as Fig.6.3, it is noticed that pointing errors worsen BER performance significantly. Further, it is noticed that BER

increases by 45% and 26% under moderate and strong turbulence condition respectively, as M increases from M=4 to M=16. This implies that effect of increasing the order of modulation on BER is more severe at moderate turbulence condition as compared to strong turbulence condition.

Fig. 6.6 shows the comparison of BER of 4-PSK modulation with and without pointing errors under weak, moderate and strong turbulence conditions. At CNDR of 35 dB BER obtained is 4.57 x 10^{-11}, 0.005828 & 0.01815 for 4PSK modulation without pointing errors under weak, moderate, and strong turbulence condition respectively. Similarly, BER obtained is 0.0001141, 0.01403& 0.04855 for 4PSK modulation with Pointing errors under weak, moderate, and strong turbulence condition respectively. The study reveals that BER performance degrades by 98% for weak, 58% for moderate and 62% for strong turbulence condition due to pointing errors. It is clearly inferred that Pointing error degrades in the BER irrespective of turbulence conditions.

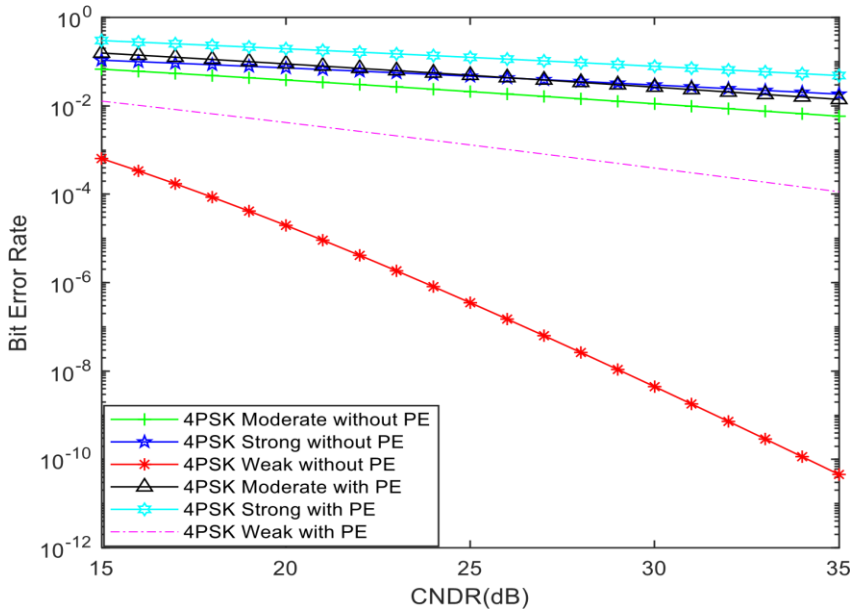

Fig.6.6: Comparison of BER of 4PSK modulation scheme with and without pointing errors under weak, moderate and strong turbulence conditions.

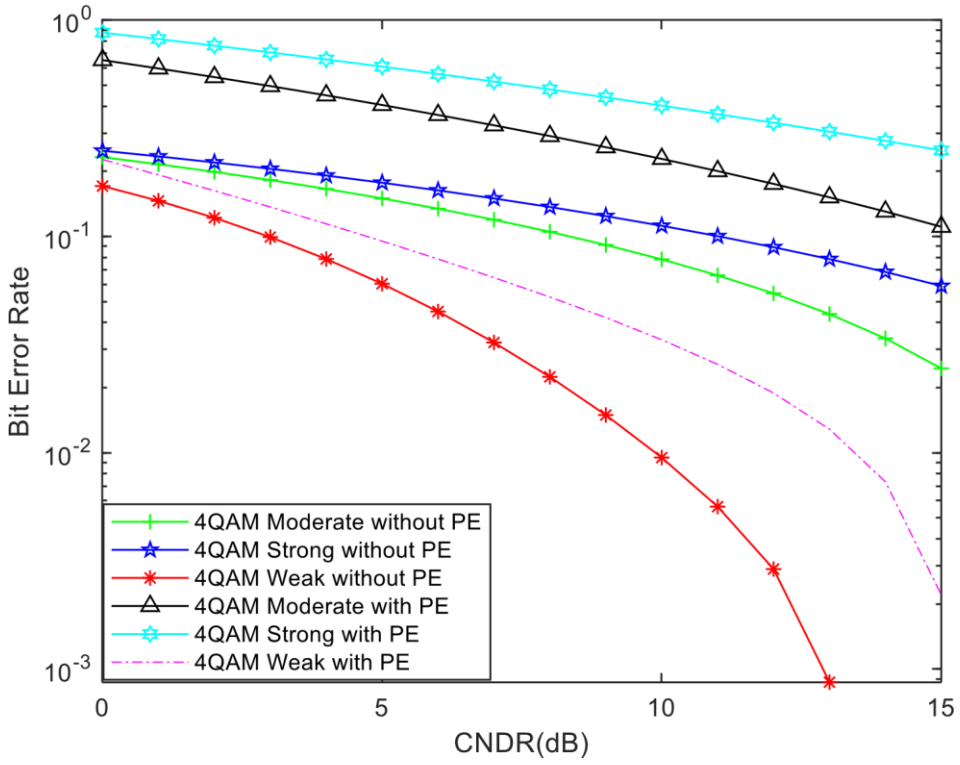

Fig.6.7: Comparison of BER of 4QAM modulation scheme with and without pointing errors under weak, moderate and strong turbulence conditions.

Fig.6.7 shows the comparison of BER of 4-QAM modulation with and without pointing errors under weak, moderate and strong turbulence conditions. Similar to Fig.6.6 here BER degrades by 93% in weak, 77% in moderate and 76% in strong turbulence condition due to pointing errors. Further, BER degrades significantly when fading severity increases from weak to moderate as compared to moderate to strong. Also, the effect of PE is more intense on BER when OFDM RoFSO link is under weak turbulence as compared to moderate and strong turbulence conditions.

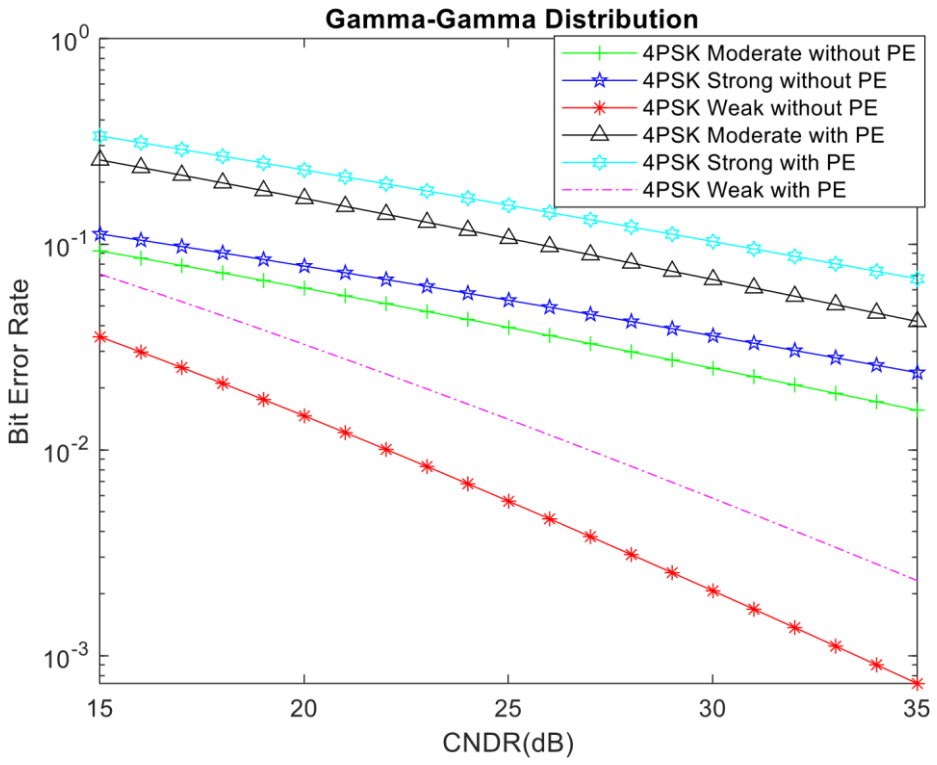

Fig.6.8: Comparison of BER of 4PSK modulation scheme over Gamma-Gamma fading with and without pointing errors under weak, moderate and strong turbulence conditions

Fig.6.8 shows the comparison of BER of 4-PSK modulation over Gamma-Gamma fading with and without pointing errors under weak, moderate and strong turbulence conditions. It noteworthy to mention that Gamma-Gamma distribution is obtained as a special case of Generalized Double Gamma distribution by inserting $m_i = 1$. It is noticed that at CNDR of 35 dB BER obtained is 0.0007342, 0.01564 & 0.02381 under weak, moderate and strong turbulence condition respectively for 4PSK modulation without pointing errors. Whereas, it is 0.002321, 0.0422& 0.0681 under weak, moderate and strong turbulence condition respectively for 4PSK modulation with Pointing errors. Observation of BER under different modulation and/or turbulence condition is similar to those over Double generalized Gamma distribution.

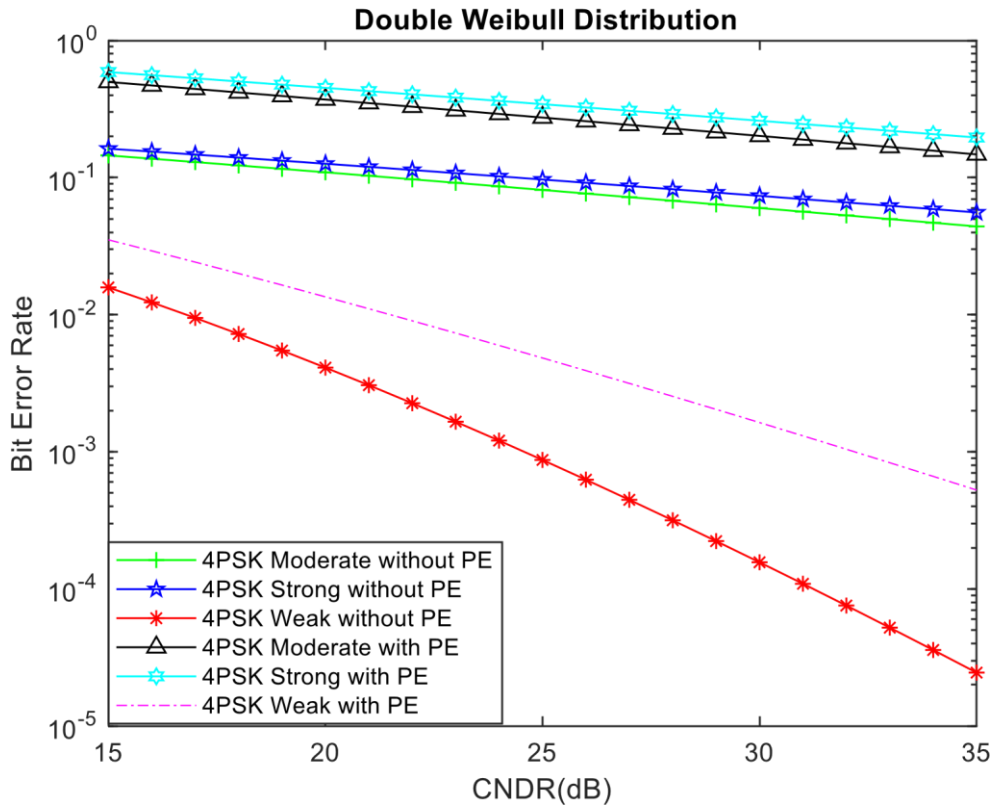

Fig.6.9: Comparison of BER of 4PSK modulation scheme over Double Weibull fading with and without pointing errors under weak, moderate and strong turbulence conditions

Fig.6.9 shows the comparison of BER of 4-PSK modulation over Double Weibull fading with and without pointing errors under weak, moderate and strong turbulence conditions. It is again important to mention that Double Weibull distribution is a special case of Generalized Double Gamma distribution obtained by putting γ_i= 1 and Ω_i= 1 BER is 2.45 x 10^{-5}& 5.2 x10^{-4} in absence and presence of pointing errors respectively under weak turbulence conditions. This shows that effect of pointing error is more under weak turbulence condition as compared to moderate and strong turbulence conditions.

Fig.6.10 shows the comparison of BER of 4QAM modulation over Gamma-Gamma fading with and without pointing errors under weak, moderate and strong turbulence conditions.

A similar observation is made that has been observed in Fig.6.8.

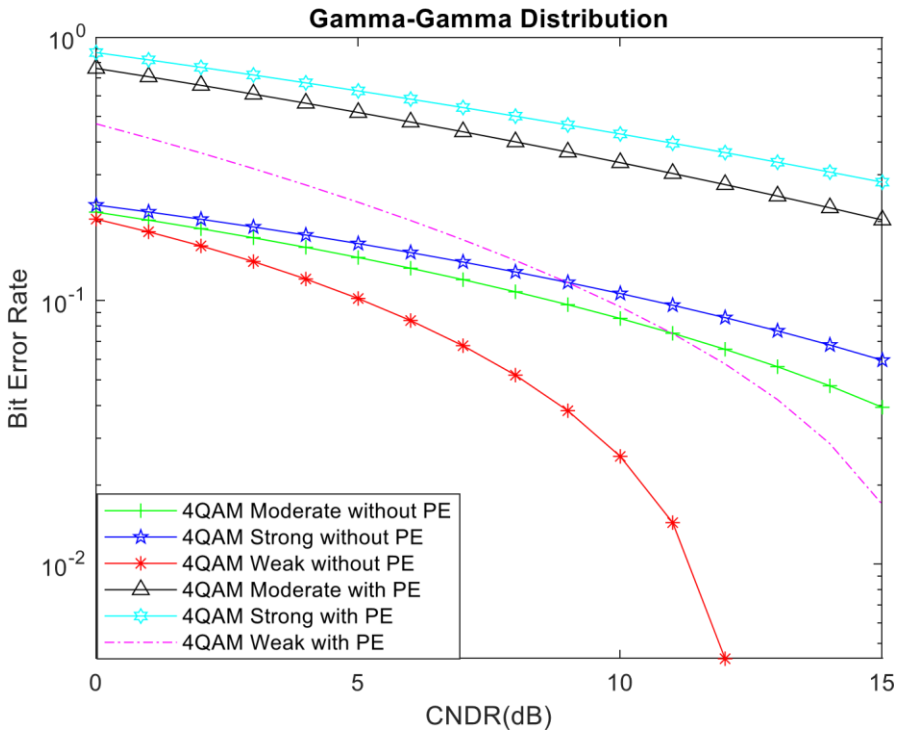

Fig.6.10: Comparison of BER of 4QAM modulation scheme over Gamma-Gamma fading with and without pointing errors under weak, moderate and strong turbulence conditions

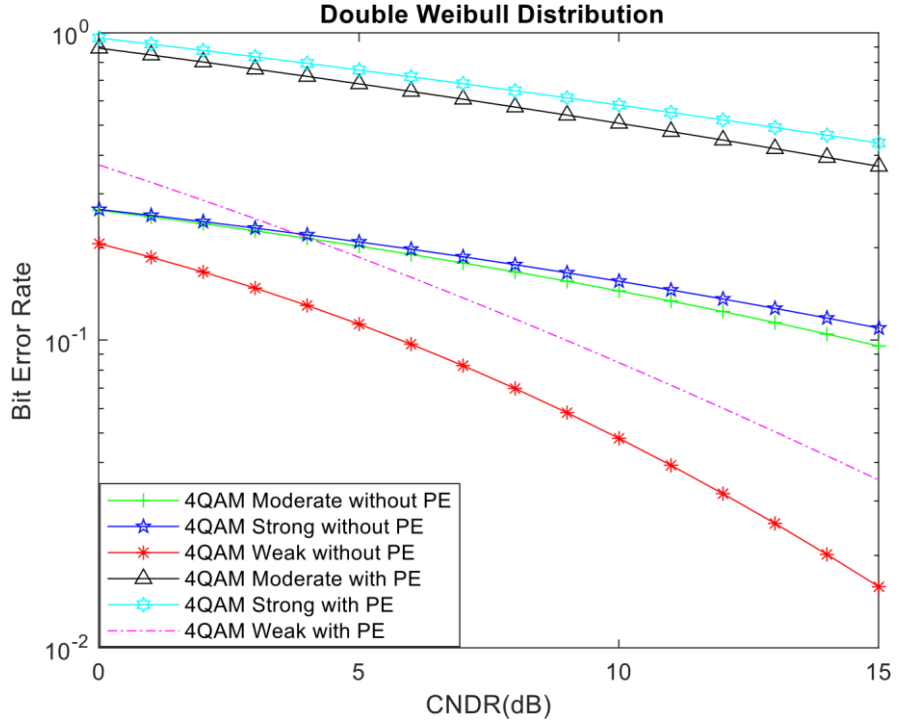

Fig.6.11: Comparison of BER of 4QAM modulation scheme over Double Weibull fading with and without pointing errors under weak, moderate and strong turbulence conditions

Fig.6.11 shows the comparison of BER of 4-QAM modulation over Double Weibull fading with and without pointing errors under weak, moderate and strong turbulence conditions. Observations from Fig.6.11 are similar to Fig.6.9, pointing error degrades the performance irrespective of all turbulence conditions.

Summary

In this chapter, License free spectrum, high data rates and ease of installation make Radio on Free space optical (Ro-FSO) ubiquitous for upcoming generation of communication system. However, atmospheric turbulence induced fading and/or pointing error are the challenging issues of Ro-FSO system. The effects of these issues on performance of RoFSO has been thoroughly analyzed by presenting closed form expressions under different turbulence conditions for different schemes. Specifically, BER of M-QAM and K-PSK modulation schemes over Double Generalized Gamma Fading distribution, under weak, moderate, and strong turbulence conditions, for OFDM based Ro-FSO system has been analyzed by presenting closed form expressions for respective measures. Further, closed form expressions and in turn the presented analysis is based on with and without pointing errors. Furthermore, presented expressions have been deduced over Gamma-Gamma and double Weibull fading as a special case of Double Generalized Gamma Fading distribution. BER of M-QAM and K-PSK modulation schemes for different values of K/M, different values of turbulence conditions and with or without pointing errors has been observed numerically. Observation shows that irrespective of severity of turbulence be it strong or be it moderate an increase in order of modulation causes in an increase in BER. Also, pointing errors deteriorate the BER irrespective of severity and/or order of modulation schemes. Finally, it is observed that the effect of the order of modulation scheme on BER is more severe under moderate turbulence condition than under strong turbulence condition. Whereas, the effect of pointing error on BER is more under weak turbulence than under strong turbulence conditions.

CHAPTER 7

CONCLUSION AND FUTURE WORK

This thesis has undertaken an in-depth investigation into the performance analysis of a dual-hop RF/FSO communication system, which combines the robustness of RF channels and the high data rate capabilities of FSO links. The proposed system leverages Mixture Gamma (MG) distribution to model the RF channel and Double Generalized Gamma (Double GG) distribution to model the FSO channel. This modelling approach accurately reflects real-world channel impairments, including atmospheric turbulence, pointing errors, and multipath fading.

7.1. Summary of the Work Done in Thesis

The key contributions and findings of this research are summarized below:

1. Modelling and Analysis of Dual-Hop RF/FSO System:

   A dual-hop communication system was modelled where the RF hop is represented using the Mixture Gamma distribution and the FSO hop is modelled using the Double GG distribution. This combination enables effective performance characterization under diverse atmospheric and channel conditions, including weak, moderate, and strong turbulence.

2. Outage Capacity and Ergodic Capacity (EC):

   Analytical closed-form expressions for Outage Capacity and Ergodic Capacity were derived across multiple fading scenarios. Results show that:

   - Outage Capacity decreases with increasing outage threshold and turbulence severity but increases with average SNR.
   - Ergodic Capacity improves with increasing SNR and decreases with increasing path loss.
   - Nakagami-m fading outperforms Rayleigh fading due to its flexibility in representing a wider range of fading environments.

3. Capacity Analysis under EGC Scheme:

   In the FSO subsystem, Equal Gain Combining (EGC) was applied to combat atmospheric turbulence. The Average Capacity (AC) under EGC was analyzed using the MGF-based approach, and closed-form expressions were derived. It was observed that:

- Increasing the number of diversity branches (L) enhances capacity, but the gain diminishes beyond L = 2.
- Capacity reduction is more significant under strong turbulence than under weak or moderate conditions.

4. Symbol Error Rate (SER) Analysis:
   Closed-form expressions for SER of M-PSK and M-QAM modulation schemes over Double GG fading with EGC were developed using Fox-H functions. Key observations include:
   - SER increases with turbulence severity and modulation order.
   - The performance degradation is more significant when transitioning from weak to moderate turbulence than from moderate to strong.
5. OFDM-based Ro-FSO Link with Pointing Error Analysis:
   An OFDM Radio-over-FSO system was designed and analyzed, with BER expressions derived for M-QAM and K-PSK under both pointing error and no pointing error scenarios. The findings reveal:
   - Pointing errors significantly degrade BER performance, especially under weak turbulence.
   - Higher-order modulations are more susceptible to performance degradation due to increased sensitivity to SNR variations.
6. Validation through MATLAB Simulations:
   All derived analytical results were validated using MATLAB simulations. The simulations strongly agree with theoretical predictions, proving the reliability of the proposed models and derived expressions.

In conclusion, this thesis successfully demonstrates that hybrid dual-hop RF/FSO systems, modelled with advanced fading distributions, provide a robust and flexible communication architecture capable of meeting the demands of next-generation wireless networks, despite the presence of challenging environmental conditions.

7.2. Future Scope

Although this thesis has made significant contributions to the understanding and optimization of dual-hop RF/FSO systems in complex channel environments, several promising avenues remain for future research.

1. Extension to MIMO-RF/FSO Systems:

- Incorporating Multiple Input Multiple Output (MIMO) techniques into the dual-hop RF/FSO framework could further enhance the system capacity and reliability.
- MIMO-FSO with spatial diversity and spatial multiplexing could mitigate turbulence and pointing errors more effectively.

2. Machine Learning and AI-based Channel Estimation:
    - Real-time channel estimation and prediction using machine learning algorithms (e.g., reinforcement learning, deep neural networks) could dynamically adapt transmission parameters to changing weather and channel conditions.
    - Such techniques could optimize modulation schemes, coding rates, and relay selection in real-time.
3. Experimental Testbed and Field Trials:
    - Practical deployment and experimentation of the proposed models using testbeds would help validate the results under real atmospheric turbulence, building sway, and environmental noise.
    - Implementation on drones or high-rise buildings could be explored for urban communication scenarios.
4. Advanced Relay Protocols:
    - Exploring other relaying strategies such as Decode-and-Forward (DF), Compress-and-Forward (CF), or adaptive relaying can yield better throughput and energy efficiency compared to the current Amplify-and-Forward (AF) scheme.

Publications Related to the Thesis

Published Journal Papers:

1. Piyush Jain, Jayanthi. N and Lakshmanan. M. "ABER of M-QAM and K-PSK Modulations over Double-GG Fading Channel", Published in International Journal of Electronics, ISSN 0020-7217 (Print) 1362-3060 (Online), Vol. 110, No. 5, 2023, pp. 934 – 954. (SCI/Scopus) (IF = 1.336).
   (DOI: https://doi.org/10.1080/00207217.2022.2068196)

2. Piyush Jain, Jayanthi. N and Lakshmanan. M. "Closed Form Expressions of AC and SER for Double GG Fading Distribution under EGC Scheme in FSO Communication System", Published in Wireless Personal Communications, ISSN 0929-6212 (Print) 1572-834X (Online), Vol. 127, No.4, 2022, pp. 2935 – 2954. (SCI/Scopus) (IF = 1.671). (DOI: https://doi.org/10.1007/s11277-022-09904-7)

Conference Papers:

1. Piyush Jain, N. Jayanthi and Lakshmanan. M. "Ergodic Capacity of Mixture Gamma and Double Generalized Gamma Distribution in Dual Hop RF/FSO Transmission System", Published in IEEE Xplore in the proceedings of 2nd IEEE International Conference on Vision Towards Emerging Trends in Communication and Networking Technologies (ViTECoN), held at VIT University, Vellore, India on May 05 & 06, 2023. (Scopus) . (DOI: https://doi.org/10.1109/ViTECoN58111.2023.10157813)

2. Piyush Jain, N. Jayanthi and Lakshmanan. M. "Outage Capacity of Mixture Gamma and Double Generalized Gamma Distribution in Dual Hop RF/FSO Transmission System", Published in IEEE Xplore in the proceedings of 2nd IEEE International Conference on Vision Towards Emerging Trends in Communication and Networking Technologies (ViTECoN), held at VIT University, Vellore, India on May 05 & 06, 2023 (Scopus).
   (DOI: https://doi.org/10.1109/ViTECoN58111.2023.10157741)

3. Piyush Jain, Jayanthi. N, Lakshmanan. M. "Performance of Hybrid LPPM-POLSK-SIM in FSO over Double GG Fading Distribution", Shashwat Rai, Vineet Singh and Shreyanshi Agrawal, Published in IEEE Xplore in the proceedings of IEEE Sponsored International

Conference on Advance Computing and Innovative Technologies in Engineering (ICACITE 2021) held at Galgotias College of Engineering and Technology, Greater Noida, India on March 04 & 05, 2021, pp. 832 – 835. (Scopus).
(DOI: https://doi.org/10.1109/ICACITE51222.2021.9404658)

4. Piyush Jain, N Jayanthi, M Lakshmanan "BER Analysis of PolSK Modulation for FSO Communication System with Generalized Pointing Error over Double GG Turbulence Channel", Tushar Sharma, Siddharth Saini, Shambhavi, Published in IEEE Xplore in the proceedings of IEEE Sponsored International Conference on Advance Computing and Innovative Technologies in Engineering (ICACITE 2021) held at Galgotias College of Engineering and Technology, Greater Noida, India on March 04 & 05, 2021, pp. 1 – 5. (Scopus).

   (DOI: https://doi.org/10.1109/ICACITE51222.2021.9404594)

References

[1] Kashani, M.A., Uysal, M. and Kavehrad, M., 2015. A novel statistical channel model for turbulence-induced fading in free-space optical systems. *Journal of Lightwave Technology*, *33*(11), pp.2303-2312.

[2] Khalighi, M.A. and Uysal, M., 2014. Survey on free space optical communication: A communication theory perspective. *IEEE communications surveys & tutorials*, *16*(4), pp.2231-2258.

[3] Alkholidi, A. and Altowij, K., 2012. Effect of clear atmospheric turbulence on quality of free space optical communications in Western Asia. *Optical Communications Systems*, p.41.

[4] Anbarasi, K., Hemanth, C. and Sangeetha, R.G., 2017. A review on channel models in free space optical communication systems. *Optics & Laser Technology*, *97*, pp.161-171.

[5] Willebrand, H.A. and Ghuman, B.S., 2001. Fiber optics without fiber. *IEEE spectrum*, *38*(8), pp.40-45.

[6] M. A. Esmail, H. Fathallah and M. Alouini, "Analysis of fog effects on terrestrial Free Space optical communication links," *2016 IEEE International Conference on Communications Workshops (ICC)*, Kuala Lumpur, 2016, pp. 151-156.

[7] McCartney, E.J., 1976. Optics of the atmosphere: scattering by molecules and particles. *New York, John Wiley and Sons, Inc., 1976. 421 p.*

[8] Yi, X., Yao, M. and Wang, X., 2017. MIMO FSO communication using subcarrier intensity modulation over double generalized gamma fading. *Optics Communications*, *382*, pp.64-72.

[9] Liu, H., Liao, R., Wei, Z., Hou, Z. and Qiao, Y., 2015. BER analysis of a hybrid modulation scheme based on PPM and MSK subcarrier intensity modulation. *IEEE Photonics Journal*, *7*(4), pp.1-10.

[10] Al-Nahhal, M., & Ismail, T. (2019). Enhancing spectral efficiency of FSO system using adaptive SIM/M-PSK and SIMO in the presence of atmospheric turbulence and pointing errors. *International Journal of Communication Systems*, *32*(9), e3942.

[11] Andrews, L.C. and Phillips, R.L., 2005. Laser beam propagation through random media (Vol. 152). Bellingham, WA: SPIE press.

[12] Belmonte, A., Comerón, A., Rubio, J.A., Bará, J. and Fernández, E., 1997. Atmospheric- turbulence-induced power-fade statistics for a multiaperture optical receiver. Applied optics, 36(33), pp.8632-8638.

[13] Aloui ni, M.S. and Goldsmith, A.J., 1999. A unified approach for calculating error rates of linearly modulated signals over generalized fading channels. IEEE Transactions on Communications, 47(9), pp.1324-1334.

[14] Popoola, W.O., Ghassemlooy, Z., Allen, J.I.H., Leitgeb, E. and Gao, S., 2008 Free-space optical communication employing subcarrier modulation and spatial diversity in atmospheric turbulence channel. IET optoelectronics, 2(1), pp.16-23.

[15] Simon, M.K. and Vilnrotter, V.A., 2005. Alamouti-type space-time coding for free-space optical communication with direct detection. IEEE Transactions on Wireless Communications, 4(1), pp.35-39.

[16] Wilson, S.G., Brandt-Pearce, M., Cao, Q. and Baedke, M., 2005. Optical repetition MIMO transmission with multipulse PPM. IEEE journal on Selected Areas in Communications, 23(9), pp.1901-1910.

[17] Uysal, M., Li, J. and Yu, M., 2006. Error rate performance analysis of coded free-space optical links over gamma-gamma atmospheric turbulence channels. IEEE Transactions on wireless communications, 5(6), pp.1229-1233.

[18] Chatzidiamantis, N.D., Sandalidis, H.G., Karagiannidis, G.K., Kotsopoulos, S.A. and Matthaiou, M., 2010, April. New results on turbulence modeling for free-space optical systems. In 2010 17th International Conference on Telecommunications (pp. 487-492). IEEE.

[19] Jurado-Navas, A., Garrido-Balsells, J.M., Paris, J.F. and Puerta-Notario, A., 2011. A unifying statistical model for atmospheric optical scintillation. arXiv preprint arXiv:1102.1915.

[20] Peppas, K.P., 2011. A simple, accurate approximation to the sum of Gamma–Gamma variates and applications in MIMO free-space optical systems. IEEE Photonics Technology Letters, 23(13), pp.839-841.

[21] Faridzadeh, M., Gholami, A., Ghassemlooy, Z. and Rajbhandari, S., 2012. Hybrid pulse position modulation and binary phase shift keying subcarrier intensity modulation for free space optics in a weak and saturated turbulence channel. JOSA A, 29(8), pp.1680- 1685

[22] Song, X. and Cheng, J., 2013. Subcarrier intensity modulated MIMO optical communications in atmospheric turbulence. Journal of Optical Communications and Networking, 5(9), pp.1001-1009.

[23] Luong, D.A., Thang, T.C. and Pham, A.T., 2013. Effect of avalanche photodiode and thermal noises on the performance of binary phase-shift keying-subcarrier-intensity modulation/free-space optical systems over turbulence channels. IET Communications, 7(8), pp.738-744.

[24] Malik, A., & Singh, P. (2015). Free space optics: current applications and future challenges. International Journal of Optics, 2015.

[25] Singhal, P., Gupta, P. and Rana, P., 2015, April. Basic concept of free space optics communication (FSO): An overview. In 2015 International Conference on Communications and Signal Processing (ICCSP) (pp. 0439-0442). IEEE.

[26] Jagadeesh, V.K., Palliyembil, V., Muthuchidambaranathan, P. and Bui, F.M., 2015. Free space optical communication using subcarrier intensity modulation through generalized turbulence channel with pointing error. Microwave and Optical Technology Letters, 57(8), pp.1958-1961.

[27] Kaur, P., Jain, V.K. and Kar, S., 2015. Performance analysis of free space optical links using multi-input multi-output and aperture averaging in presence of turbulence and various weather conditions. IET Communications, 9(8), pp.1104-1109.

[28] Liu, H., Liao, R., Wei, Z., Hou, Z. and Qiao, Y., 2015. BER analysis of a hybrid modulation scheme based on PPM and MSK subcarrier intensity modulation. IEEE Photonics Journal, 7(4), pp.1-10.

[29] Vellakudiyan, J., Muthuchidambaranathan, P., Bui, F.M. and Palliyembil, V., 2015. Performance of a subcarrier intensity modulated differential phase-shift keying over generalized turbulence channel. AEU-International Journal of Electronics and Communications, 69(11), pp.1569-1573.

[30] Aminikashani, M., Kavehrad, M. and Gu, W., 2016, February. Error performance analysis of FSO links with equal gain diversity receivers over double generalized gamma fading channels. In Broadband Access Communication Technologies X

(Vol. 9772, p. 97720R). International Society for Optics and Photonics.

[31] Bhatnagar, M.R. and Ghassemlooy, Z., 2016. Performance analysis of gamma–gamma fading FSO MIMO links with pointing errors. Journal of Lightwave technology, 34(9), pp.2158-2169.

[32] Esmail, M.A., Fathallah, H. and Alouini, M.S., 2016. An experimental study of FSO link performance in desert environment. IEEE Communications Letters, 20(9), pp.1888- 1891.

[33] Giri, R.K. and Patnaik, B., 2017. Bit error rate performance analysis of hybrid subcarrier intensity modulation-based FSO with spatial diversity in various weather conditions. Journal of Optical Communications.

[34] Yacoub, M.D., 2007. The $\alpha $-$\mu $ Distribution: A Physical Fading Model for the Stacy Distribution. IEEE Transactions on Vehicular Technology, 56(1), pp.27-34.

[35] Arimoto, Y., 2010, February. Near field laser transmission with bidirectional beacon tracking for Tbps class wireless communications. In Free-Space Laser Communication Technologies XXII (Vol. 7587, p. 758708). International Society for Optics and Photonics.

[36] Ciaramella, E., Arimoto, Y., Contestabile, G., Presi, M., D'Errico, A., Guarino, V. and Matsumoto, M., 2009. 1.28 Terabit/s (32x40 Gbit/s) WDM transmission system for free space optical communications. IEEE Journal on selected areas in communications, 27(9), pp.1639-1645.

[37] Sova, R.M., Sluz, J.E., Young, D.W., Juarez, J.C., Dwivedi, A., Demidovich, N.M., Graves, J.E., Northcott, M., Douglass, J., Phillips, J. and Driver, D., 2006, September. 80 Gb/s free-space optical communication demonstration between an aerostat and a ground terminal. In Free-Space Laser Communications VI (Vol. 6304, p. 630414). International Society for Optics and Photonics.

[38] Kvíčala, R., Kvičera, V., Grabner, M. and Fišer, O., 2007. BER and availability measured on FSO link. Radio engineering, 16(3), p.7.

[39] Bell, A.G., 1880. Upon the production and reproduction of sound by light. Journal of the Society of Telegraph Engineers, 9(34), pp.404-426.

[40] Uysal, M., Li, J. and Yu, M., 2006. Error rate performance analysis of coded free-space optical links over gamma-gamma atmospheric turbulence channels. IEEE Transactions on wireless communications, 5(6), pp.1229-1233.

[41] Moon Todd, K., Error correction coding: mathematical methods and algorithms. 2005 by John Wiley & Sons.

[42] Kahn, J.M. and Barry, J.R., 1997. Wireless infrared communications. Proceedings of the IEEE, 85(2), pp.265-298.

[43] Wong, K.K., O'Farrell, T. and Kiatweerasakul, M., 2000. The performance of optical wireless OOK, 2-PPM and spread spectrum under the effects of multipath dispersion and artificial light interference. International Journal of Communication Systems, 13(7-8), pp.551-576.

[44] Doss-Hammel, S., Oh, E., Ricklin, J.C., Eaton, F.D., Gilbreath, G.C. and Tsintikidis, D., 2004, October. A comparison of optical turbulence models. In Free-Space Laser Communications IV (Vol. 5550, pp. 236-247). International Society for Optics and Photonics.

[45] Ricklin, J.C., Hammel, S.M., Eaton, F.D. and Lachinova, S.L., 2006. Atmospheric channel effects on free-space laser communication. Journal of Optical and Fiber Communications Reports, 3(2), p.111.

[46] Mohammed, Nazmi A., et al. "Performance evaluation of FSO link under NRZ-RZ line codes, different weather conditions and receiver types in the presence of pointing errors." The Open Electrical & Electronic Engineering Journal 6.1 (2012).

[47] Porras, R.A.B., 2013. Exponentiated Weibull fading channel model in free-space optical communications under atmospheric turbulence (Doctoral dissertation, Universitat Politècnica de Catalunya).

[48] Sandalidis, H.G. and Tsiftsis, T.A., 2008. “Outage probability and ergodic capacity of free-space optical links over strong turbulence”. Electronics Letters, 44(1), pp.46-47.

[49] Magableh, A.M. and Matalgah, M.M., 2009. “Moment generating function of the generalized α-μ distribution with applications”. IEEE Communications Letters, 13(6), pp.411-413.

[50] Dohler, M. and Arndt, M., 2006. Inverse incomplete gamma function and its application. Electronics Letters, 42(1), pp.35-36.

[51] Pesek, J., Fiser, O., Svoboda, J. and Schejbal, V., 2010. Modeling of 830 nm FSO Link Attenuation in Fog or Wind Turbulence. Radio engineering, 19(2).

[52] Nistazakis, H.E., Assimakopoulos, V.D. and Tombras, G.S., 2011. Performance estimation of free space optical links over negative exponential atmospheric turbulence channels. OPTIK-International Journal for Light and Electron Optics, 122(24), pp.2191- 2194.

[53] Barrios, R. and Dios, F., 2012, October. Probability of fade and BER performance of FSO links over the Exponentiated Weibull fading channel under aperture averaging. Unmanned/Unattended Sensors and Sensor Networks IX (Vol. 8540, p. 85400D). International Society for Optics and Photonics.

[54] Peppas, K.P., Stassinakis, A.N., Topalis, G.K., Nistazakis, H.E. and Tombras, G.S., 2012. Average capacity of optical wireless communication systems over IK atmospheric turbulence channels. IEEE/OSA Journal of Optical Communications and Networking, 4(12), pp.1026-1032.

[55] Mohammed, N.A., El-Wakeel, A.S. and Aly, M.H., 2012. Performance evaluation of FSO link under NRZ-RZ line codes, different weather conditions and receiver types in the presence of pointing errors. Open Electrical & Electronic Engineering Journal, 6, pp.28- 35.

[56] Vats, A. and Kaushal, H., 2014. Analysis of free space optical link in turbulent atmosphere. Optik-International Journal for Light and Electron Optics, 125(12), pp.2776- 2779.

[57] Kumar, A., Dhiman, A., Kumar, D. and Kumar, N., 2013. Free space optical communication system under different weather conditions. IOSR Journal of Engineering (IOSRJEN), 3(12), pp.52-58.

[58] Singh, N.S. and Singh, G., 2013. Performance Evaluation of Log-normal And Negative Exponential Channel Modeling Using Various Modulation Techniques in OFDM-FSO Communication. International Journal of Computers & Technology, 4(2c2), pp.639-647.

[59] Gradshteyn, I.S. and Ryzhik, I.M., 2014. Table of integrals, series, and products. Academic press.

[60] Khalighi, M.A. and Uysal, M., 2014. Survey on free space optical communication: A communication theory perspective. IEEE communications surveys & tutorials, 16(4), pp.2231-2258.

[61] Giri, R.K. and Patnaik, B., 2019. Bit error rate performance analysis of hybrid subcarrier intensity modulation-based FSO with spatial diversity in various weather conditions. Journal of Optical Communications, 40(3), pp.307-314.

[62] AlQuwaiee, H., Ansari, I.S. and Alouini, M.S., 2016. On the maximum and minimum of double generalized gamma variates with applications to the performance of free-space optical communication systems. IEEE Transactions on Vehicular Technology, 65(11), pp.8822-8831.

[63] Kashani, M.A., Uysal, M. and Kavehrad, M., 2015, June. On the performance of MIMO FSO communications over double generalized gamma fading channels. In 2015 IEEE International Conference on Communications (ICC) (pp. 5144-5149). IEEE.

[64] Li, J., Liu, J.Q. and Taylor, D.P., 2007. Optical communication using subcarrier PSK intensity modulation through atmospheric turbulence channels.

[65] Kaur, P., Jain, V.K. and Kar, S., 2015. Performance analysis of free space optical links using multi-input multi-output and aperture averaging in presence of turbulence and various weather conditions. IET Communications, 9(8), pp.1104-1109.

[66] Saeed, R.A. and Abbas, E.B., 2018, August. Performance Evaluation of MIMO FSO Communication with Gamma-Gamma Turbulence Channel using Diversity Techniques. In 2018 International Conference on Computer, Control, Electrical, and Electronics Engineering (ICCCEEE) (pp. 1-5). IEEE.

[67] Johnsi, A.A. and Saminadan, V., 2013, April. Performance of diversity combining techniques for fso-mimo system. In 2013 International Conference on Communication and Signal Processing (pp. 479-483). IEEE.

[68] Saber, M.J. and Keshavarz, A., 2018, May. On performance of adaptive subcarrier intensity modulation over generalized FSO links. In Electrical Engineering (ICEE), Iranian Conference on (pp. 358-361). IEEE.

[69] Sadiku, M.N., Musa, S.M. and Nelatury, S.R., 2016. Free space optical communications: An overview. European scientific journal, 12(9).

[70] Dabiri, M.T., Sadough, S.M.S. and Khalighi, M.A., 2017. FSO channel estimation for OOK modulation with APD receiver over atmospheric turbulence and pointing errors. Optics Communications, 402, pp.577-584.

[71] Kaur, G., Singh, H. and Sappal, A.S., 2017. Free space optical using different modulation techniques—a review. International Journal of Engineering Trends and Technology (IJETT), 43(2).

[72] Popoola, W.O. and Ghassemlooy, Z., 2009. BPSK subcarrier intensity modulated free- space optical communications in atmospheric turbulence. Journal of Lightwave technology, 27(8), pp.967-973.

[73] Prabu, K. and Kumar, D.S., 2015. BER analysis for BPSK based SIM–FSO communication system over strong atmospheric turbulence with spatial diversity and pointing errors. Wireless Personal Communications, 81(3), pp.1143-1157.

[74] Jiang, T., Zhao, L., Liu, H., Deng, D., Luo, A., Wei, Z. and Yang, X., 2019. Performance Improvement for Mixed RF–FSO Communication System by Adopting Hybrid Subcarrier Intensity Modulation. Applied Sciences, 9(18), p.3724.

[75] Faridzadeh, M., Gholami, A., Ghassemlooy, Z. and Gatri, A., 2014, September. BPSK- SIM-PPM modulation for free space optical communications. In 7'th International Symposium on Telecommunications (IST'2014) (pp. 794-798). IEEE.

[76] Faridzadeh, M., Gholami, A., Ghassemlooy, Z. and Rajbhandari, S., 2012, July. Hybrid 2-PPM-BPSK-SIM with the spatial diversity for free space optical communications. In *2012 8th International Symposium on Communication Systems, Networks & Digital Signal Processing (CSNDSP)* (pp. 1-5). IEEE.

[77] Tiwari, Pawan, Nikhil Kumar, Pragati Singh, Chhavi Srivastava, M. Lakshmanan, Piyush Jain, and Saurabh Katiyar. "Modeling and Analysis of Hybrid SIM with L-PPM and MSK over Double Generalized Gamma Distribution in Free Space Optical Communication System." In *2019 International Conference on Vision Towards Emerging Trends in Communication and Networking (ViTECoN)*, pp. 1-4. IEEE, 2019.

[78] Balti, E., & Guizani, M. (2018). Mixed RF/FSO cooperative relaying systems with co- channel interference. IEEE Transactions on Communications, 66(9), 4014-4027.

[79] Wang, Z., Shi, W., & Liu, W. (2019). Two-way mixed RF/FSO relaying system in the presence of co-channel interference. IEEE Photonics Journal, 11(2), 1-16.

[80] Sun, Q., Zhang, Z., Zhang, Y., Lopez-Benitez, M., & Zhang, J. (2021). Performance analysis of dual-hop wireless systems over mixed FSO/RF fading channel. IEEE Access.

[81] Ashrafzadeh, B., Zaimbashi, A., Soleimani-Nasab, E., & Uysal, M. (2020). Unified performance analysis of multi-hop FSO systems over double generalized gamma turbulence channels with pointing errors. IEEE Transactions on Wireless Communications, 19(11), 7732-7746.

[82] Petkovic, M. I., Ansari, I. S., Djordjevic, G. T., & Qaraqe, K. A. (2019). Error rate and ergodic capacity of RF-FSO system with partial relay selection in the presence of pointing errors. Optics Communications, 438, 118-125.

[83] Siddharth, M., Shah, S., Vishwakarma, N., & Swaminathan, R. (2021). Performance analysis of adaptive combining based hybrid FSO/RF terrestrial communication. IET Communications, 14(22), 4057-4068.

[84] Atapattu, S., Tellambura, C., & Jiang, H. (2011). A mixture gamma distribution to model the SNR of wireless channels. IEEE transactions on wireless communications, 10(12), 4193-4203.

[85] Palliyembil, V., Vellakudiyan, J., Muthuchidamdaranathan, P., & Tsiftsis, T. A. (2018). Capacity and outage probability analysis of asymmetric dual-hop RF–FSO communication systems. IET Communications, 12(16), 1979-1983.

[86] Yang, L., Hasna, M. O., & Ansari, I. S. (2017). Unified performance analysis for multiuser mixed $\eta $-$\mu $ and $\mathcal {M} $-distribution dual-hop RF/FSO systems. IEEE Transactions on Communications, 65(8), 3601-3613.

[87] Kamga, G. N., Aïssa, S., Rasethuntsa, T. R., & Alouini, M. S. (2019). Mixed RF/FSO communications with outdated-CSI-based relay selection under double generalized gamma turbulence, generalized pointing errors and Nakagami-m fading. IEEE Transactions on Wireless Communications.

[88] Balti, E., & Guizani, M. (2018). Mixed RF/FSO Cooperative Relaying Systems With Co- Channel Interference," IEEE Transactions on Communications, vol. 66, no. 9, pp. 4014–4027, Sep. 2018,

[89] Liang, H., Gao, C., Li, Y., Miao, M., & Li, X. (2021). Performance analysis of mixed MISO RF/SIMO FSO relaying systems. Optics Communications, 478, 126344.

[90] Gupta, J., Dwivedi, V. K., & Karwal, V. (2018). On the performance of RF-FSO system over Rayleigh and Kappa-Mu/inverse Gaussian fading environment. IEEE Access, 6, 4186-4198.

[91] Samimi, H. (2019). Outage analysis of mixed dual-hop RF-FSO communication system over fading channels with pointing errors. Wireless Personal Communications, 109(3), 1557-1569.

[92] Mathur, A., Bhatnagar, M. R., Ai, Y., & Cheffena, M. (2018). Performance analysis of a dual-hop wireless-power line mixed cooperative system. IEEE Access, 6, 34380-34392.

[93] Yi, X., Shen, C., Yue, P., Wang, Y., & Ao, Q. (2019). Performance of decode-and-forward mixed RF/FSO system over κ− μ shadowed and exponentiated Weibull fading. Optics Communications, 439, 103-111.

[94] Vellakudiyan, J., Palliyembil, V., Ansari, I. S., Muthuchidambaranathan, P., & Qaraqe, K. (2019). Performance analysis of the decode-and-forward relay-based RF-FSO communication system in the presence of pointing errors. IET Signal Processing, 13(4), 480-485.

[95] Petkovic, M. I., & Trpovski, Z. (2018). Exact outage probability analysis of the mixed RF/FSO system with variable-gain relays. IEEE Photonics Journal, 10(6), 1-14.

[96] Xu, G., & Song, Z. (2020). Performance analysis for mixed κ-μ fading and M-distribution dual-hop radio frequency/free space optical communication systems. IEEE Transactions on Wireless Communications, 20(3), 1517-1528.

[97] Sharma, S., Madhukumar, A. S., & Swaminathan, R. (2019). Switching-based cooperative decode-and-forward relaying for hybrid FSO/RF networks. Journal of Optical Communications and Networking, 11(6), 267-281.

[98] Wang, Y., Wang, P., Liu, X., & Cao, T. (2018). On the performance of dual-hop mixed RF/FSO wireless communication system in urban area over aggregated exponentiated Weibull fading channels with pointing errors. Optics Communications, 410, 609-616.

[99] Hajji, M., & El Bouanani, F. (2017, November). Performance analysis of mixed Weibull and Gamma-Gamma dual-hop RF/FSO transmission systems. In 2017 International Conference on Wireless Networks and Mobile Communications (WINCOM) (pp. 1-5). IEEE.

[100] Rai, S., Pattanayak, D. R., Dwivedi, V. K., & Singh, G. (2017, March). New results on turbulence modelling for Rayleigh-double generalized gamma mixed RF-FSO cooperative system. In 2017 International Conference on Wireless Communications, Signal Processing and Networking (WiSPNET) (pp. 2483-2487). IEEE.

[101] AlQuwaiee, H., Ansari, I. S., & Alouini, M. S. (2015). On the performance of free-space optical communication systems over double generalized gamma channel. IEEE journal on selected areas in communications, 33(9), 1829-1840.

[102] Al-Ahmadi, S., & Yanikomeroglu, H. (2010). On the approximation of the generalized- K distribution by a gamma distribution for modeling composite fading channels. IEEE Transactions on Wireless Communications, 9(2), 706-713.

[103] Lei, H., Gao, C., Guo, Y., & Pan, G. (2015). On physical layer security over generalized gamma fading channels. IEEE Communications Letters, 19(7), 1257-1260.

[104] Malik, S., & Sahu, P. K. (2020). Performance analysis of free space optical communication system using different modulation schemes over weak to strong atmospheric turbulence channels. In Optical and Wireless Technologies: Proceedings of OWT 2018 (pp. 387-399).

[105] Khallaf, H. S., Elfiqi, A. E., Shalaby, H. M., Sampei, S., & Obayya, S. S. (2018). On the performance evaluation of LQAM-MPPM techniques over exponentiated Weibull fading free-space optical channels. Optics Communications, 416, 41-49.

[106] Tsiftsis, T. A., Sandalidis, H. G., Karagiannidis, G. K., & Uysal, M. (2008, May). FSO links with spatial diversity over strong atmospheric turbulence channels. In 2008 IEEE international conference on communications (pp. 5379-5384). IEEE.

[107] Abaza, M., Mesleh, R., Mansour, A., & Aggoune, E. H. M. (2014, April). Spatial diversity for FSO communication systems over atmospheric turbulence channels. In 2014 IEEE Wireless Communications and Networking Conference (WCNC) (pp. 382-387). IEEE.

[108] Ninos, M. P., Nistazakis, H. E., & Tombras, G. S. (2017). On the BER performance of FSO links with multiple receivers and spatial jitter over gamma-gamma or exponential turbulence channels. Optik, 138, 269-279.

[109] Alshaer, N., Ismail, T., & Nasr, M. E. (2020). Generic evaluation of FSO system over Málaga turbulence channel with MPPM and non-zero-boresight pointing errors. IET Communications, 14(18), 3294-3302.

[110] Alshaer, N., Ismail, T., & Nasr, M. E. (2020). Generic evaluation of FSO system over Málaga turbulence channel with MPPM and non-zero-boresight pointing errors. IET Communications, 14(18), 3294-3302.

[111] Nallagonda, V. R., & Krishnan, P. (2021). Performance analysis of FSO based inter-UAV communication systems. Optical and Quantum Electronics, 53, 1-20.

[112] Farooq, E., Sahu, A., & Gupta, S. K. (2018). Survey on FSO communication system— Limitations and enhancement techniques. In Optical and Wireless Technologies: Proceedings of OWT 2017 (pp. 255-264).

[113] Zafar, S., & Khalid, H. (2021). Free space optical networks: applications, challenges and research directions. Wireless Personal Communications, 121(1), 429-457.

[114] R. Gupta, S. Gangwar, Yashwardan, P. Jain, and M. Lakshmanan, "Performance Analysis of Mixture Gamma and Double Generalized Gamma RF/FSO Transmission Systems," *Telecommunications and Radio Engineering, vol.81*, no. 4, pp. 49–64, 2022.

[115] Yilmaz, F., and Alouini, M. S. (2012). A unified MGF-based capacity analysis of diversity combiners over generalized fading channels. *IEEE Transactions on Communications*, *60*(3), 862-875.

[116] Simon, M. K., and Alouini, M. S. (2005). Digital communication over fading channels (Vol. 95). John Wiley and Sons.

[117] Wolfram, The Wolfram functions site (2004), Source; Internet (online), http://functions.wolfram.com.

[118] A Kilbas, M. Saigo, H-Transforms: Theory and Applications. Analytical Meth- ods and Special Functions, CRC Press, Boca Raton, 2004.

[119] Prudnikov, A. P., Brychkov, Y. A. andMarichev, O. I. (1990) “Integral and Series: Volume More Special Functions,” CRC Press Inc.

[120] Singh, S. P., and Kumar, S. (2016). A MGF based closed form expressions for error probability and capacity over EGK fading for interference limited system. Wireless Personal Communications, 91(2), 577-593.

[121] Nistazakis, H. E., Stassinakis, A. N., Sandalidis, H. G., & Tombras, G. S. (2015). QAM and PSK OFDM RoFSO over M-turbulence induced fading channels. IEEE

Photonics Journal, 7(1). https://doi.org/10.1109/JPHOT.2014.2381670

[122] Krishnan, P., Jana, U., & Ashokkumar, B. K. (2018). Asymptotic bit-error rate analysis of quadrature amplitude modulation and phaseshift keying with OFDM RoFSO over M turbulence in the presence of pointing errors. IET Communications, 12(16), 2046–2051. https://doi.org/10.1049/iet-com.2017.0560

[123] Kumar, A., & Krishnan, P. (2020). Performance analysis of RoFSO links with spatial diversity over combined channel model for 5G in smart city applications. Optics Communications, 466,125600. https://doi.org/10.1016/j.optcom.2020.125600.